SILICON CARBIDE INTEGRITY IN TRISO FUEL PARTICLES

MHAKAMUNI WITNESS MAKAMU

Submitted in partial fulfillment of the requirements for the degree of

MSc (Applied Science) in Metallurgy

in the

Faculty of Engineering, Built Environment and Information Technology

University of Pretoria

Pretoria

April 2015

Summary

Title:	Silicon Carbide Integrity in TRISO Fuel Particles
Author:	Mhakamuni Witness Makamu
Supervisor:	Prof J.P.R. de Villiers
Co-supervisor:	Prof G.T. van Rooyen
Department:	Materials Science and Metallurgical Engineering
University:	University of Pretoria
Degree:	Masters of Science (Applied Science) in Metallurgy

Chemical vapor deposited (CVD) silicon carbide (SiC) is used as a pressure vessel material for tristructural isotropic (TRISO) coated fuel particles for the high temperature pebble-bed reactor. Experience has shown that sometimes these particles fail in operation. The fracture toughness (K_{IC}) was measured at room temperature to determine the maximum internal pressure that the CVD SiC layer in TRISO-coated fuel particles can withstand without fracturing. The K_{IC} was measured using the indentation fracture toughness method on the curved-surface and cross-section of the test piece. The most suitable test load for measuring the K_{IC} and Vickers hardness (H_V) values of the CVD SiC layer was 100 g. The Evans-Davis model for calculating the K_{IC} of ceramic materials was found to be the most appropriate for the CVD SiC layer. The average curved-surface K_{IC} value was 3.47 MPa.√m, for the 51 µm test sample, which was tougher than the average cross-section K_{IC} value of 3.17 MPa.√m. The wall thickness values of the samples tested were 28, 36, 39 and 51 µm and their corresponding measured mean curved-surface K_{IC} values were 3.13, 3.07, 3.15 and 3.47 MPa.√m, respectively, which were on par with values reported in literature. The corresponding minimum curved-surface K_{IC} values were 1.43, 1.67, 1.65 and 2.52 MPa.√m, respectively. These values were obtained from the average curved-surface K_{IC} values minus five sigma ($K_{IC} = \mu - 5\sigma$). The internal pressure that the SiC shell can handle without failing will depend on the initial crack length and the value of K_{IC}**.** The pressure that a particle can withstand assuming the leak-before-break (i.e. a particle with a crack that extends right through the shell) was also used. This represents a more conservative value for the maximum pressure allowable without fracture when the fracture toughness is known. In fact, there is a considerable wide distribution in the measured fracture toughness. Using the average fracture toughness (µ) minus five times the standard deviation (σ) represents a conservative approach. The calculated maximum allowable pressure represents an even more conservative approach when both the LBB condition and the $\mu - 5\sigma$ requirement are assumed. This is probably representative for the operation of the PBMR.

Key words: *Chemical Vapor Deposition, Silicon Carbide, Fracture Toughness, Vickers Indentation Test, Internal Pressure, Fuel Particles, PBMR, CVD, SiC, TRISO*

Declaration

I, the undersigned hereby declare that:

I understand what plagiarism is and I am aware of the University's policy in this regard;

The work contained in this dissertation is my own original work,

I did not refer to work of current or previous students, lecture notes, handbooks or any other study material without proper referencing,

Where other people's work has been used this has been properly acknowledged and referenced;

I have not allowed anyone to copy any part of my thesis,

I have not previously in its entirety or in part submitted this thesis at any university for a degree.

Makamu MW

26535582

14 April 2015

Acknowledgments

I would like to thank the following institutions and people who made this dissertation possible:

- Prof J.P.R. de Villiers, Prof P.C. Pistorius and Prof G.T. Van Rooyen for constantly giving me advice that contributed towards the completion of this project
- Mr. R. Cromarty and all the personnel at the department for their valuable contribution
- Mr. M.P. Hindley from Eskom Research and Innovation Center for his contribution more especially in statistics
- The Department of Materials Science and Metallurgical Engineering at the University of Pretoria and IMMRI for allowing me to have access to their facilities at all times.
- SANHARP for their financial support
- PBMR for the provision of test samples

Thanks are also due to all my friends who gave me support when I needed it most.

Dedication

To my kids Appreciate, Gingirikani, Ntivo and Thwala

Table of contents

List of figures

List of tables

List of equations[1]

[1] ***Note:*** The unit of one variable will depend on the units of the other variables in the equation in use. It can also depend on the preferred units. For instance the crack length can be expressed in m, mm or µm.

Abbreviations, Acronyms, Symbols and Conversions[2]

PBMR	=	Pebble Bed Modular Reactor
TRISO	=	Tristructural Isotropic
CVD	=	Chemical Vapor Deposition
SiC	=	Silicon Carbide
CeSiC	=	Carbon-SiC (also known as CeSIC, CSiC, CSIC, C-SiC, and C-SIC)
SAFARI-1	=	South African fundamental Atomic Reactor Installation
MW	=	Megawatts
HTR	=	High Temperature Reactor
HTGR	=	High Temperature Gas-Cooled Reactor
PyC	=	Pyrolytic Carbon
MeV	=	Mega electron Volts
$n.m^{-2}$	=	Neurons per square meter
SEM	=	Scanning Electron Microscope
f	=	Applied load
H_V	=	Vickers Hardness
HK	=	Knoop Hardness
MTS	=	Methyltrichlorosilane
μ	=	mean
μm	=	Micron meters
2α	=	Indent Diagonal
a	=	Half indent Diagonal
l	=	Crack Length measured from the edge of an indentation
c	=	Crack length for edge crack or one half crack length for internal crack
c_c	=	Critical Crack Length
d	=	Crack Depth
d_c	=	Critical Crack Depth
t	=	Thickness
B	=	Critical Specimen Thickness
K	=	Stress intensity factor
K_{IC}	=	Plain Strain Fracture Toughness
K_{IIC}	=	Plain Stress Fracture Toughness
Y	=	Shape Factor
σ	=	Stress
σ_c	=	Critical Stress
σ_d	=	Design Stress
σ_y	=	Yield Stress

[2] The symbol used in this document might vary from the standard known symbols to avoid confusion. For instance, *d*, means indent diagonal in the standard Vickers hardness equation whereas **2a** also means the same in the equation used to calculate the fracture toughness of ceramics. Therefore **2a** means indent diagonal in this document.

P	=	Pressure
P_c	=	Critical Pressure
P_{max}	=	Maximum Pressure
E	=	Young's Modulus/Elastic Modulus
D	=	Mean Diameter
t	=	wall thickness
1 kg	=	9.80665 N;
1 kg/mm^2	=	9.80665 MPa;
1 atm	=	0.101325 MPa;
π	=	3.141592654
Kolmogorov-Smirnov	=	K-S
Anderson-Darling	=	A-D

Chapter 1: Introduction

1.1 BACKGROUND

Pebble Bed Modular Reactor (PBMR) (Pty) Limited was established in 1999 and was responsible for the overall design of the entire PBMR plant. PBMR (Pty.) Ltd. was also intended to market small-scale, high-temperature nuclear reactors, both locally and internationally. The concept is based on experience in the US and mainly Germany where prototype reactors were operated successfully between the late 1960s and 1980s [1, 2].

The PBMR has a simple design, with inherent safety features that require no human intervention, and which cannot be bypassed. The basis for the safety of pebble bed reactors is the very low power density of the reactor, which means that the amount of energy and heat produced is volumetrically low and that there are natural mechanisms such as conductive and radiative heat transfer that will remove the heat even if no forced cooling is provided [2].

The PBMR [1, 2] was designed as a helium-cooled, graphite-moderated high temperature reactor (HTR) utilizing a closed cycle gas turbine for electricity generation. It would produce a power of approximately 400 MW (thermal) [as compared to 20 MW (thermal) from the SAFARI-1 reactor] and net electrical output of approximately 165 MW (electrical). Heat from the PBMR can also be used for a variety of industrial process applications namely: to generate process steam for cogeneration applications, in-situ oil sands recovery, ethanol applications and refinery applications. Thus, the High Temperature Gas-cooled Reactor (HTGR) technology is receiving increasing interest in many countries around the world as a promising future energy option. The optimum size for a pebble bed was concluded to be about 250 MW (thermal) to allow for rapid and modular construction as well as maintaining its inherent safety features [1].

The PBMR [1] comprises of a 6 m diameter and 20 m high steel pressure vessel, lined with a 0.9 m thick layer of graphite bricks which serves mainly as a neutron reflector although important also in terms of heat transfer (a passive heat transfer medium). The pressure vessel holds about 452,000 fuel spheres, consisting of low enriched uranium tristructural isotropic (TRISO) coated

fuel particles contained in a molded graphite sphere. A coated fuel particle consists of a kernel of uranium dioxide surrounded by four coating layers as shown in Figure 1.

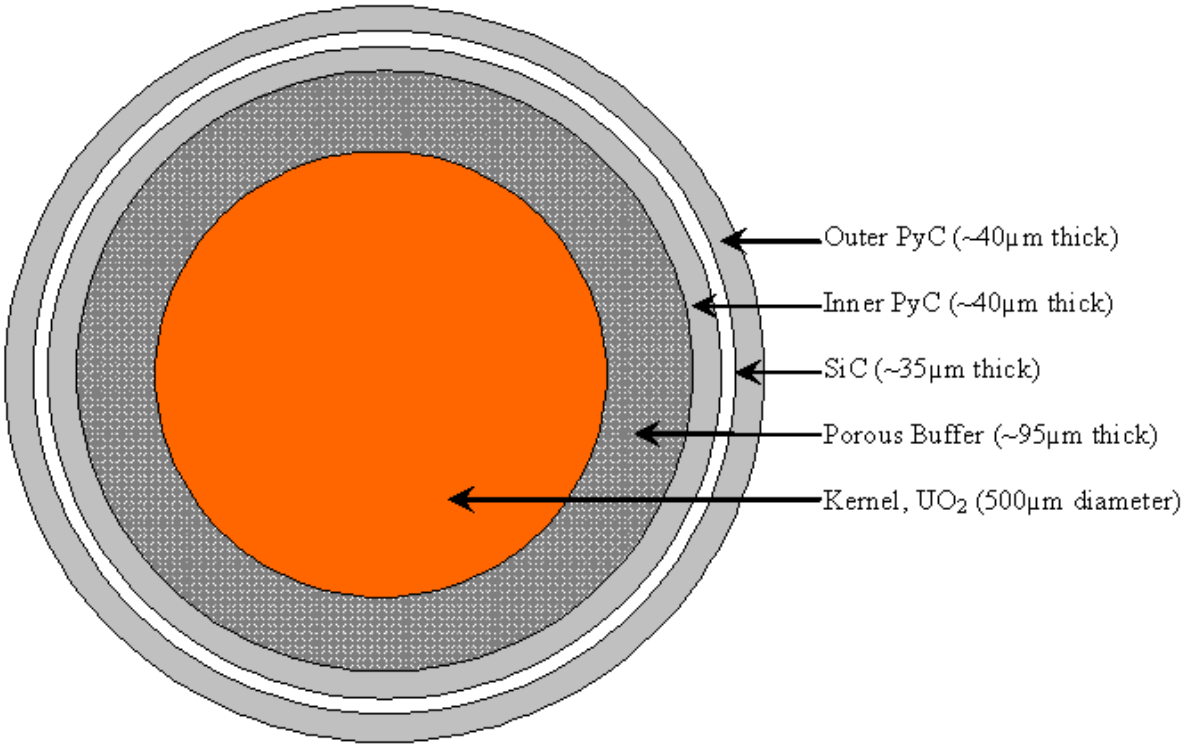

Figure 1: Schematic diagram of a typical TRISO-coated particle geometry [3]

The spherical fuel kernel used in the PBMR pebbles is coated with porous buffer pyrolytic carbon (PyC), inner PyC, SiC and outer PyC layers. The primary function of each layer in a TRISO particle was well explained by Gregory *et al* [4] and discussed in detail under section 2.3 of this thesis.

High-purity stoichiometric Chemical Vapour Deposition (CVD) processed-SiC was widely used as a pressure vessel material for fuel-particles in HTGR. This project is focusing only on the SiC layer of the TRISO coated particles used in the PBMR pebbles. The main reason for focusing on the SiC is that this layer was treated as the primary containment which serves as a pressure vessel as well as a diffusion barrier. That means if the SiC layer was to fail, the radioactive fission products (metallic and gaseous fission products) would leak, releasing radiation into the fuel spheres and then into the reactor pressure vessel and gas coolant system. Thus, it has been considered as a worst case scenario.

Wolf *et al* [5] found that the principal cause of fission product release from TRISO-coated fuel is the mechanical failure of the SiC coating at temperatures up to 1150 ^{o}C. This is because structural defects and crack nucleation sites will always exist in the SiC coating. Niihara [6] found that degradation of toughness is not observed up to 500 ^{o}C and that the toughness of the SiC increases with increasing temperature above 1100 ^{o}C. Ghosh *et al* [7] as well as other authors [6, 8 and 9] also reported that the fracture toughness of SiC was independent of temperature from 20 ^{o}C to 1400 ^{o}C. However, others [9 and 10] reported that the fracture toughness of SiC increases slightly with temperature. Higher fracture toughness (K_{IC}) of annealed materials appears to be due to crack bridging by elongated grains [9].

Under normal operation, a maximum internal TRISO pressure of not exceeding 30 MPa has been reported in the literature [11 and 12]. The particles were strong enough to withstand this pressure without undue failures [12]. Since the maximum internal pressure of 30 MPa depends on modeling assumptions and assumptions for the material properties, it is nevertheless important to experimentally determine the maximum internal pressure that a 35 µm CVD SiC layer in TRISO-coated fuel particle with a defect can withstand without failure. The K_{IC} and the hardness of the CVD SiC layer in TRISO-coated fuel particles were determined at room temperature since the mechanical properties were reported [6, 7, 8, 9 and 10], not to be negatively affected by temperature up to 1700 ^{o}C, which is above the operating temperature of the PBMR.

1.2 PROBLEM STATEMENT

The TRISO coated particles are subjected to an internal gas pressure that is generated during fission and from fission products of the fuel kernel material. The internal pressure will cause stress that may lead to the failure of the TRISO layers and a release of the fission products to the environment. Thus, it is important to determine the fracture toughness in order to determine the critical crack size at pressures prevailing inside the TRISO kernel. Radioactive fission products need to be retained within the fuel particle, therefore the fracture strength of the SiC layer is of concern. Thus, there is a need to determine the maximum internal pressure that the SiC layer can withstand without cracking, to ensure a safe working environment.

1.3 OBJECTIVE OF THIS STUDY

The aim of this project was to determine the maximum internal pressure that the 35 µm CVD SiC in TRISO fuel particles can *withstand* without cracking. This was achieved through the determination of the mechanical properties (fracture toughness and hardness) of a bulk hot-pressed (HP) polycrystalline SiC and polycrystalline CVD SiC in TRISO particles using the indentation technique at room temperature.

Why Fracture toughness? Since most manufactured materials contain defects such as cracks, there is a need to determine the critical crack size necessary to cause failure at a particular stress value, leading to catastrophic crack propagation.

Chapter 2: Literature Review

2.1 Ceramics as structural materials

Ceramics are strong, hard, and durable. This makes them attractive structural materials. The one significant drawback is their brittleness, but this problem is being addressed by the development of composite materials. Ceramics can withstand high temperatures and do not expand greatly when heated. This makes them excellent thermal barriers, for various applications. While some of these ceramics are good thermal insulators, some of them such as the SiC are very good conductors.

The processing of crystalline ceramics follows the basic steps that have been used for ages to make clay products. The materials are selected, prepared, formed into a desired shape, and sintered at high temperatures. Glasses are processed by pouring in a molten state, working into shape while hot, and then cooling. Newer processing techniques such as *chemical vapour deposition* and sol-gel processing have been developed.

The reason for putting more emphasis on the ceramic materials was that the scope of this investigation focused on the SiC, which is one of leading refractory ceramic materials. The above discussion also helps to understand why this ceramic material (i.e. SiC) was used instead of other solid materials. The rest of the chapter will focus on the SiC, its properties, applications in the nuclear industry as well as various methods for testing its properties.

2.2 Silicon Carbide and its Applications in The Nuclear Industry

There are two groups of SiC materials, which are both multi-phase and single-phase materials. The single-phase SiC materials are CVD, hot pressed (HP) and sintered SiC. The multiphase SiC materials are reaction bonded SiC, converted SiC and Carbon SiC (CeSiC). Multiphase SiC materials have SiC phases intermixed with phases of Si and/or carbon whereas a single-phase SiC materials are 99 % to 99.9999 % pure SiC, depending on the manufacturing conditions [13].

CVD SiC has high purity (99.99 % pure on a metals basis) with a cubic β-SiC crystal structure, while hot-pressed or sintered SiC has a hexagonal or trigonal α-SiC structure. Other polytypes may also be produced using the CVD technique [14].

Multiple-phase materials have non-uniform and less repeatable mechanical properties because of internal stresses that are introduced during cooling after sintering. This is caused by different thermal expansion coefficients of the different phases of the multiphase materials [13].

Single-phase materials provide uniform and repeatable mechanical properties because of their high purity than multiphase materials [13]. Cockeram [8, 14] concluded that the CVD SiC material is isotropic with respect to strength and elastic/Young's modulus.

CVD is a complex chemical process and is one of the most attractive techniques capable of producing highly dense and pure ceramic materials. SiC produced by CVD is a potential candidate for high temperature structural applications because of its excellent high temperature oxidation resistance, corrosion, erosion and/or abrasion resistance; its high elastic modulus and strength, and a high thermal shock resistance [15]. It is therefore used as diffusion barrier coatings for susceptors in the semiconductor industries, oxidation resistance coatings for re-usable space vehicles, coatings for continuous filaments, and matrices for fiber-reinforced composites and more interestingly; as a coating for fuel particles in HTGRs [15].

An example where SiC finds its application in the nuclear industry is shown in Figure 2. Figure 2 shows a scanning electron microcopy (SEM) cross-section micrograph of a heavily irradiated cracked TRISO fuel particle with SiC still intact [15]. The SiC layer should provide containment of gaseous and metallic fission products.

It has been reported by Snead [15] that during fission of the fuel kernel material, gaseous products such as Krypton (Kr), Xenon (Xe), Carbon monoxide (CO) and Carbon dioxide (CO_2) are released. CO and CO_2 are not direct fission products. They are generated from carbon layers reacting with oxygen released from the oxide fuel during operation. Gaseous products within the kernel, together with kernel swelling due to radiation damage and fission product accumulation

cause internal pressure and tensile stresses in the pyrocarbon layers. Eventual cracking of the carbon layers, due to internal pressurization and irradiation, can cause a stress concentration at the interface between the carbon and SiC layers [15] (see Figure 2).

Figure 2: Irradiated TRISO showing cracked PyC [15]

2.3 TRISO FUEL PARTICLES

Chemical vapor deposition of SiC is also applied to TRISO-coated spherical fuel particles for HTGRs. The spherical fuel particles are surrounded by four layers with the first layer being the porous PyC [containing about 50 % porosity] followed by a dense PyC, SiC and another dense PyC. The porous PyC absorbs fission products generated within the kernel, and it also serves as a reservoir for fission products and accommodates kernel swelling without transmitting forces to the outer coatings. The inner dense PyC layer protects the kernel from reactions with chlorine during the deposition of the SiC layer, provides structural support for the SiC layer; and protects the SiC layer from fission products and carbon monoxide during operation [4].

A high-density, high strength SiC layer provides the TRISO-coated particle with the ability *to contain the high pressure* generated inside the kernel/buffer region by fission products. This SiC

layer can therefore be called a fission gas 'pressure vessel'. The outermost layer in the TRISO system is another high density, isotropic PyC layer that protects the SiC during the remainder of the fabrication process and provides structural stability to the particle during irradiation [4].

The TRISO coating system has become one of the techniques for fabricating fuels for the currently operating gas cooled reactors as well as the next generation HTGRs such as the pebble bed reactor and various HTRs being studied under the international Generation IV reactor program [15].

There are various kernel materials [UO_2, UC_2, UO_2 + UC_2, (Th, U)O_2, (Th, U)C_2] reported to have been tested as nuclear fuel for HTGRs [16]. Particles with UO_2 have the advantage over those with UC_2 of better retaining certain fission products (such as the rare earths) and of better stability at temperatures of 2000 to 2500 °C (that might be encountered in a core heat up accident). However, in a coated particle fuel with UO_2 kernels, there is excess oxygen released during fission. For every two-oxygen atoms (O_2) produced, other fission products combine with 1.6 atoms, leaving an excess of 0.4 atoms [17]. This excess oxygen will react with the buffer to form CO gas. Under high burn-up conditions, excess CO is generated and could lead to a higher-pressure buildup inside the pressure vessel (i.e. SiC) resulting in a mechanical failure of this pressure vessel and could also accelerate kernel migration (the so called the "amoeba effect") [5, 16]. As explained by Wolf, the amoeba effect is defined as the migration of the fuel kernel into the coating material in a temperature that weakens the coating. Wolf also mentioned that there are various factors influencing the amoeba such as irradiation temperature and the amount of free oxygen within the particle when oxide kernels are used. In the pebble bed reactor, the fuel temperatures and the temperature gradients across the particles are low enough to avoid damage by the amoeba effect [5].

The reaction of the excess oxygen in the oxide fuel $UO_{2\pm x}$ with the buffer carbon at higher temperatures to produce noticeable pressures of CO and CO_2 has also been reported by Guéneau [18]. The oxygen source for CO formation comes from the $UO_{2\pm x}$ fuel and it is governed by the oxygen chemical potential in $UO_{2\pm x}$. The more the O/U ratio increases, the more the CO pressure increases. CO_2 pressure is the major gaseous species at high temperature

whereas CO is the major one at lower temperature (i.e. 1000 ^{o}C). At 1500 ^{o}C, CO_2 contributes significantly to the gas pressure (see Figure 3) [18].

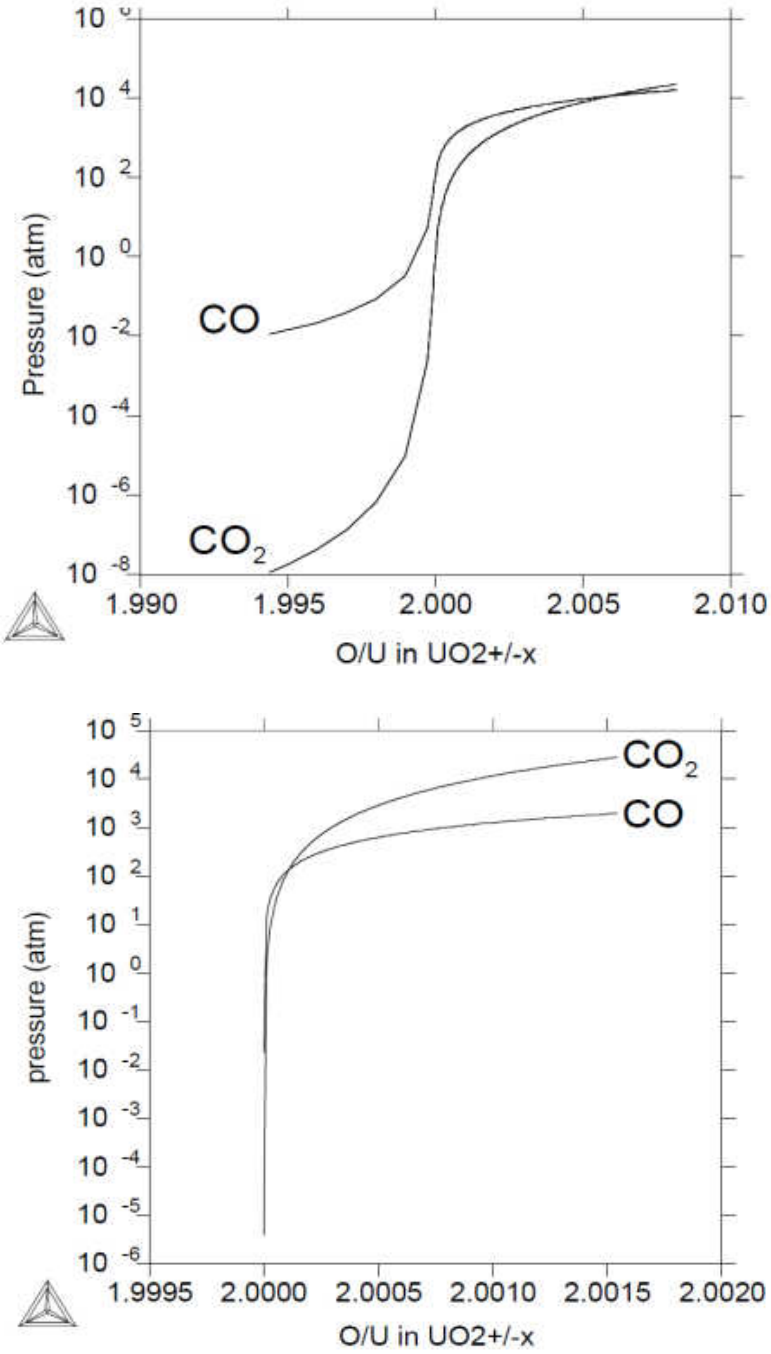

Figure 3: Calculated CO and CO_2 partial pressures versus O/U ratio in UO2±x fuel in equilibrium with carbon at 1000 ^{o}C (top diagram) and 1500 ^{o}C (bottom diagram) and at a fixed volume of 7.18 x 10^{-6} m^3 [18]

As discussed in this section, the main purpose of these coating layers is to retain fission products within the particle. In particular, the SiC layer acts as a diffusion barrier to metallic fission products and as a pressure vessel of the particle. During the generation of the fission products, there is a pressure build up within the vessel. As seen in in Figure 2, the SiC layer is the only layer still in a good condition to contain the fission products and if the maximum internal pressure exceeds the maximum pressure that can be contained by SiC alone, the SiC would eventually fail.

2.4 AN OVERVIEW OF THE CVD PROCESS

CVD is a generic name for a group of processes that involve depositing a solid material from a gaseous phase. CVD can be performed in a 'closed' or 'open' system. In the 'closed' system, a reversible chemical reaction is possible. In the 'open' system, after deposition the reaction chemicals are removed from the reactor, with the recovery of the reactants made only if the expense justifies it [19].

According to Choy, the CVD system has the following unique advantages [19]:

- Good uniformity and high purity when depositing SiC at a high temperature and a high pressure
- Deposition of films directly from vapours or gases
- Reproducibility of films
- Coating of complex shaped components
- Ability to control crystal structure
- Control of crystal structure, surface morphology and orientation of the CVD products
- Deposition rate can be adjusted readily
- Reasonable processing cost for the conventional CVD technique and flexibility of using a wide range of chemical precursors such as halides, hydrides, which enable the deposition of a large spectrum of materials including metals, carbides, nitrides, oxides, sulphides, III–V and II–VI materials.

- Relatively low deposition temperatures enable the deposition of refractory materials at a fraction of their melting temperatures. For example, refractory materials such as SiC (sublimation point: 2700 ^{o}C) can be deposited at 1000^{o}C using the combination of methyltrichlorosilane (MTS) and H_2 as shown by the following chemical reaction:

$$CH_3SiCl_3\,(MTS)\,(g) \rightarrow^{H2} SiC(s) + 3HCl\,(g)$$ [19].

The *drawbacks* of the CVD process include chemical and safety hazards caused by the use of toxic, corrosive, flammable, or explosive precursor gases and the use of more sophisticated reactors or vacuum systems by CVD variants such as low pressure or ultrahigh vacuum CVD, plasma assisted CVD and photo-assisted CVD, which tends to increase the cost of fabrication [19].

The distinctive advantages of CVD, under specific conditions, outweigh its limitations. In general, CVD is a versatile deposition technique. It has become one of the main processing methods for the deposition of amorphous, single-crystalline or polycrystalline thin films and coatings for a wide range of applications [19].

There is no universal CVD equipment. Each piece of CVD equipment is individually tailored for specific coating materials or substrate geometry, whether it is used for R&D or commercial production. In general, the CVD equipment consists of three main components for example: *chemical-vapour precursor supply system*, *the CVD reactor* and *the effluent gas handling system* [19].

The chemical-vapour precursor supply system generates vapour precursors and then delivers them to the reactor. The design of the CVD reactor depends on whether the starting material is solid, liquid or gas. The sublimation of a solid precursor depends on surface area of the solid and contact time. Liquid sources often use a bubbler to vaporise the reactants, and a carrier gas (reactive gases such as H_2 or inert gases such as Ar) to transport the vaporised reactants into the reactor [19].

The *CVD reactor* is used to heat the substrate to the deposition temperatures. There are various reactor configurations; for instance, fluidized bed, horizontal, vertical, semi-pancake, barrel and multiple wafers [19].

The *effluent gas handling system* consists of a neutralizing part for the exhaust gases, and/or a vacuum system to provide the required reduced pressure for the CVD process that performs at low pressure or high vacuum during deposition. The main function of the effluent gas handling system is to remove the hazardous by-product and the toxic un-reacted precursor safely. Therefore, the effluent gas handling system needs to be tailored to the individual CVD system [19].

The CVD equipment is designed to produce give a coating with uniform thickness, surface morphology, structure and composition. The design has taken into consideration the temperature control, reactant depletion, fluid dynamics and heat transfer in the system. Most of the CVD reactor systems are designed empirically. The commercial production equipment is more sophisticated and complex in design as compared to the laboratory CVD coater [19].

The TRISO coating is normally formed using a fluidized bed chemical vapour deposition (FBCVD) method. FBCVD is usually used at a high temperature and at atmospheric pressure in order to suspend fuel particles. For SiC layer deposition, MTS is used as a source/reactant. Hydrogen is used as a carrier gas and diluent gas, to control the concentration of the mixture of MTS vapour and the carrier gas (H_2). The combination of MTS (methyltrichlorosilane) and H_2 is the most popular, partly because MTS contains the same number of silicon and carbon atoms, making deposition of stoichiometric films easy [19].

The SiC layer in TRISO coated fuel particles is a critical layer since it is a protective layer against diffusion of fission products and provides mechanical strength for the fuel particle. Therefore, mechanical properties of the SiC layer are important and will depend on the process parameters such as deposition temperature, pressure and deposition rate. As the deposition temperature increases, the grain size and deposition rate increase while the chemical composition

changes with increasing temperature, the preferred orientation on the surface of the depositing layer also changes from (111) to (220) and (311) planes in the cubic variety of SiC [20].

The process parameters should be adjusted to prevent co-deposition of free Si with SiC or free C with SiC. For instance, if the fluidizing gas is pure hydrogen and the ratio of H_2/MTS ranged from 239 to 1028, β-SiC single phase is deposited between 1500 and 1700^{o}C and free Si is co-deposited with β-SiC between 1150 ^{o}C and 1500^{o}C. If the fluidizing gas is a mixture of H2 and Ar and the ratio of (H2+Ar)/MTS was around 250, β-SiC single phase is deposited between 1400 ^{o}C and 1600 ^{o}C and free Si is co-deposited with β-SiC between 1150 ^{o}C and 1400 ^{o}C. When the fluidizing gas is pure argon and the ratio of Ar/MTS is 248, free C was co-deposited with SiC at 1300 ^{o}C and 1600 ^{o}C [21].

2.5 MECHANICAL PROPERTIES IN GENERAL

Mechanical properties describe the way in which a material responds to forces, loads, and impacts. Ceramics are hard materials that are also resistant to corrosion (durable). These properties, along with their low densities and high melting points, make ceramics attractive structural materials. Ceramic materials are somewhat limited in applicability by their low fracture toughness property, which in many respects are inferior to those of metals. The principal limitation of ceramics is their brittleness and low fracture toughness, i.e., the tendency to fail suddenly with little plastic deformation or very little energy absorption.

Hardness, toughness, strength, brittleness, and *ductility* are *mechanical properties* used as measurements of how metals behave under a load. These properties are described in terms of the types of force or stress that the metal must withstand and how these are resisted. For the purpose of this investigation it is important to define and discuss in general the relationship between the hardness, toughness, elasticity and strength of materials.

2.5.1 Hardness

Hardness is the property of a material, which gives it the ability to resist being permanently deformed, scratched, cut, indented or changed in shape when a load (that can cause cutting, scratching, deformation or indentation) is applied. The greater the hardness of the metal, the greater resistance it has to deformation.

In metallurgy hardness is defined as the ability of a material to resist plastic deformation. It is also defined as the resistance of a material to indentation. This is the usual type of hardness test carried out in most materials, in which a pointed or rounded indenter is pressed into a surface under a test load. Hardness is one of the most frequently measured properties of a ceramic. Its value helps to characterize resistance to deformation, densification, and fracture.

There are macro-, micro- and nano-hardness measurements, depending on the loading force value and the indentation dimensions. *Macro-hardness* tests (Rockwell, Brinell, and Vickers) are the most widely used methods for rapid routine hardness measurements. The indenting forces in macro-hardness tests are in the range of 50 N to 30000 N. *Micro-hardness* test (micro-Vickers and Knoop) is applicable when hardness of coatings, surface hardness, or hardness of different phases in the multi-phase material is measured. A small diamond pyramid is used as indenter loaded with a small force of 10 g to 1000 g. A *nano-hardness* test uses minor loads of about one nano-Newton followed by precise measuring of the depth of indentation.

Macro-hardness measurement is a quick and simple method of obtaining mechanical property data for the bulk material from a small sample. It is also widely used for the quality control of surface treatment processes. However, when concerned with coatings and surface properties, the macro-indentation depth would be too large relative to the surface-scale features.
Where a material's microstructure is multi-phase, non-homogeneous or prone to cracking, macro-hardness measurements will be highly variable and will not identify individual surface/microstructural features. It is here that micro-hardness measurements are appropriate.

Micro hardness is the hardness of a material as determined by forcing an indenter such as a Vickers or Knoop indenter into the surface of the material under 10 g to 1000 g load and the indentations are small. The indentations are made using a square-based pyramid indenter for the Vickers hardness scale or an elongated, rhombohedral-shaped indenter for the Knoop hardness scale. The impression length, measured microscopically, and the test load are used to calculate a hardness value. The hardness values obtained are useful as indicators of materials properties and expected service behavior. *Micro-hardness* tests are capable of determining hardness of different micro constituents within a structure, or measuring steep hardness gradients such as those encountered in case hardening.

The hardness of a material is always specified in terms of the particular test that was used to measure this property because there are several methods of measuring hardness. There are three types of tests used with accuracy by the metals industry; they are the Brinell hardness (HB) test, the Rockwell hardness (HR) test, and the Vickers hardness (HV) test. The way these three hardness tests measure a metal's hardness is to determine the metal's resistance to the penetration of a non-deformable ball or cone. The tests determine the depth which such a steel ball, diamond cone or diamond pyramid will sink into the metal, under a given load, within a specific period.

Hardness of ceramic materials is usually tested by Vickers or Knoop Methods, using diamond indenters. The principle of any hardness test method is forcing an indenter into the sample surface followed by measuring the dimensions of the indentation (depth or actual surface area of the indentation). The hardness value depends on the combination of yield strength, tensile strength and modulus of elasticity.

The *Vickers hardness test* is the standard method for measuring the hardness of a material, calculated from the size of an impression produced under load by a pyramid-shaped diamond indenter. The diagonal of the resulting indention/impression (usually no more than 0.5 mm) is measured under a microscope from tip to tip along both axes. The average measurement is converted to a Vickers hardness value according to a formula or a conversion table based on the formula. Standard test methods used was BS EN ISO 6507 part 1, 2, 3 and 4.

The Vickers hardness (H_V) values were calculated using the following formula:

Equation 1
$$H_V = 1.854\left(\frac{f}{(2a)^2}\right)$$

Where f is the applied load, (kg)
$2a$ is the indent diagonal, (mm)

The micro Vickers hardness test is usually required for testing very small or thin parts or in tight locations, close to specimen edges, etc. Generally, the main requirement for the test sample in Vickers hardness testing is a flat, polished-finish test surface and loads applied for 10 to 15 seconds. Samples also need to be securely mounted perpendicular to the indenter to prevent any rocking during the test. A result to be reported should include the type of hardness tester and the test load used (e.g. H_{V30} means a Vickers hardness tester with a 30 kg test load was used). If a non-standard time is used it should be listed after the test load.

The Vickers test is reliable for measuring the hardness of metals and ceramic materials. The Vickers indenter is a 136 degrees square-based diamond indenter, the diamond material of the indenter has an advantage over other indenters because it does not deform over time and use. The advantages of the Vickers hardness test are that extremely accurate readings can be taken, and just one type of indenter is used for all types of metals and surface treatments.

2.5.2 Fracture Toughness

The ability of a material to resist fracture in presence of defects or a crack is termed fracture toughness. The key to toughness is a good combination of strength and ductility. A material with high strength and high ductility will be tougher than a material with low strength and high ductility. Several standard types of toughness tests include fracture toughness, impact toughness and notch toughness tests. The last two tests are discussed under the section 2.5.7 whereas the fracture toughness test is discussed in this section. Material toughness can also be measured by calculating the area under the stress strain curve from a tensile test as shown in Figure 4. Fracture

toughness is one of the most important properties of any material for virtually all design applications. If a material has a large value of fracture toughness it will probably undergo ductile fracture. Materials with low fracture toughness fail in a brittle manner.

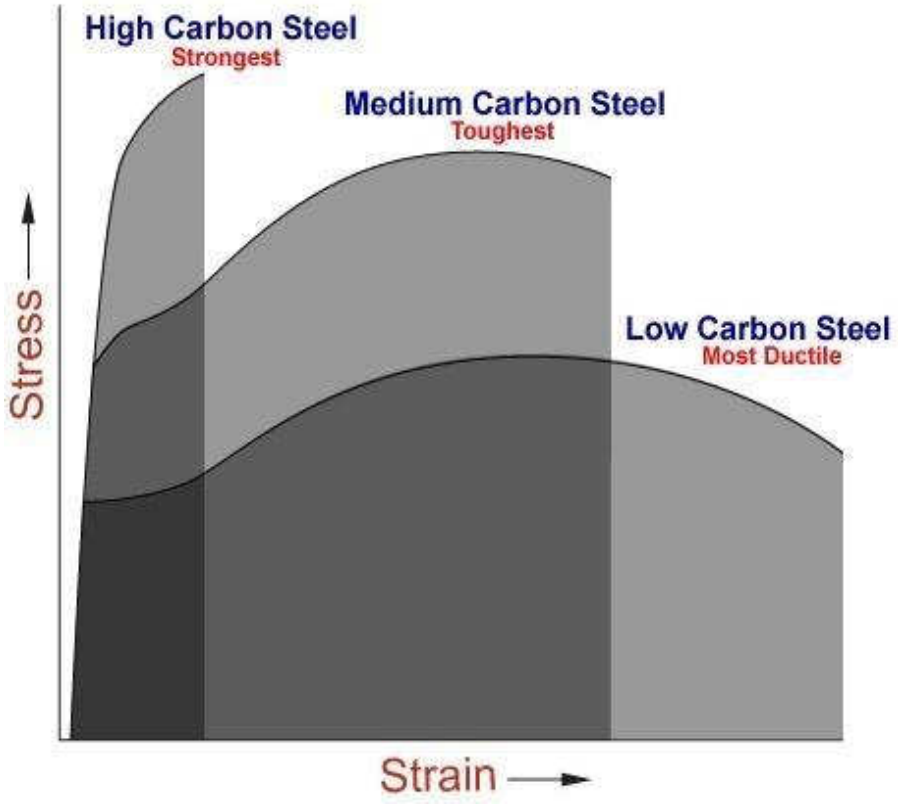

Figure 4: A stress strain curve [22]

Fracture toughness can be used to indicate the amount of stress required to propagate a pre-existing flaw, since the occurrence of flaws is not completely avoidable in the processing, fabrication, or service of a material/component. *Fracture toughness is defined as a property indicative of a material's resistance to fracture when a crack is present.* Therefore, it is a very important material property. Flaws may appear as cracks, voids, metallurgical inclusions, weld defects, design discontinuities, or some combination thereof. Since engineers can never be very sure that a material is flaw free, it is common practice to assume that a flaw of a certain size will be present in a number of components and they can then use the linear elastic fracture mechanics (LEFM) approach to design critical components. This approach uses the flaw size and features,

component geometry, loading conditions and the material property called fracture toughness to evaluate the ability of a component containing a flaw to resist fracture.

A parameter called the stress-intensity factor (K) is used to determine the fracture toughness of most materials. The stress-intensity factor is followed by a Roman numeral subscript to indicate the mode of fracture and there are three modes of fracture as illustrated in Figure 5(a). There is mode-I crack opening under a normal tensile stress perpendicular to the crack. This is the usual mode for fracture toughness tests and it is designated K_I and has the units of MPa.√m. The material can be made thick enough to resist shear (mode-II) or tear (mode-III).

Specimens having different absolute sizes produce different values for K_I. This results because the stress state adjacent to the flaw changes with the specimen thickness, B, until the thickness exceeds some critical dimension (see Figure 5(b) and Equation 5). Once the thickness exceeds the critical dimension, the value of K_I becomes relatively constant and this value, K_{IC}, is a true material property, which is called the plane-strain fracture toughness.

The stress intensity factor, K_I, represents the level of "stress" at the tip of the crack and the fracture toughness, K_{IC}, is the highest value of stress intensity that a material under plane-strain conditions can withstand without fracture. As the stress intensity factor reaches the K_{IC} value, unstable fracture occurs. The stress intensity factor is a function of loading, crack size, and structural geometry and it is represented by the following equation:

Equation 2 $$K_{IC} = Y\sigma_c\sqrt{\pi c_c}$$

Where:

K_{IC} is a basic material property (fracture toughness), (MPa.√m)

Y is a dimensionless factor dependent on the geometry of the crack and material

σ_c is the critical stress, (MPa)

c_c is the critical crack length, (mm)

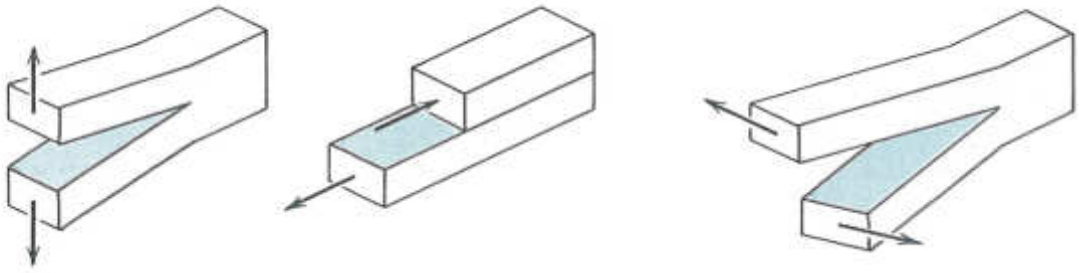

(a) Mode-I crack opening (Left), mode-II (middle) and mode-III (Right).

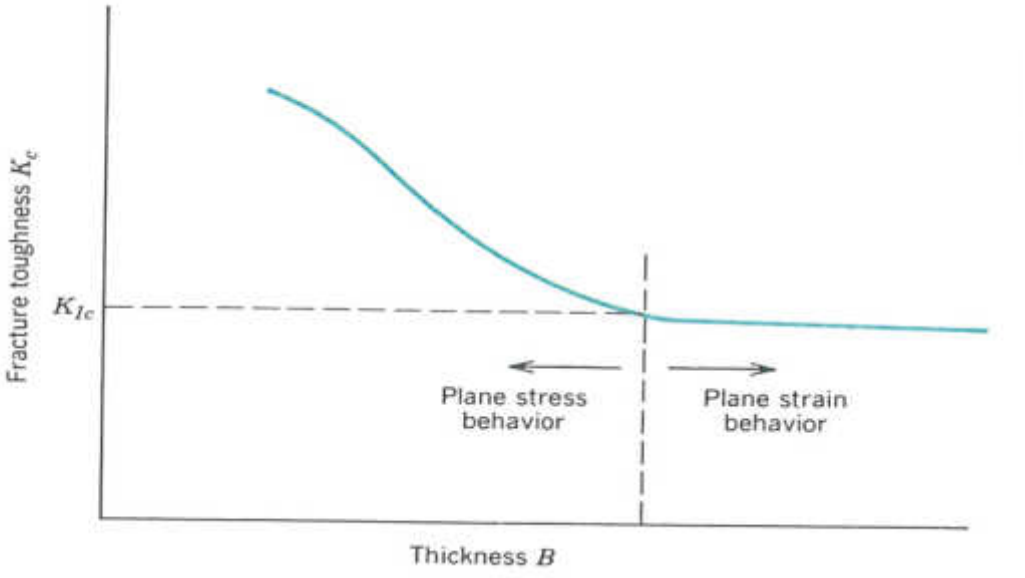

(b)

Figure 5: (a) Three modes of fracture and (b) the effect of specimen thickness on K_{IC} [22]

Figure 6, shows that c is not always the total length of the crack as for edge cracks, but is sometimes half the crack length for internal cracks. The values of Y for short cracks subjected to a tension load vary with respect to the shape and location of the crack as follows:

- Y = 1.00 for an interior crack similar to the crack shown in Figure 6(a)
- Y = 1.12 for a through-thickness surface crack as shown in Figure 6(b)
- Y = 0.73 for a half-circular surface crack as shown in Figure 6(c)

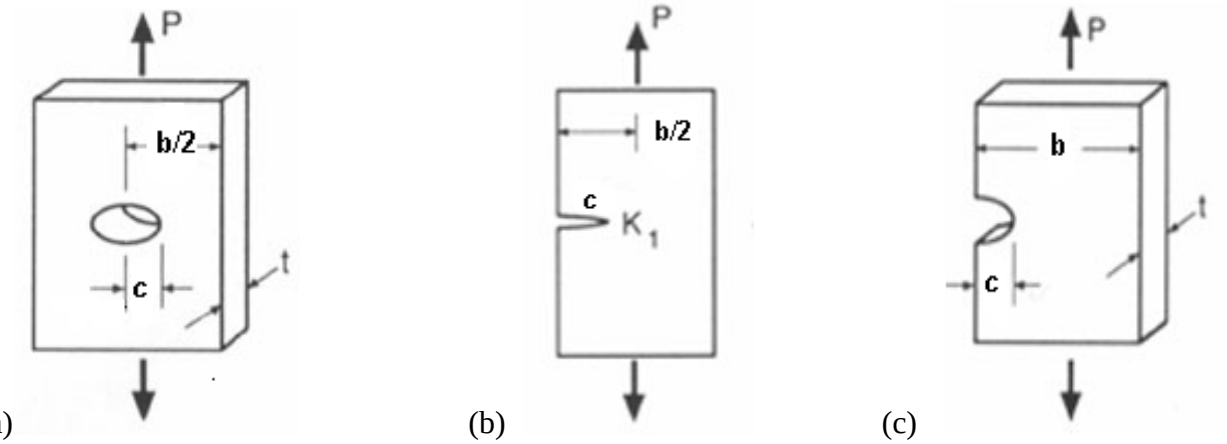

(a) (b) (c)

Figure 6: Crack Profile (a) A specimen with an interior crack. Note that the entire crack length is equal to 2c. (b) A specimen with a through-thickness crack. (c) A specimen with a half circle surface crack. [23]

There are two cases for mode-I loading. For a thin specimen the stress state is *plane stress* while for thick specimens there is a *plane-strain* condition. *The plane-strain condition* represents the more severe stress state and the values of K_C are lower than for *plane-stress specimens*. Plane strain values of critical stress intensity factor K_{IC} are valid material properties, independent of specimen thickness, to describe the fracture toughness or the resistance of the material to failure in the presence of a crack-like defect. Therefore, the plain-strain fracture toughness can be mathematically expressed as in Equation 2.

The Plane-Strain Fracture Toughness, $K_{IC,}$ values are used to determine the critical crack length when a given stress is applied to a component and also to calculate the critical stress value when a crack of a given length is found in a component.

Equation 3 $$c_c = \frac{1}{\pi}\left(\frac{K_{IC}}{\sigma_c Y}\right)^2$$

Equation 4 $$c_c \leq \left(\frac{K_{IC}}{Y\sqrt{\pi c_c}}\right)$$

Where:

c is the crack length for edge cracks or one half-crack length for internal crack, (mm)

c_c is the critical crack length, (mm)

K_{IC} is the plane-strain fracture toughness, (MPa.√m)

Y is a constant related to the sample material and its geometry

σ is the stress applied to the material, (MPa)

σ_c is the critical applied stress that will cause failure, (MPa)

In thin walled pressure vessels, one may not necessarily find plane strain conditions but rather plane stress conditions. Using the plane strain fracture toughness K_{IC} rather than the plane stress fracture toughness K_{IIC} is a conservative approach since $K_{IC}<K_{IIC}$ for thin section thicknesses.

When performing a fracture toughness test, the most commonly used fracture toughness test specimen configurations are the single-edge notch bend (SENB) or three-point bend and the compact tension (CT) specimens. The compact specimen has the advantage that it requires less material, but is more expensive to machine and more complex to test compared with the SENB specimen. If limited material is available, it is possible to fabricate SENB specimens by welding extension pieces (for the loading arms) to the material sample. (Electron beam welding is typically used, because the weld is narrow and causes little distortion).

Various methods are used to determine fracture toughness of brittle materials. These include indentation fracture (IF) technique, indentation strength (IS), surface crack in flexure (SCF), chevron-notched beam (CNB) technique, SENB technique and single-edge-V-notched beam (SEVNB) technique.

The SENB method was developed as a simple and inexpensive alternative, but the results can be influenced by the tip radius of the sawed notch. Recently a technique was introduced by Nishida *et al* [24] to taper a saw cut to a sharp V-notch using a razor blade sprinkled with diamond paste. This method is known as the SEVNB method. It was reported to be user-friendly, easy and cheap to conduct, reliable and accurate.

An accurate determination of the plane-strain fracture toughness requires a specimen whose thickness exceeds some critical thickness B. Testing has shown that plane-strain conditions generally prevail when:

Equation 5 $$B \geq 2.5\left(\frac{K_{IC}}{\sigma_y}\right)^2$$

Where:

B is the minimum thickness that produces a plain-strain condition at the crack tip

K_{IC} is the fracture toughness of the material, (MPa.√m)

σ_y is the yield stress of the material, (MPa)

When a material of unknown fracture toughness is tested, a specimen of full material section thickness is tested or the specimen is sized based on a prediction of the fracture toughness. If the fracture toughness value resulting from the test does not satisfy the requirement of the above equation, the test must be repeated using a thicker specimen.

When a test fails to meet the thickness and other test requirement that are in place to ensure plane-strain conditions, the fracture toughness values produced is given the designation K_C. Sometimes it is not possible to produce a specimen that meets the thickness requirements. For example, when a relatively thin plate product with high toughness is being tested, it might not be possible to produce a thicker specimen with plain-strain conditions at the crack tip.

2.5.3 Modulus of Elasticity

Detail information about elasticity of the material can be found from Materials Science and Engineering: An Introduction by Callister [22]. When a material has a load applied to it, the load causes the material to deform. Elasticity is the ability of a material to return to its original shape after the load is removed. The Young's modulus *E* is the elastic modulus for tension, or tensile stress. In general, elastic modulus is not the same as stiffness.

Ceramics are generally quite inelastic and do not bend like metals. Stiffness varies with the composition and crystal structure. The ability to deform reversibly is measured by the elastic modulus. Materials with strong bonding require large forces to increase space between particles and have high values for the modulus of elasticity. Young's Modulus of Elasticity is defined as the ratio of stress (force per unit area) to corresponding strain (deformation) in a material under tension or compression in the range of stress in which Hooke's Law holds. This can be experimentally determined from the slope of a stress-strain curve created during tensile tests conducted on a sample of the material.

According to Hooke's law, the strain is proportional to stress, and therefore the ratio of the two is a constant that is commonly used to indicate the elasticity of the substance. When stress and strain are not directly proportional, E may be represented as the slope ($E = \Delta S/\Delta\varepsilon$, where ΔS is change in stress and $\Delta\varepsilon$ is change in strain) of the tangent or the slope of the line connecting two points of the initial straight segment on the stress-strain curve. The modulus is then designated as tangent modulus or secant modulus at stated values of stress. The modulus of elasticity applying specifically to tension is called Young's modulus.

Young's modulus is not always the same in all orientations of a material. However, for most metals and ceramics, along with many other materials their mechanical properties are the same in all orientations. However, metals and ceramics can be treated with certain impurities, and metals can be mechanically worked to make their grain structures directional. These materials then become anisotropic as well as their Young's modulus, depending on the direction the force is applied from. Anisotropy can be seen in many composites as well.

2.5.4 Plasticity

Plasticity is the ability of a material to deform permanently without breaking or rupturing. Plasticity or plastic deformation is accepted as unrecoverable strain. Plastic deformation is retained even after the release of the applied stress. Brittle materials, like ceramics, do not experience minor plastic deformation and will fracture under relatively low stress [22].

2.5.5 Ductility and Malleability

Ductility is the property that enables a material to stretch, bend, or twist without cracking or breaking. This property makes it possible for a material to be drawn out into a thin wire. In comparison, malleability is the property that enables a material to deform by compressive forces without developing defects. A malleable material is one that can be stamped, hammered, forged, pressed, or rolled into thin sheets [22].

2.5.6 Brittleness

A brittle metal is one that breaks or shatters before it deforms. These materials experience very little or no plastic deformation. White cast iron and glass are good examples of brittle materials. Generally, brittle metals are high in compressive strength but low in tensile strength [22].

2.5.7 Strength

Strength is the property that enables a metal to resist deformation under load. The ultimate strength is the maximum strain/load a material can withstand. There are various ways in which a load can be applied to a material. Therefore, this will vary the type of strength the material should have in order to resist the applied load.

Strength measurements could be define as *yield, compression, tensile, fatigue, fracture or impact* strengths according to the forces applied and the experimental design. The most common instrument used to measure strength of material is a tensile tester.

Yield strength is the lowest stress that gives permanent deformation in a material. In some materials, like aluminium alloys, the point of yielding is hard to define, thus it is usually given as the stress required to cause 0.2% plastic strain.

Compressive strength is a limit state of compressive stress that leads to compressive failure in the manner of ductile failure or in the manner of brittle failure. *Tensile strength* is a limit state of tensile stress that leads to tensile failure in the manner of ductile failure (yield as the first stage of failure, some hardening in the second stage and break after a possible "neck" formation) or in the manner of brittle failure (sudden breaking in two or more pieces with a low stress state). Tensile strength can be given as either a true stress or engineering stress. A tensile tester is not only used to determine tensile strength, it can also be used to determine yield and compressive strength.

Impact strength is the ability of a metal to resist suddenly applied loads. Often measured with the Izod impact strength test or Charpy impact test, both of which measure the impact energy required to fracture a sample. A notched sample is generally used to determine impact strength. Impact is a very important phenomenon in governing the life of a structure.

Fatigue strength is the ability of material to resist various kinds of cyclical stress and it is expressed by the magnitude of alternating stress, for a specified number of cycles. *Fracture strength* is the minimum tensile stress that will cause fracture. *Fracture strength* is calculated from the load at the beginning of fracture during a tension test, and the original cross-sectional area of the specimen. Modern tensile testers are designed for tensile, compression, flexural (bending), shear, peel, fatigue cycling, and constant load tests on various materials such metals, plastics, paper and finished products.

Before looking at impact testing, let us first define what is meant by 'toughness' since the impact test is the only one method by which this material property is measured. As discussed in section 2.5.2, in general toughness is a measure of the amount of energy required to cause an item (a test piece or a pressure vessel) to fracture and fail. The more energy that is required then the tougher the material.

The area beneath a stress/strain curve produced from a tensile test is a measure of the toughness of the test piece under slow loading conditions. However, in the context of an impact test we are looking at notch toughness, a measure of the metal's resistance to brittle or rapid fracture in the presence of a flaw or notch and rapid loading conditions. The study of fracture toughness gave

rise to a range of tests used to characterise 'notch toughness' of which the *Indentation Fracture* test described in this investigation is one.

2.5.8 The Relationships among the Mechanical Properties

For ceramic materials, simple relations exist between mechanical properties (Young's modulus E, Hardness H_V, and Fracture toughness K_{IC}) which allow calculating them all as long as two of these three properties are known. The relationship between these properties is given by Evans-Davis equation as shown in the following expression:

Equation 6 $$K_{IC} = 0.4636 \left(\frac{f}{a^{3/2}}\right)\left(\frac{E}{H_V}\right)^{2/5} 10^{F}$$

Where:

K_{IC} is the plane-strain fracture toughness, (MPa.√m)

f is Test load, (N)

a is half diagonal length of the indent, (mm)

c is half crack length, which is measured from the centre of the indentation, (mm)

E is Young's Modulus, (GPa)

H_V is Vickers hardness in, (GPa)

F is $-1.59 - 0.34B - 2.02B^2 + 11.23B^3 - 24.97B^4 + 16.23B^5$ and $B = \log_{10}\left(\frac{c}{a}\right)$

2.6 FACTORS THAT INFLUENCE THE MECHANICAL PROPERTIES OF CVD SIC

A literature review on the factors that affect the mechanical properties of CVD SiC was conducted. The mechanical properties of the SiC include hardness, fracture toughness, elastic modulus, fracture strength, and thermal creep. The type of bonding (ionic or covalent) and the internal structure (crystalline or amorphous) affect the properties of *ceramic* materials. This study examines *CVD growth direction*, which is one of the factors affecting the hardness and the fracture toughness of the SiC.

2.6.1 The mechanical properties of CVD SiC as manufactured

The physical properties of a typical CVD SiC in the as-received form are shown in Appendix 7.1. Table 1 below summarizes the hardness and fracture toughness values of CVD SiC at various test loads obtained from various literature sources. As presented in Table 1, some authors like Pharr referred to Vickers-indentation fracture toughness technique as Indentation test and they are both the same test. The table shows that the test load does not affect these mechanical properties since they are more or less the same. However, it is not expected for the data in Table 1 to have exact fracture toughness values because the unknown manufacturing conditions might be slightly different. As highlighted on the table the K_{IC} values of CVD SiC manufactured by various companies was almost the same at 100 g, 500 g and 1000 g. These K_{IC} values were also obtained from various test methods. As a results of this, a test load as low as 100 g can be used to evaluate the K_{IC} values of a very thin layer of CVD SiC in TRISO particles.

Table 1: The mechanical properties of SiC at room temperatures as manufactured

Load (g)	**K_{IC} (MPa. m$^{1/2}$)**	**H_V (GPa)**	***E* (GPa)**	**Test Method**	**Process**	Reference
100	3.5	35	446	Vickers Indentation Test	CVD	Pharr [25]
	3.5			Vickers Indentation Test	CVD	Snead *et al* [15]
	3.2			Chevron Notched Beam	CVD	Snead *et al* [15]
2000	5.1	38	490	Vickers Indentation Test	CVD	Nogami *et al*
1000	2.8	36	503	Vickers Indentation Test	CVD	Osborne [26]
	3.4			Chevron V-Notched Beam	Sintered	Orange *et al* [27]
1000	3.1	36		Surface Crack in Flexure (SCF)	Sintered	Munro R.G. [28]
500	3.1	26		Surface Crack in Flexure	Sintered	Munro R.G. [28]
300	3.5			Vickers indentation Test	CVD	Zhang *et al* [29]

2.6.2 The effect of sample orientation

The fracture toughness of a material commonly varies with specimen orientation direction. Therefore, it is customary to specify specimen and crack orientations. The micro-hardness of polycrystalline SiC films was found [30] to be affected by the preferred orientation of SiC, which

varied greatly with deposition parameters. The (111) oriented films had higher hardness values than (220) oriented films.

According to Cockeram [8], the chevron-notched fracture toughness values measured on both curved-surface and cross-sectional area were identical from room temperature to 1090 ^{o}C, which indicates that the fracture toughness values are independent of the CVD growth direction. He also mentioned that this isotropic nature is notably different from hot-pressed alpha SiC and is likely a result of cubic β-SiC microstructure produced by the CVD process and the transgranular fracture mode.

According to Lee *et al* [31], both the fracture toughness and hardness results are independent of the orientation for hot pressed SiC. Cockeram [14] also reported that the flexural strength is shown to be independent of the CVD growth direction. The question remains whether or not, will the K_{IC} remain isotropic in all directions when measured using the indentation technique?

CVD SiC in TRISO particles showed that the growth direction of the SiC is parallel to the hoop stress (σ_h). Hoop stress is defined as $\sigma_h = \left(\frac{\mathrm{Pr}}{2t}\right)$ for spherical vessels. For a spherical thin-walled pressure vessel the hoop stress and axial stress are equal and is one-half of the hoop stress in the cylindrical pressure vessel. This makes the spherical pressures vessel more “efficient” pressure vessel geometry. Thus, a lot of work was done to investigate the effect of the growth direction on the mechanical properties of the SiC.

2.6.3 The effect of grain size

Kodama *et al* [9] have used a dense-fine-grained SiC ceramic, fabricated by a hot-pressing technique, using pyrolyzed polycarbosilane powders, to determine the effect of grain size on the fracture toughness of this material. It was found [10] that the samples with the smallest mean grain size (0.2 µm) and the largest mean grain size (1.4 µm) showed a minimum fracture toughness whereas the maximum fracture toughness (5.1 MPa.m$^{1/2}$) was observed at the average grain size of ~0.7 µm. Also, the fracture toughness of the samples having similar grain sizes

increased with increasing relative density. The fracture mode of the SiC can either be intergranular or transgranular depending on the grain size. The fracture surface showing a mixture of both transgranular and intergranular fracture modes was observed in the samples with the smallest grain size and in the samples with the largest grain size, whereas the sample with the maximum toughness had the fracture surface broken mainly in the intergranular fracture mode.

Niihara [6] reported a similar relationship in the wide grain size region (0.1 to 100 µm) for CVD SiC with a maximum K_{IC} of ~4 MPa.m$^{1/2}$ being obtained at the average grain size of 1 µm to 3 µm. The reason for the grain-size dependence of K_{IC} was reported to be residual internal stress and resultant micro crack formation in CVD SiC.

Since indentation hardness is a measure of the material's resistance to penetration by a diamond indenter (i.e. resistance to plastic deformation) and the movement of dislocations generated by the indenter is influenced by the microstructure, the hardness increases with decreasing grain size.

2.6.4 The effect of irradiation and temperature

Despite the fact that the experimental work has to be carried out at a room temperature, it was interesting to note the effect of irradiation on the hardness and the fracture toughness of the CVD SiC. It was reported [30] that the hardness of the CVD SiC increases with increasing irradiation exposure and quickly reached a plateau after exposure to a fluence of 0.5 x 10^{25} n.m^{-2}, E > 0.1 MeV.

Clinard *et al* [32] found featureless and straight cracks on the un-irradiated samples but on the irradiated materials (Al_2O_3 and MgO), they found that cracks experienced void intersection, changes of direction, crossing and branching. Thus, the indentation fracture toughness of these materials increased. It was also suggested that the toughening observed in Al_2O_3 might be attributable to the combined effect of a number of mechanisms operating simultaneously. However, crack-void interaction (i.e. crack pinning and deflection due to the defect cluster) was the dominating factor. He suggested that this effect might be occurring in the CVD SiC, because

the cluster formation is similar and clusters are known to exist in different sizes. Nogami *et al* [10] made the same conclusion by observing that the increase of K_{IC} for CVD SiC with temperature was also due to the increase of the mobility of dislocations and crack pinning and deflection. Park *et al* [33] verified the toughening mechanisms in SiC (see Figure 7) due to irradiation in his studies but the reason for the increase in toughness with ion beam irradiation was not given, instead the explanation was based on the work of other authors such as Clinard *et al* [32].

Nogami [10] investigated the indentation fracture toughness of CVD SiC irradiated up to 10^{24}–10^{25} n.m^{-2} (E_n> 0.1 MeV) at the temperature of 80–1150 ^{o}C. Nogami found that the hardness rapidly increases with the irradiation temperature below 100 ^{o}C and showed almost no change above 100 ^{o}C while a small reduction in fracture toughness was seen below 400 ^{o}C, with a significant increase as temperature is increased up to about a temperature of 1000 ^{o}C. It was finally concluded that these mechanical properties were significantly dependent on the irradiation temperature, while generally independent on the irradiation dose. Young's modulus of the material is also taken into consideration during the calculations of the K_{IC}. Price [34] found no significant change in the elastic modulus or modulus of rupture after exposure to a fluence of 2.8 x 10^{21} n.cm^{-2} (E >0.18 MeV).

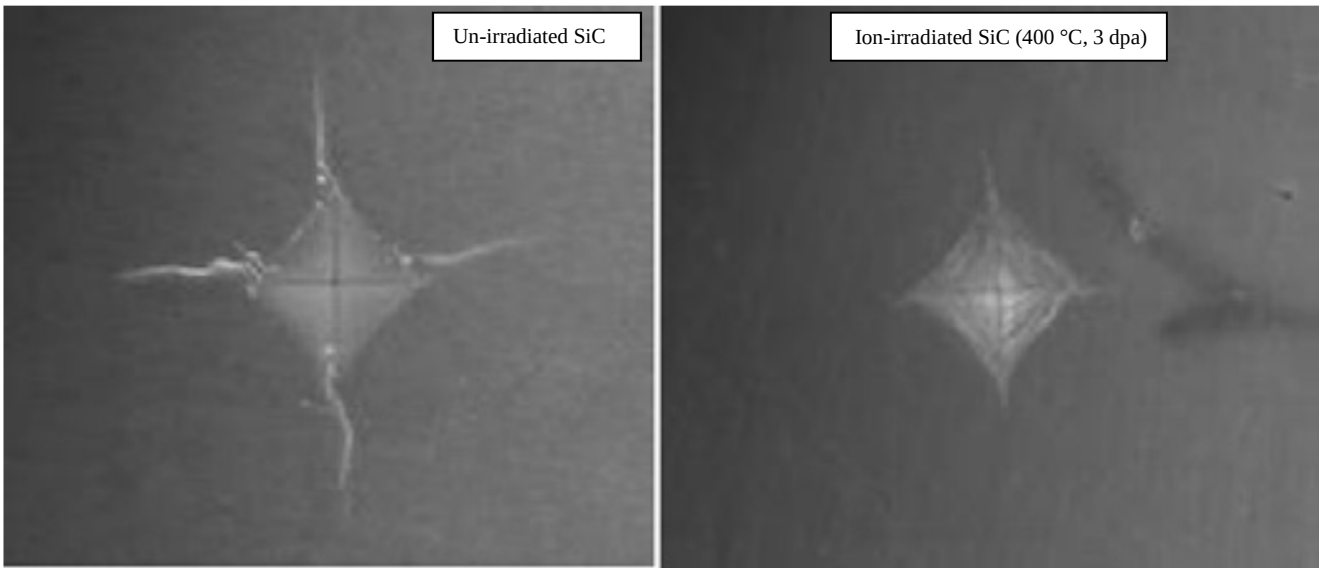

Figure 7: An indent on the surface of the CVD SiC without (left) and with (right) Si-ion bombardment as a function of irradiation temperature [33]

Hardness is related to the yielding phenomenon in crystalline materials; therefore, the hardness is dependent on how easily dislocations can move through the material. Neutron irradiation at temperatures <1000 °C produces density changes in crystalline SiC by a variety of mechanisms [26]. Reduced defect populations with increasing irradiation temperatures result from the recombination of interstitial vacancy pairs and the agglomeration of vacancies to form sessile loops. The ease with which dislocations move is dependent on the size and density of the defect barriers. The defect cluster size is known to increase as the irradiation temperature increases, resulting in an increase in stress required to move dislocations.

Niihara [6] reported that a rapid fall in hardness at high temperatures, observed for sintered materials, was not detected up to 1500 ^{o}C for CVD SiC and Si_3N_4. Several investigations [6, 10, 26, 27, 30, 32 and 33] concluded that the fracture toughness of the SiC does not degrade at elevated temperature but it increases with irradiation temperature. Henshall *et al* [35] have reported that α-SiC single crystals showed an increase in toughness above 800 ^{o}C. It was assumed that this increase in toughness at high temperatures was due to small plastic deformation at crack tips. This explanation may be applied to CVD SiC, because the substantial increase in plasticity, as observed for α-SiC single crystals, was also confirmed by the high-temperature indentation work above about 1000 ^{o}C for CVD SiC [26].

Kim *et al* [30] have reported that the fracture toughness of hot pressed SiC estimated by the Vickers indentation method was 1.9 MPa.m$^{1/2}$ and increased to 6.1 MPa.m$^{1/2}$ after grain growth by annealing at 1850 ^{o}C for 12 hrs. He also concluded that higher fracture toughness of annealed materials appeared to be a result of crack bridging by large elongated grains. Ghosh *et al* [7] concluded that the fracture toughness of sintered α-silicon carbide is about 3 MPa.m$^{1/2}$ and independent of temperature from 20 to 1400 ^{o}C.

2.6.5 The effect of impurities

Coated fuel particles may be contaminated by metallic impurities during the fuel manufacturing processes and therefore, care should be taken to prevent the fuel from being contaminated with those elements that react with SiC. Impurities detected by Minato *et al* [36] were Fe, Ni and Co.

They have been contained as impurities in the graphite matrix, which surrounded the coated particles. These elements are more stable thermodynamically in the presence of SiC than in the presence of graphite at irradiation temperatures. Thus, they react with the SiC layer to form more stable silicides {i.e. FeSi, NiSi, and CoSi) as shown in the following equation: (M(s) + SiC(s) → MSi(s) + C(s)} [36].

2.6.6 The effect of residual stress

The residual stress of CVD beta silicon carbide depends on the deposition temperature. The residual stress increases with decreasing deposition temperature [37]. The residual stress of CVD beta silicon carbide is always compressive and can be relaxed by recovery and recrystallization processes because intrinsic stress is the predominant stress in the films [37].

Niihara [6] concluded that the CVD SiC deposited should contain a high internal stress, due to a spontaneous fracture of this material during the CVD process, which results in micro crack formation. The relaxation effects of the *residual internal stress* must also be responsible for toughness increase although its effect might be small since it was not clearly observed after 10 hrs of annealing at 1500 ^{o}C [9]. Although the CVD materials include residual internal stresses produced during the CVD process, the variation in toughness at various temperatures due to residual stress was deemed to be small or negligible [9]. The relationship between the grain size and the residual stresses is discussed further in section 2.9.

2.7 Test Methods for Fracture Toughness Measurements of CVD SiC

The methods for evaluating the fracture toughness of ceramics include the single edge notched beam technique (SENB), chevron notched beam (CNB) technique, indentation fracture (IF) technique and fractographic methods. In this research, the fracture toughness of SiC was examined using the indentation fracture technique, which involves the measurements of crack length introduced by an indentation using a diamond indenter. According to Nogami *et al* [10], this is one of the best techniques available for measuring the toughness of brittle materials like an irradiated ceramic because it can be evaluated by the crack growth behaviour in a very small region.

The advantages of the indentation technique include the use of a very small specimen, specimen preparation is very simple requiring the provision of a polished-reflective plane surface, cracks can be measured optically without difficulty and it is both quick and cost effective [38]. The conventional methods to determine K_{IC} require a complex experimental procedure and a minimum number of samples, which have quite large dimensions. Therefore, the indentation method is a simpler technique to obtain the K_{IC} of brittle materials.

Many researchers, such as Osborne [26] and Nogami [10], continue to use the Vickers micro indentation technique because it is applicable to a very small specimen. Many authors, using this technique, have already investigated the K_{IC} and hardness of SiC. However, the sample sizes used by these authors were not as small as the SiC layer in TRISO. Therefore, it is important to ensure that the fracture toughness of a very small (in this case 35-µm) sample is the same as that of large samples used in the conventional methods.

The general statement by Hong *et al* [39] mentioned that the techniques, which are available to determine the mechanical properties of bulk materials, are not suitable for TRISO particles.

2.8 INDENTATION EQUATIONS

Many equations (Table 2, and Table 16, Appendix 7.2) were used to evaluate the fracture toughness of ceramics by various authors. The only equations that can be used for silicon carbide material are shown in Table 2. From the list of equations that are suitable for evaluating the fracture toughness of SiC materials in Table 2, only the Evans-Davis equation (i.e. equation AA) was found [6, 10] to give results equivalent to conventional methods.

Table 2: Equations for determining the fracture toughness from various authors

Equation	Radial Median crack equations	Model (others user)	Ref.	factor
A	$K_{IC} = 0.016*(E/H_V)^{1/2}*(P / c^{3/2})$	Lawn *et al*(Orange)	[40, (27)]	0.03162
B	$K_{IC} = 0.043*(E.H_o)^{1/2}*(a^2/ c^{3/2})$	Gong *et al*	[41]	31.62
C	$K_{IC} = 0.16 * H_V * a^{1/2} * (c / a)^{-3/2}$	Lee *et al*	[31]	31.62
Equation	**Palmqvist crack equations**			
AA	$K_{IC} = 0.4636 * (P/a^{1.5})* (E/H_V)^{0.4} 10^{F}$	Osborne *et al* (Nogami *et al*)	[26, (10)]	0.03162
BB	$K_{IC} = 0.018 *HV*a^{0.5}*(E/H_V)^{0.4}*[(c/a) - 1]^{-0.5}$	Niihara *et al* (Strecker *et al**)	[6, (42]	31.62

Where $\boldsymbol{K_{1C}}$ = fracture toughness (MPa.√m), $\boldsymbol{H_V}$= Vickers hardness (GPa), ***P***= load (N).***a*** is a half diagonal length of the indent (mm), ***l*** and ***c*** are crack lengths as indicated on Figure 9, ***E***= Young's Modulus, $\boldsymbol{H_o}$ is the true hardness and ***F***= (-1.59-0.34*B-2.02*B^2+11.23*B^3-24.97*B^4+16.23*B^5) and **B** = log (c/a). *an error of using a/c instead of c/a in equation BB was corrected

Figure 8 is a schematic representation of a plane and cross sectional views of the cracks from the corners of the indent. These parameters were used in this investigation to measure both the hardness and the K_{IC} values. Crack profiles induced by indentation may be classified into two types: median/halfpenny type and Palmqvist type as shown in Figure 8. It was reported [26] that the fracture toughness obtained using Evans-Davis equation (i.e. equation AA in Table 2) is independent of the crack system. Therefore, in this investigation, it was not important to determine the crack type. The selected equation was based on the work of other researchers such as Osborne *et al* [26]. Osborne confirmed that a load of 2.94 N (300 g) could be producing a halfpenny crack system. Two of the five equations were designed for the Palmqvist crack system as shown in Table 2. However, all the equations were used at various loads and K_{IC} values were compared.

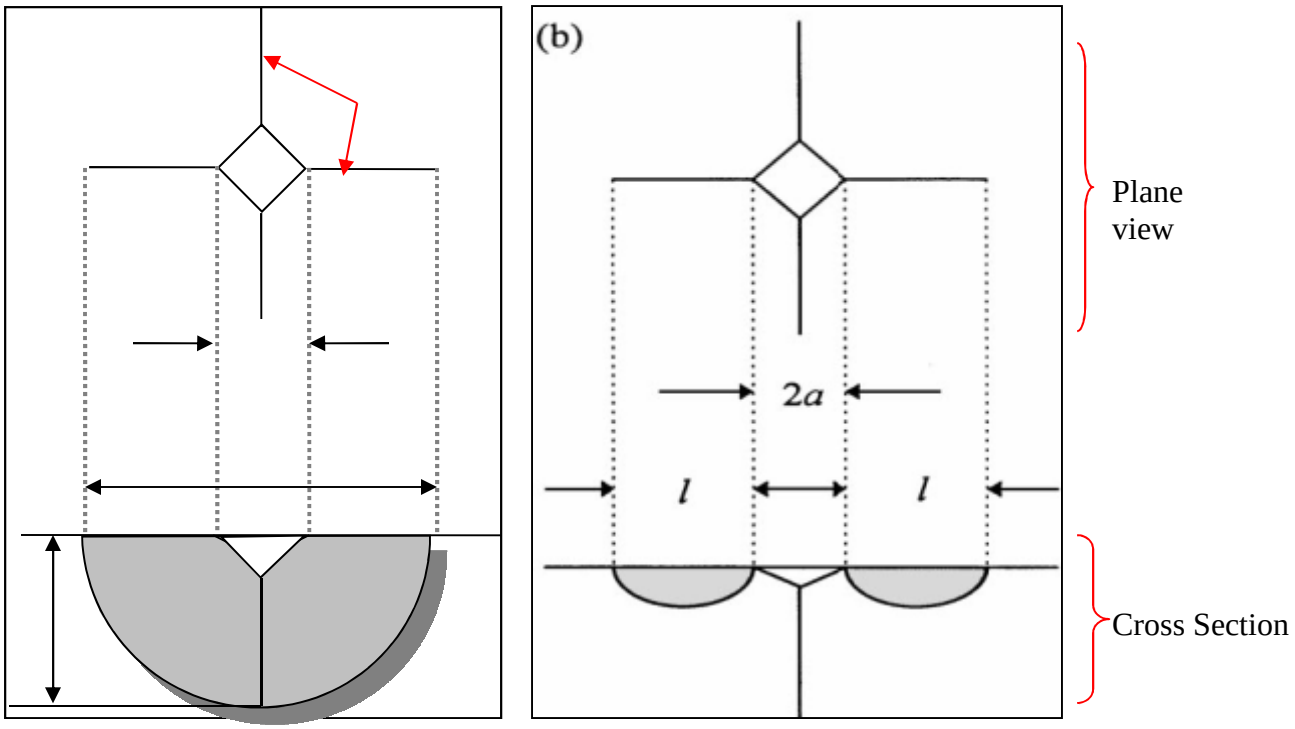

Figure 8: Comparison of (a) median/radial and (b) Palmqvist cracks around a Vickers indentation [43]

Where,

a is a half diagonal length of the indent,

d is a subsurface median cracks or crack depth and

l is a crack length measured from the corner of the indentation impression. The units can be either µm or mm.

2.9 FAILURE MECHANISMS OF THE TRISO PARTICLES

The mechanisms [17] by which a particle could fail, which would ultimately lead to fission product release are as follows:

- Pressure vessel failure caused by internal gas pressure
- Pyrocarbon layer cracking and/or debonding due to irradiation induced shrinkage which ultimately leads to the failure of the SiC layer
- Fuel kernel migration (amoeba effect) which leads to interactions of the fuel kernel with the coating layers

- Fission product/ coating layer chemical interactions
- Matrix/ OPyC interaction
- As-manufactured defects (cracks, porosity, etc.) and contamination (e.g. Fe) produced during fabrication of fuel particles or during pressing of fuel compacts/spheres [i.e. Impurities (e.g. Fe) attack the SiC layer during the final heat treatment at 1700 ^{o}C]
- Thermal decomposition of the SiC layer at very high temperatures
- Enhanced SiC permeability and/or SiC degradation due to fast neutron fluence and/or burn-up

The main contributing factor to the above failure mechanisms is temperature. The literature survey section briefly explains the relationship between the mechanical properties (i.e. HV and K_{IC}), and temperature, irradiation, residual stress, grain size, impurities and the SiC growth direction. Even though the purpose of this investigation was to conduct the experimental work at room temperature, the literature survey has also focused on the effect of temperature on mechanical properties of the CVD β-SiC.

Fracture toughness values for the CVD SiC are reported to be independent of the CVD growth direction and test temperature from ambient to 1100 °C. Both hardness and indentation fracture toughness increase after irradiation exposure. The variation in toughness at various temperatures due to residual stresses was deemed small or negligible. The hardness increases with decreasing grain size while the highest K_{IC} was found at an average grain size (~0.7 µm) since the samples with the smallest and the largest grains showed almost minimum K_{IC} values [9].

The literature survey has resulted in a better understanding of the mechanisms that affect the integrity of SiC with respect to the retention of fission products. The integrity of the CVD SiC will depend on continuously maintaining the quality of TRISO coating. This experimental work will ignore the beneficial compressive forces induced by both the IPyC and OPyC on the SiC in order to estimate the actual stress that can be handled by the SiC layer alone. The actual maximum internal pressure generated by the fission products will therefore be compared with the maximum internal pressure that can be handled by the SiC layer ignoring the support from the carbon layers. Thus, there will be a better understanding of the integrity of the SiC layer in TRISO particles with respect to the internal gas pressure generated during irradiation.

Chapter 3: Experimental Procedure

3.1 MATERIAL PREPARATION

3.1.1 Material used to conduct the experiment

Most authors, whose work was reviewed, did not mention the geometry of the sample they used to conduct their experiments; however, the sample sizes used in some experiments were not as small as the thickness of the SiC layer in TRISO coated fuel particles. Therefore, the SiC samples of two different forms (i.e. hot pressed (HP) and CVD were used for this research project. The first type was 0.1 mm and 5.0 mm thick, bulk polycrystalline SiC plates, which were produced by *GoodFellows* using the hot pressing technique. The choice of the HP SiC was due to its availability in the bulk form as compared to the CVD SiC.

The other sample type consisted of TRISO coated zirconia particles containing polycrystalline β-SiC layers (see Table 3), which were produced by the PBMR (Pty) Ltd using a CVD process. The SiC was chemically vapor deposited on pyrolytic carbon-coated zirconia particles in a fluidized bed reactor using methyltrichlorosilane with hydrogen. The deposits usually consist of pure *β*-SiC, (*β*-SiC + Si) or (*β*-SiC + C) depending on deposition conditions. The conditions aimed at producing a very pure beta SiC, however the composition of the samples used in this study was unknown. Four batches of the TRISO particles (see Table 3) were prepared to conduct the experiments for this investigation. The thickness of the CVD SiC ranged from 28 to 51 µm with the density ranging from 3.16 g/cm^3 to 3.19 g/cm^3.

Table 3: TRISO-coated fuel particles that were used for this investigation

Sample/Batch NO	**Thickness, (µm)**				**Density, g/cm^3**
	Buffer	**IPyC**	**SiC**	**OPyC**	**SiC**
CPT-T-G165	99	56	28	46	3.18
CPT-T-G148	115	76	36	55	3.18
CPT-T-G131	108	77	39	0	3.19
CPT-B-B10	60	15	51	45	3.16

3.1.2 Sampling Procedure

Sample preparation is time-consuming and might be expensive; therefore, thoughts were given in the selection of samples with respect to the number and location or orientation within the test piece. The 51 µm CVD SiC in TRISO coated fuel particles was used for this purpose. Although it was reported that the CVD SiC materials are isotropic as discussed in section 2.2, it is important to define the orientation of the CVD SiC.

The CVD SiC in TRISO coated fuel particles was prepared in both directions, i.e. perpendicular to the CVD growth direction for indentation tests on a polished cross-section and parallel to the CVD growth direction for indentation tests on a polished curved-outer surface as shown in Figure 9 and Figure 10 respectively.

All Vickers indentations perpendicular to the CVD growth direction were called ***Cross-Section Indentation***. All Vickers indentations parallel to the CVD growth direction (i.e. indentation on the polished curved-outer surface) were called ***Curved Surface Indentation***.

Cross sectional view of a TRISO particle is shown at the bottom left of Figure 10 with three arrows illustrating the polished surface for *Curved Surface Indentation*. To prepare samples for indentation on a curved surface the particles are mounted in a black resin and then polished in the direction of these arrows shown in Figure 10 until a SiC is exposed to the surface with enough area to make an indentation. *Curved Surface Indentations* were done on particles where the SiC layer has the smallest diameter on the polished section, i.e. where the SiC layer has been polished away the least as shown in Figure 10.

When indents are made on the samples surface that is prepared on the *cross-sectional direction*, the crack direction depends on the indents position and indent orientation as shown under SEM images in the appendix. An experiment has been performed on the samples prepared for *cross-section indentation* to determine the effect of indent orientation.

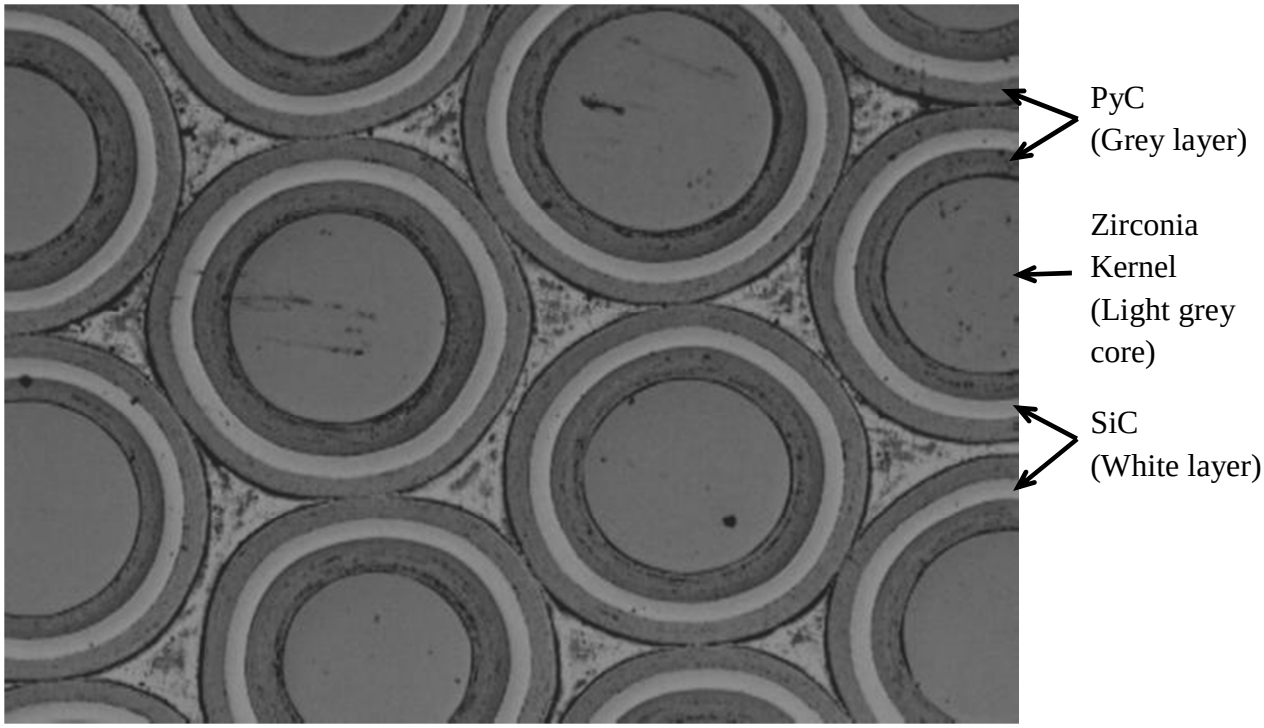

Figure 9: SEM micrograph showing polished cross-section of the TRISO coated fuel particles.

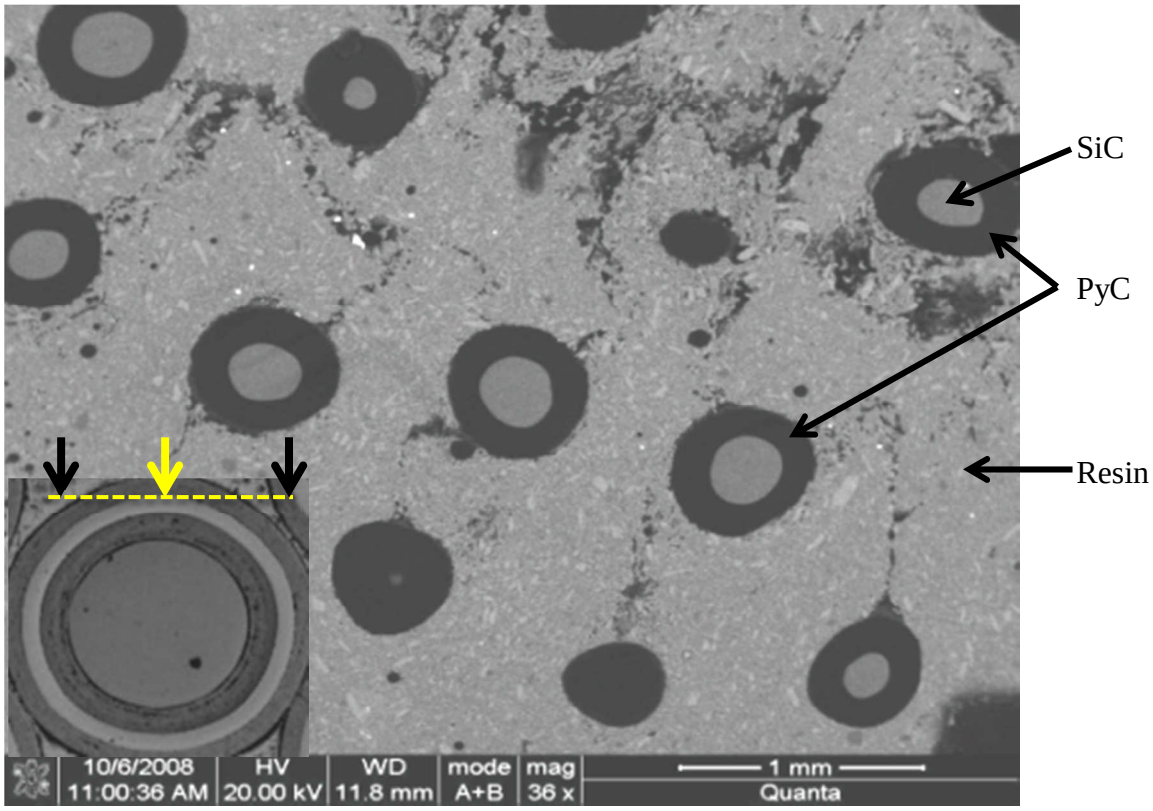

Figure 10: SEM micrograph showing polished outer/curved surface of the CVD SiC TRISO particles embedded in the mounting black resin.

The samples used were from the same batch, meaning that their properties would be similar. In order to determine the correct sample size, the following procedure was followed. *First*, ten indentations per particle for ten particles per batch were made and the differences between the mean values of the ten particles will be compared statistically using ANOVA. In this investigation, minimal differences would be an indication that only a few indents per particle can be used to conduct the test. The *second* test was conducted by using 50 particles from the same batch and the differences calculated. In this case, small differences would be an indication that statistically few particles per batch, as determined by the test results, can be used instead of too many particles.

The standard error of a statistic is the standard deviation of the sampling distribution of that statistic. The standard error of any statistic depends on the sample size, the larger the sample size the smaller the standard error. Standard errors are important because they reflect how much sampling fluctuation a statistic will show, i.e. how good an estimate of the population the sample statistic is. The standard error has been used to describe the deviation from the mean and the frequency of this deviation since it takes into account the sample size.

$$Standard\ error\ = \sqrt{(\ variance/(sample\ size)\ )}$$

3.1.3 Ceramography

Metallography is the science and art of preparing a metal surface for analysis by grinding, polishing, and etching to reveal microstructural constituents. Since the material used in this investigation was a ceramic material and may be prepared using metallographic techniques, the terms ceramography was used instead of metallography. *Ceramography* is the microstructure evaluation of ceramics.

Sectioning allows the sampling of the required sample size from a large piece. In this investigation the sample size was too small to be sectioned, however, it was required to prepare the sample to be able to carry out the experiment. Since orientation of the test piece was critical, the CVD SiC particles were prepared to allow testing to be done on surfaces that are respectively perpendicular and parallel to the growth direction of the deposited CVD layer.

The samples to be tested / indented on the *curved outer surface* were polished to reveal the outer surface of a SiC ranging from 30 µm to 200 µm in diameter [see Figure 10]. It is important to note that SiC surfaces with minimal surface areas are the most suitable for indentation since only a minimal thickness has been polished away.

The samples to be tested / indented on the *cross-sectional* area were also mounted and polished to the particle diameter as shown in Figure 9. The mounting and polishing techniques are not explained in detail in this investigation because all samples were prepared by PBMR (Pty) Ltd using propriety methods.

The above-mentioned ceramography was specifically for the CVD SiC layer in TRISO particles. The 0.1 mm HP SiC sample was mounted prior to polishing using a clear resin. The 5 mm thick HP SiC sample was thick enough and was polished un-mounted. These samples were polished using 1-micron diamond abrasive. Polished samples were gold coated prior to indentation tests using the Sputter Coater. Coating thickness was kept constant for all samples by coating all samples at 10 milliamps (mA) for 50 seconds.

Gold coating prior to indentation reduces the time taken between indentation and crack length measurement. Ponton and Rawlings [44] showed that pre-coating would not affect the post-indentation crack length, whereas post-coating may do so. Gold coating prior to indentation also enhances the visibility of the crack path and ensures better imaging by reducing sample charging when the crack length measurement is conducted using a SEM.

3.1.4 Test Load

To determine the influence of test load a 243 H_V calibration block was used with test loads ranging from 25 g to 1000 g. The Vickers hardness numbers (H_V) of a 243 H_V calibration block were compared at various loads to determine whether, the variation was within the acceptable range, taking into consideration human errors and equipment used. The samples were examined microscopically immediately after indentation as discussed in the following section.

The 5 mm HP SiC sample and the 51 µm CVD SiC layer in TRISO particle were also tested at various test loads to determine an appropriate test load, which will be suitable for thin layers without compromising the properties of the material. In this investigation, the loads used for the 5 mm HP SiC sample were 25, 50, 100, 200, 300, 500 and 1000 g, whereas for the 51 µm CVD SiC layer in TRISO particles the test loads used were 50, 100 and 200 g.

Various authors, such as Qian *et al* [45], used a wide range of loads ranging from 50 g to 294.20 N to conduct their experiments. However, a minimum indenter load of ~49.03 N [44] was recommended if the surface radial crack lengths are to be measured optically. Li *et al* [46] has reported that the Vickers hardness is constant above the load of 2.94 N, and was supported by Dieter [47] who mentioned that the hardness of the material increases with decreasing testing load below 2.94 N. Thus, various test loads used were necessary to establish a suitable test load for the CVD SiC ceramic materials. The suitable test load was found to be 100 g. It was used on various samples of the CVD TRISO particles for validation.

3.2 MATERIAL EXAMINATION

3.2.1 Hardness Test

A Micro Vickers hardness tester created an indentation with cracks emanating from the four corners of an indent. The difficulties in acquiring accurate and precise hardness readings are often not appreciated. Below are some of the factors associated with hardness measurements in ceramics that need to be avoided in order to have consistent results.

- At low indentation loads, problems arise from the load dependence of hardness and from measurement uncertainty due to the small indentation size.
- At higher indentation loads, cracking and sprawling become problematic; in some instances, they make credible measurement impossible.
- The indentation size effect, in which hardness increases with decreasing indentation load, is found with both Knoop hardness and Vickers hardness. A constant hardness is only reached

at specific loads, depending on the ceramic. Since hardness is strongly dependent on indentation load, the load should always be reported with the hardness results.

- Hardness is inversely proportional to the square of the diagonal length of the indentation, therefore any small error in indentation diagonal length measurement doubled the hardness value. Therefore, it is crucial to measure the diagonal length carefully, particularly for ceramics in which the indentation size is small and the percentage error larger. Smaller diagonal lengths are produced in ceramics than in most metals for a given load, and these result in inconsistent hardness measurements.

Hardness is usually measured on conventional micro hardness instruments with either Knoop or Vickers diamond indenters. For research purposes, Vickers, Knoop, and Berkovich (triangular pyramid) indenters are customary; Rockwell and Brinell indenters are rarely suitable for ceramics research. For engineering and characterization applications, approximately 60% of worldwide published ceramic hardness values are Vickers, with loads typically in the range of a few Newtons to 9.8 N (1000 g) and occasional for soft or high-toughness ceramics as high as 98 N.

Although the Knoop hardness test is a micro indentation method of determining the hardness of dense ceramics, the Vickers hardness test was an ideal technique for this investigation because four well-defined cracks emanating from the edges of an indent are available for fracture toughness measurements. The Vickers hardness tester (Model Micromet^{TM} 3, Buehler, Ltd), with a load range of 10 g – 1000 g, was first calibrated using a 243 H_V standard block prior to the experimental work.

The hardness test was carried out by applying a standard Vickers diamond indenter to a polished (but not etched) and gold coated surface using loads as discussed in section 3.1.4, typically 100 g. The test load was applied for 15 s before the indenter was retracted. The indention diagonal ($2a$, µm, in Equation 1) was measured under both the SEM and the light microscopes; the Vickers hardness (H_V) was calculated from the load (f) and the square of the diagonal length using the Equation 1. The constant in the equation accounts for the actual contact area of the indenter. The use of the Equation 1 instead of the conversion table was used because the average

indented diagonal length was outside the range of the tabulated values available. The space between indentations was more than enough to prevent an interaction between indentations and free edges. The required numbers of the indentations are discussed in detail in section 3.1.2.

3.2.2 Indentation Fracture Toughness

Testing operators usually seek to avoid cracking that interferes with the hardness measurement. However, the fracture toughness can be calculated from the length of the cracks that emanate from the corners of a Vickers indentation. The lengths of the cracks, the indentation half-diagonal size, the hardness values and the elastic modulus are related to the fracture toughness by an analytical expression.

Early work [46] claimed that calculated fracture toughness using the indentation fracture-toughness technique was only accurate to within 30 to 40 %, representing a considerable uncertainty. However, the accuracy of indentation technique was improved with later investigations. The Evans–Davis model (Equation 6), as discussed in section 2.5.8, was used for the evaluation of indentation fracture toughness in this investigation and it has been proved to yield fracture toughness values of ceramic materials with high accuracy when compared to conventional methods [10, 25]. Although it is not universally accepted, other authors such as Pharr, Nogami and Osborne has also use the Evans-Davis model to determine the fracture toughness of the SiC.

3.3 Analytical Tools

3.3.1 Scanning Electron Microscope

After the gold-coated sample was indented using a Vickers micro hardness tester, the length of the cracks emanating from the corners and the diagonals of an indentation were immediately measured using a scanning electron microscope (SEM). An optical microscope was only used to measure the diagonal length of the indent and it provided an indication of the hardness of the material. Indentations that produced multiple cracks from the corners, cracks from the

indentation sides, and/or subsurface cracks were not included in the analysis. Such cracking is indicative of existing cracks or other local defects that interfere with the development of cracks at the corners of the indentation.

3.3.2 Indentation Equations

Surface cracks associated with Vickers indentation are used to estimate the fracture toughness of ceramics. In general, when the indent is made, four cracks emanate from the corners of the indents and the average crack length of the four cracks is used to estimate the K_{IC}. However, in this investigation each crack length was treated individually in measuring the K_{IC}, because of the importance of the SiC material in TRISO particles. The use of an average crack length was avoided since the procedure will produce average toughness values material as compared to the use of each crack individually. Many authors [10, 25 and 26] have recommended the Evans-Davis equation and it was used in this investigation (see Equation 6).

3.3.3 Leak-before-break Condition

A leak-before-fracture condition could develop in a manner shown in Figure 11. Assuming that a semi-circular crack exists as shown in Figure 11, the length of the through-thickness flaw would be 2*c* or equivalent to twice the vessel wall thickness, 2*t*. Hence, the stress-intensity factor for this crack is defined by Equation 6. Leak before break describes a pressure vessel designed such that a crack in the vessel will grow through the wall, allowing the contained fluid to escape and reducing the pressure, prior to growing so large, as to cause fracture at the operating pressure.

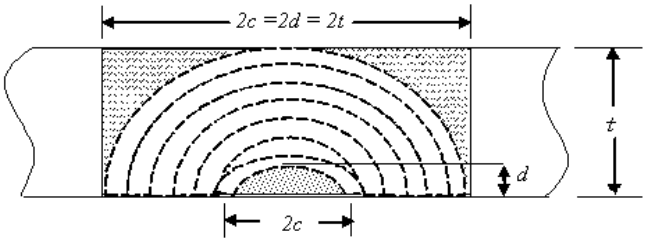

Figure 11: Diagram showing the growth of a semi-elliptical surface flaw to semi-circular configuration. At leak condition (2c = 2d =2t), unbroken ligaments (shaded areas) break open to form a through-thickness crack [48]

The Leak-before-break (LBB) condition is used to access the ability of a pressure vessel to accommodate cracks without bursting in a catastrophic fashion. For this to happen the fracture toughness should be high-enough to accommodate a through thickness crack with a surface length equal to twice the thickness of the pressure vessel (see Figure 11). Thus, the vessel would then leak its contents without bursting. Any cracks that do not penetrate the wall of the pressure vessel would be able to contain the contents without bursting. It is also possible to apply LBB condition to the SiC shell in a TRISO coated particle to determine the maximum pressure when the material starts leaking [49].

Equation 7 and Equation 8 below were used to estimate the internal pressure that a SiC shell can safely withstand as a function of a crack length and the fracture toughness at a LBB condition. The lower bound pressure will be the leak-before-break condition because the SiC shell may contain a whole spectrum of defects [48]. In general, LBB condition could exist when a crack of length up to at least twice the vessel wall thickness could be tolerated at the operating internal pressure [48]. The following Equation 7 has been derived from Equation 2.

Equation 7 $$K_{IC} = Y\sigma_c\sqrt{\pi t}$$

Where $2c = 2d = 2t$ at a LBB,

t is a vessel wall thickness, (mm)

all other variables are as discussed in the previous sections

The following Equation 8 gives stress in a thin-walled spherical pressure vessel.

Equation 8 $$\sigma_c = \frac{P_c D}{4t}$$

Where P_c is a critical internal pressure, (MPa)

D is a mean diameter, (mm)

t is a vessel wall thickness, (mm)

σ_c is a critical hoop stress, (MPa)

K_{IC} is the stress intensity factor for crack propagation and Y is a shape factor related to the crack geometry, e.g. Y is equal to one for a straight through internal cracks of length $2c$, and is equal to 1.12 for edge cracks of length c and $2/\pi$ for penny-shaped cracks of radius c [50]. To calculate the allowable pressure for cracks to penetrate the shell the shape factor given below was used.

Equation 9
$$K = Y * \frac{2}{\pi} \sigma_c \sqrt{c}$$

Equation 10
$$Y = 1.99 - 0.41\frac{c}{t} + 18.7\left(\frac{c}{t}\right)^2 - 38.48\left(\frac{c}{t}\right)^3 + 53.85\left(\frac{c}{t}\right)^4$$

Where, c < t and all variables are as discussed in the previous sections

At the initial stage, the crack size is very small with a semi-circular shape and the suitable shape factor to be used is Y = 2/π. When the crack starts propagating, up to an estimated crack length equal to half the wall thickness, the suitable correctional factor is shown in Equation 10 [51] and when the crack shape is semicircular (i.e. 2c = 2t), the suitable shape factor is Y = 1. Equations 9, 10 and 11 were used to estimate the maximum internal pressure at the minimum K_{IC} value (i.e. average K_{IC} value minus five times the standard deviation, μ - 5σ) *up to an estimated crack length equal to half the wall thickness*. A conservative approach would be to assume that K_{IC} values less than (μ - 5σ) would also apply to those particles that has a crack length equal to the shell thickness i.e. the leak before break condition (LBB).

3.3.4 Statistical Analysis

There are statistical methods and tools that are useful in research when planning/designing experiments or communicating the results of experiments. Interpretation of statistics can lead to errors in description and interpretation. These errors can lead to incorrect decisions.

Brittle material such as CVD SiC exhibits a large scatter of strength measurements, which makes it difficult to define the exact failure load [52]. A guideline, in Hindley [52], for statistical analysis of strength measurements of graphite material has been applied for the analysis of fracture toughness measurement of the CVD SiC in the work. It is therefore important to

determine statistically whether the fracture toughness measurements of the CVD SiC fit a specific distribution. The Weibull and normal distribution are chosen for analysis purpose. The statistic methods were further utilised for the following:

- to determine if enough samples were used to conduct the experiment,
- to determine the minimum $K_{IC,}$
- to compare various processes by using the mean K_{IC}
- to determine whether the use of minimum K_{IC} would be a conservative approach

MATLAB statistical tools have been used to determine if the data (i.e. fracture toughness measurements) fits either a normal or Weibull distribution. The statistical techniques used were probability plots and Anderson-Darling (A-D) goodness of fitness. The choice of a distribution was first determined from the probability plots visually and then using an A-D goodness of fit test with a significance of 0.05. [52]

The probability plot is a graphical technique for assessing whether or not data set follows a given distribution such as normal or Weibull. Probability plot determines what distribution fits the sample data and if a given distribution, such as Weibull, provides a good fit to data [53]. The data are plotted against a theoretical distribution (e.g. normal) on a probability plot in such a way that the points should approximately lie on a straight line. Departures from this straight line indicate departures from a particular distribution (e.g. departure from normality from a normal probability plot) [53].

A-D Goodness of Fit is used to test if a sample of data came from a population with a specific distribution (is the data from normal, log-normal, Weibull, exponential, or logistic distributions). It is derived from Kolmogorov-Smirnov (K-S) [54] test and it gives more weight to the tails than does the K-S test [53]. The A-D test makes use of the specific distribution in calculating critical values. This has the advantage of allowing a more sensitive test and the disadvantages that critical values must be calculated for each distribution, which depends on the sample size [52-53]. There constants are available in literature [54 - 57] and therefore, for a certain sample size a critical value can be calculated. The fit is compared to this critical value to determine if the fit passes or fails the A-D test [52].

Chapter 4: Results and Discussions

4.1 INDENTATION TECHNIQUE

The experimental work helped to develop the K_{IC} test procedure for the SiC in the TRISO particles. Some of the factors that contributed in achieving the results are listed in Appendix 7.3. The following sub-sections validate and finalize the analytical tool (indentation technique) used for this investigation.

4.1.1 Material

Reliable results were obtained by using both the 5 mm HP SiC and the 51-µm CVD SiC samples. The reliability of the indentation technique was further tested using various thicknesses of the CVD SiC samples as discussed in the previous section. The thickness of these test samples was not less than twice the crack length (2*c*) and the adjacent indent centers were about 4*c* apart. The longest crack, 2c, at 100 g test load as shown in Appendix 1.1, was ~18 µm, which made the sample thickness suitable to conduct the experimental work.

The 0.1mm HP SiC was not suitable to conduct the experiments due to the surface defects (e.g. pre-existing cracks and porosities) that were causing the cracks to propagate catastrophically during indentation test as shown in Figure 12(a). The thick arrows on the image in Figure 12(b) shows cracks caused by the polishing technique due to pre-existing cracks shown by a thin arrow on the same image.

Good indentation impressions were produced on the SiC in TRISO particles as shown in Figure 13 and appendix 7.5. A micro-Vickers hardness tester and a test load of 200 g were used to obtain this impression. The experimental work has been completed using the CVD SiC in TRISO coated fuel particles with the thickness ranging between 28 µm and 51 µm.

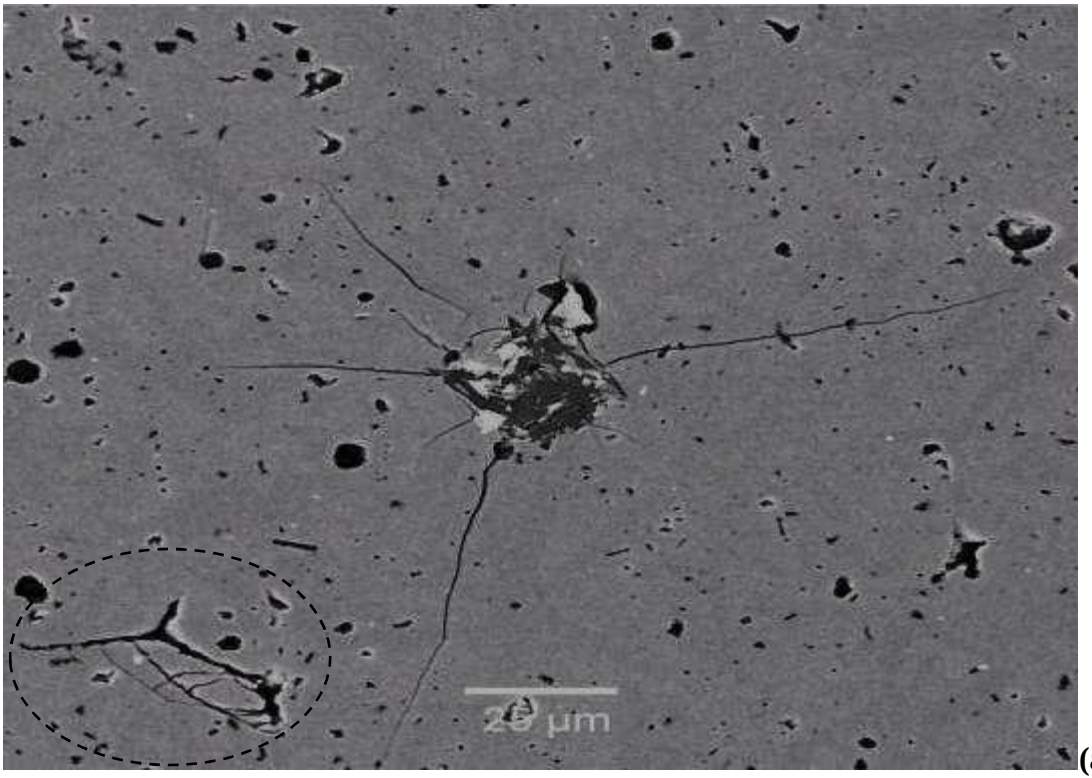

(a)

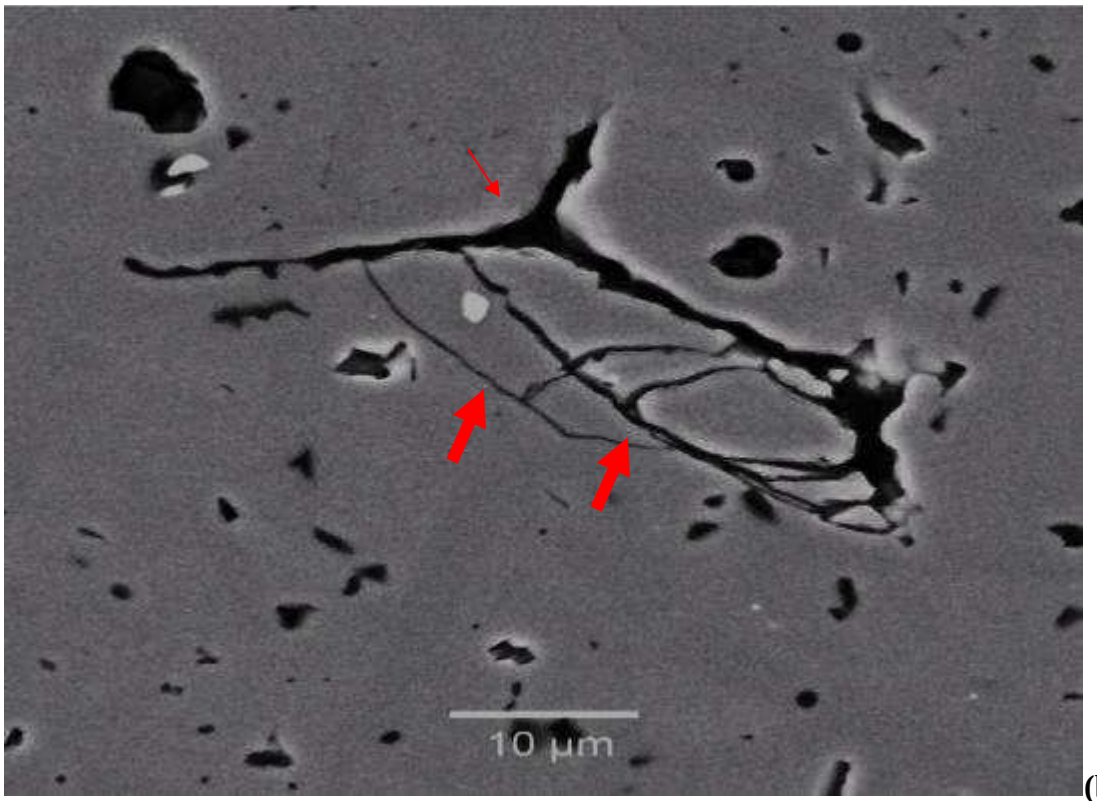

(b)

Figure 12: Cracks found on the surface of the 0.1 mm HP SiC. The cracks in (a) were the results of an indentation test, whereas in (b) they formed near a pre-existing crack.

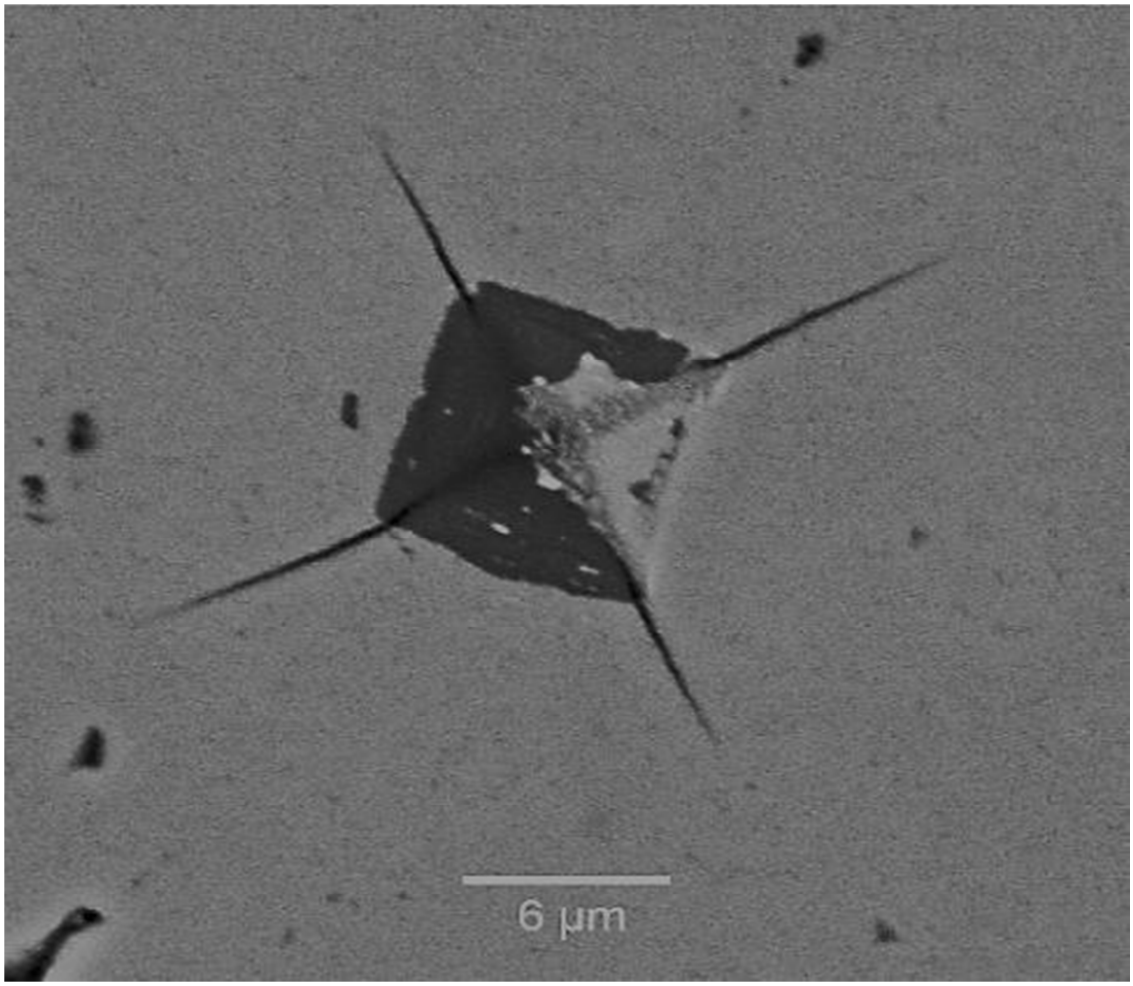

Figure 13: SEM photomicrograph showing an indentation on the 51 µm CVD SiC in TRISO with cracks emanating at the corners of the indent

4.1.2 Sampling

Ten indentations per particle on ten particles from the same batch yielded 400 cracks (i.e. one crack from each indent corner) for estimating the K_{IC}. The mean K_{IC} value obtained using 40 cracks from each particle were compared with the mean K_{IC} value obtained using 400 cracks. The F value (F critical) in Table 4 that need to be exceeded in order to have a significant difference between treatments was not exceeded, showing that there was no significant difference between the average K_{IC} value obtained using 400 cracks and that obtained using 40 cracks. In other words, as supported by Table 20, Appendix 7.6, one particle instead of ten can be used to determine the K_{IC} as long as the surface area will allow four indents.

Similarly, the critical F value in Table 20, Appendix 7.6, was also not exceeded therefore there was no need to use 100 indents in order to produce the mean K_{IC} value that is statistically

acceptable. Therefore, at least four indents can be used to determine the mean K_{IC} value of the CVD SiC.

Table 4: Statistical variation in the mean K_{IC} results between 400 and 40 cracks. The other two reference tables are in Appendix 7.6.

Anova: Single Factor						
SUMMARY						
Groups	Count	Sum	Average	Variance		
Cross-Sectional area	400	1267.7	3.17	0.08028		
CPT-B-B10 A	40	129.9	3.25	0.102045		
CPT-B-B10 B	40	124.6	3.12	0.079769		
CPT-B-B10 C	40	128.1	3.20	0.053583		
CPT-B-B10 D	40	127.2	3.18	0.046769		
CPT-B-B10 E	40	129.4	3.24	0.097205		
CPT-B-B10 F	40	122.3	3.06	0.061994		
CPT-B-B10 G	40	126.3	3.16	0.064558		
CPT-B-B10 H	40	126.5	3.16	0.067019		
CPT-B-B10 I	40	127.8	3.20	0.129718		
CPT-B-B10 J	40	125.6	3.14	0.089128		
ANOVA						
Source of Variation	SS	Df	MS	**F**	P-value	**F crit**
Between Groups	1.152025	10	0.115203	**1.445**	0.1559	**1.843**
Within Groups	62.91153	789	0.079736			
Total	64.06355	799				
Where: SS stands for sums of squares, Df for degrees of freedom and MS for mean square						

Sample orientation has an influence on the K_{IC} of the CVD SiC as shown in Figure 14, middle top and middle bottom images. Since the dangerous cracks will be the ones that are propagating on the radial direction, therefore, it is important to determine the properties of the SiC in the CVD growth direction.

Figure 14 shows a comparison between the samples prepared for *Cross-Section Indentation* (top row) and prepared for *Curved Surface indentation* (bottom row). The first two columns have shown the cracks propagation due to 100 g and 200 g test loads. The far right images indicate how the samples were prepared for the indentation.

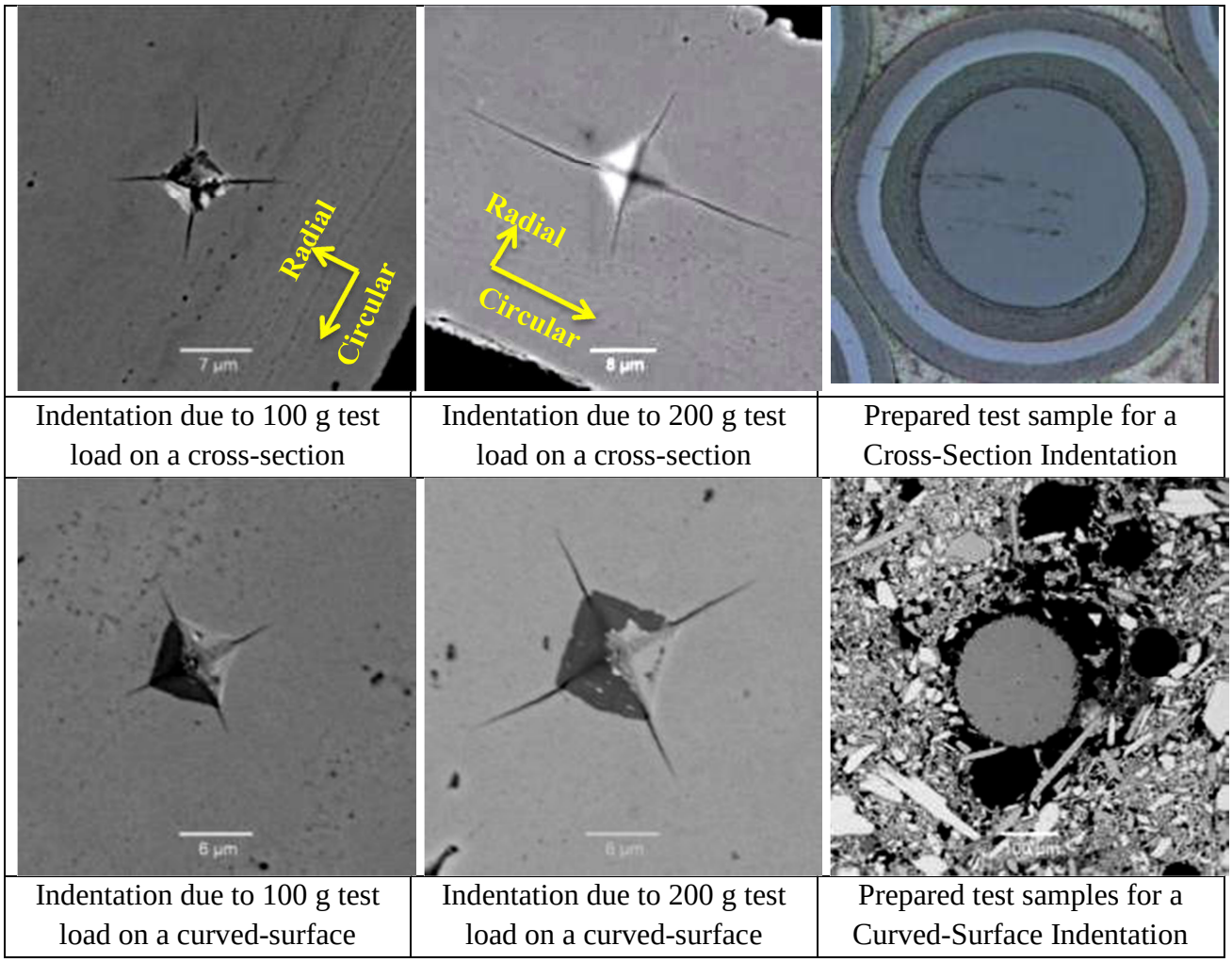

Indentation due to 100 g test load on a cross-section	Indentation due to 200 g test load on a cross-section	Prepared test sample for a Cross-Section Indentation
Indentation due to 100 g test load on a curved-surface	Indentation due to 200 g test load on a curved-surface	Prepared test samples for a Curved-Surface Indentation

Figure 14: The top row indicates indentation on the cross-section and the bottom row indicates indentation on the curved-surface using 100 g and 200 g test loads. The far right column indicates the loading direction.

The pressure inside the kernel introduces biaxial hoop tensile stresses in the CVD SiC shell, which will preferentially propagate cracks in radial direction. Therefore, the K_{IC} was determined from the curved-surface indentation although not all the indentations made on the curved-surface were exactly parallel to the CVD growth direction. For applicable K_{IC} measurements, the material thickness in comparison with the crack length must be sufficient. An extreme example of this is shown in Figure 15. Preparing CVD SiC samples for curved-surface indentation yields K_{IC} results that can be used directly to calculate the maximum internal pressure that can be sustained at a known crack length. The only cracks that will cause failure of the SiC are cracks propagating in a radial direction and therefore, circular cracks as shown in Figure 14 middle top micrograph are not important.

Figure 16 shows indents on one of the particles tested. Such test at the centre of the polished curved outer surface cannot be used because the material thickness at the centre of the sample was very thin as compared to the areas close to the edge. On the other samples, the centre of the polished surface is also very close to the inner carbon layer as shown in Figure 17. TRISO particles with the inner PyC already surfacing at the center of the SiC as shown in Figure 17 could not be used. Figure 16 shows an applicable example of an acceptable indentation, where the test area is very small. The test area should be at least between 960 μm^2 and 40,000 μm^2. The material thicknesses vary from particle to particle depending on how much of the SiC layer was removed during sample preparation.

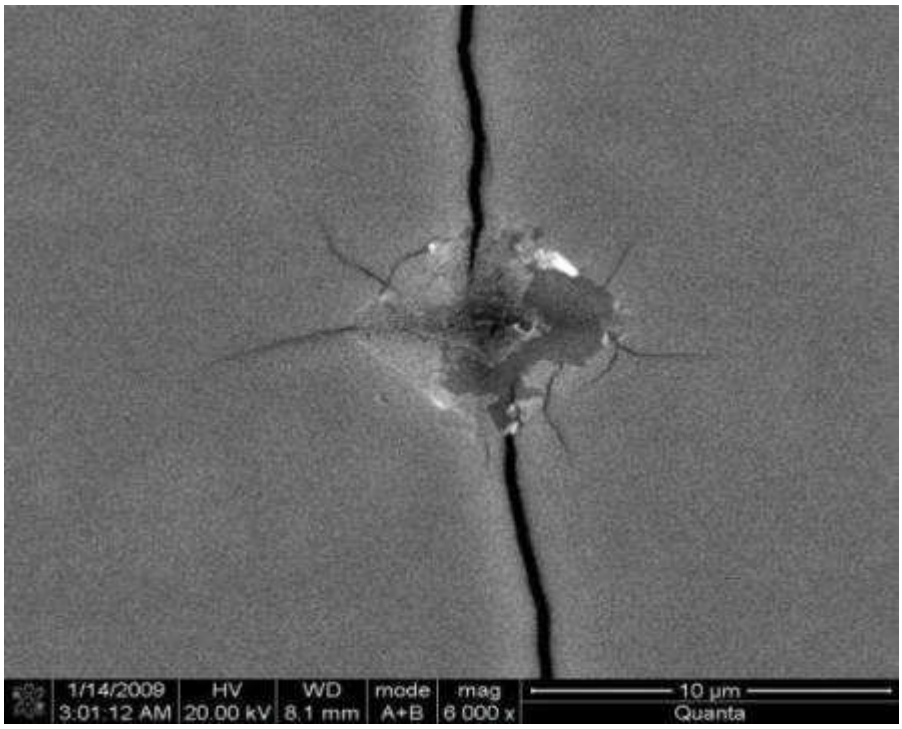

Figure 15: Indentation cracking on the CVD SiC due to insufficient material thickness

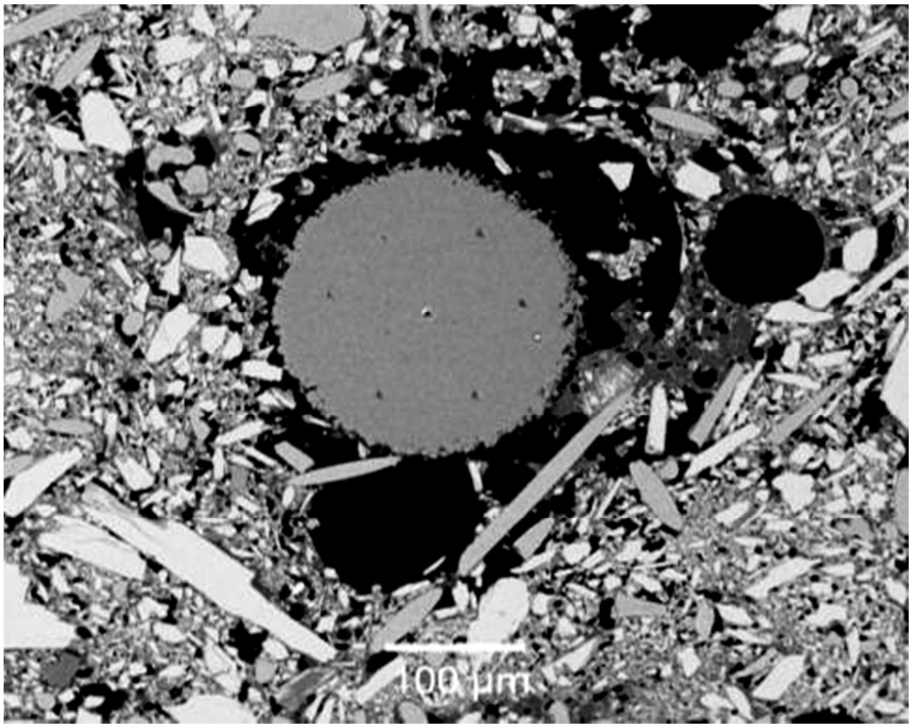

Figure 16: SEM micrograph showing indents on the polished curved-surface of sample CPT-B-10 (i.e. 51 µm CVD SiC).

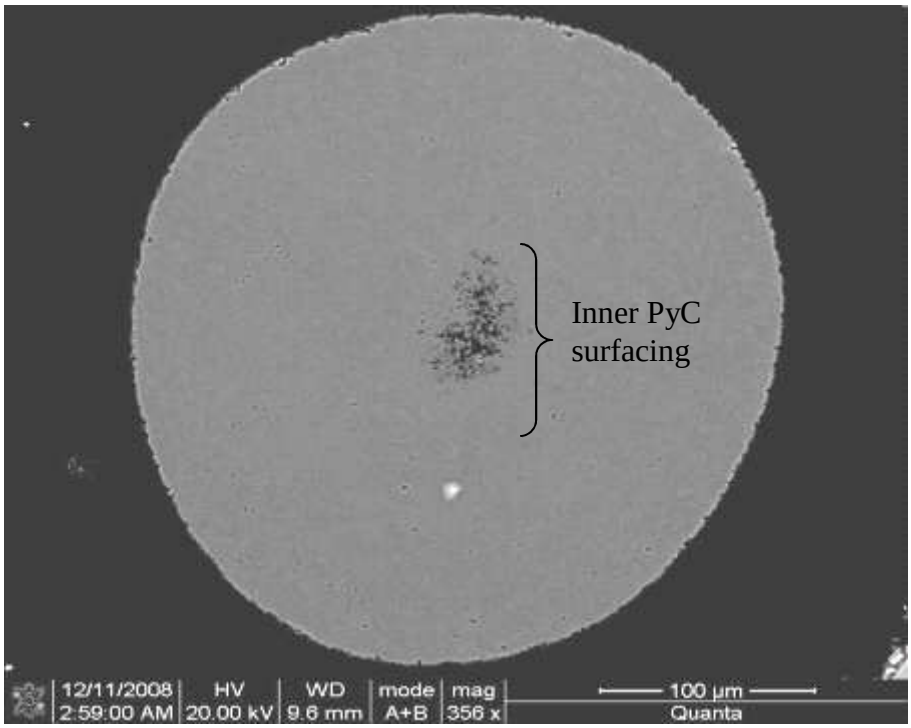

Figure 17: SEM image showing inner PyC (black) surfacing in the center of a 36 µm CVD SiC shell (white area) of sample CPT-T-G148

4.1.3 Test Load

At low loads, i.e. 25 g and 50 g, it was difficult to measure the indent diagonal length and the crack length using either the SEM or the optical light microscope. Therefore, the data was not considered appropriate to determine the hardness and K_{IC} of the HP SiC. The 243 H_V calibration block was used to verify the Vickers hardness tester. It was found that the hardness was independent of the test load as shown in Table 5 and Table 6. The F value (F critical) in Table 6 that need to be exceeded in order to have a significant difference between treatments (i.e. test loads) was not exceeded. In other words, there was no variation between the means of the hardness values obtained using any test load between 25 g and 1000 g. Thus, three low loads (50 g, 100 g, and 200 g) were selected to determine the test load suitable for testing the 35 μm thick CVD SiC shell.

Table 5: The influence of various test loads on the measured Vickers hardness of a standard calibration block with a Vickers hardness values of 243

Test	**load (g)**						
	25	**50**	**100**	**200**	**300**	**500**	**1000**
1	237	234	225	234	243	231	239
2	240	249	228	238	236	234	232
3	240	257	243	243	237	237	232
4	240	232	238	250	236	232	229
5	251	234	260	237	228	235	232
Average	**243**	**241**	**239**	**240**	**236**	**234**	**233**
error	5	10	12	6	5	2	3

Table 6: Statistical variation in the mean H_V results at various test loads

ANOVA						
Source of Variation	*SS*	*df*	*MS*	*F*	*P-value*	*F crit*
Between Groups	390	6	65	1.046218	0.417329	2.445259
Within Groups	1739.6	28	62.12857			
Total	2129.6	34				
Where: SS = sums of squares, df = degrees of freedom and MS = mean square						

The SEM micrograph in Figure 18 shows the influence of various loads on the indentations produced in the SiC shell. At a load of 50 g, it was difficult to measure the indentation diagonal length and crack length whereas at 200 g and above, cross-section indentation cracks were longer on the circumferential direction than on the radial direction. The cause of longer cracks at one direction and shorter cracks at another direction was assumed to be due to the sample fabrication technique (i.e. CVD process) and it is discussed in section 4.1.2. The CVD SiC was tough when indents are made on the curved surface. When indents are made on the cross-section, the cracks propagated easily at the circumferential direction since it was the weakest as compared to the radial direction.

Lists of SEM images showing different features are listed in appendix 7.5. 100 g was found to be the optimum load to use for the determination of the fracture toughness and it was consequently used for the bulk of the work. As discussed in the literature any test load between 100 g and 1000 g can be used to produce the same K_{IC} value for CVD SiC material. The selected 100 g was within the range of the loads used in the literature as shown in Table 1.

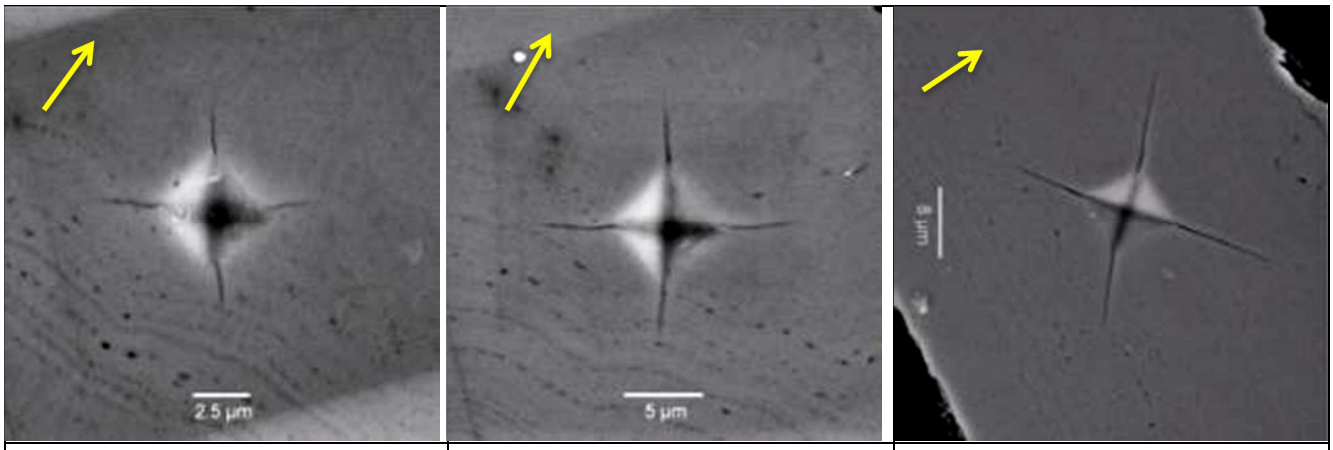

@ 50 g	@ 100 g	@ 200 g

Figure 18: SEM images of CVD SiC at three different loads showing Vickers indentations with well-defined cracks. The arrows on each image shows CVD growth direction.

4.1.4 Fracture Toughness Equation

Table 2 in chapter 2 indicates a list of equations used to determine the K_{IC} of the CVD SiC shell. The K_{IC} results using various equations at three different test loads are shown in

Table 7 with detail information in Table 21, Appendix 7.7. It was found that equation AA (Evans-Davis) together with the test load of 100 g gives an average K_{IC} value similar to the values reported in the literature as shown in Table 1. Osborne and Nogami also recommended the Evans–Davis model for CVD SiC. Furthermore, the lowest standard deviation was obtained from this equation, possibly due to a lower crack sensitivity of this equation. Thus, the following Evans-Davis equation, as discussed previously, was chosen for this investigation:

$$K_{IC} = 0.4636 \left(\frac{f}{a^{3/2}}\right)\left(\frac{E}{HV}\right)^{2/5} 10^{F}$$

$$F = -1.59 - 0.34B - 2.02B^2 + 11.23B^3 - 24.97B^4 + 16.23B^5 \quad \text{and} \quad B = log_{10}\left(\frac{c}{a}\right)$$

Where E, H_V, K_{IC} are described under the "Abbreviations, Acronyms, Symbols and Conversions" section

Table 7: The average K_{IC} values of the CVD SiC sample (i.e. CPT-B-B10 sample) measured at three different test loads. Five different equations were used for each test load.

Load	**K_{IC} (MPa.√m) @ 50 g**					**K_{IC} (MPa.√m) @ 100 g**					**K_{IC} (MPa.√m) @ 200 g**				
Equation	**A**	**B**	**C**	**AA**	**BB**	**A**	**B**	**C**	**AA**	**BB**	**A**	**B**	**C**	**AA**	**BB**
Mean	**2.9**	**3.6**	**4.6**	**2.9**	**3.1**	**2.9**	**3.6**	**3.7**	**3.3**	**3.3**	**2.2**	**2.8**	**2.9**	**3.0**	**3.0**
StdDev	0.5	0.7	0.6	0.2	0.5	0.5	0.6	0.6	0.2	0.4	0.9	1.1	1.1	0.8	0.7

4.1.5 Microscopic Examination

Comparison between the SEM and the optical light microscope was performed to determine the best analytical tool that can be used to examine the indent features. Vickers hardness results of the CVD SiC were used to indicate how effective and accurate the SEM is as compared to the optical light microscope. Thus, the optical light microscope results were compared to the SEM results as shown in Table 8. Noticeable errors were observed when using an optical light microscope to measure Vickers hardness, H_V, as compared to the errors observed when using a SEM.

The higher error values were due to the difficulties in measuring the edges of the diagonal length, as they were not as clearly resolved by an optical microscope as compared to a SEM. This is an indication that small indentations will result in large errors when measured using the optical light microscope. A backscattered electron image, produced by a small spot size (e.g. 4.1, which has no units), an acceleration voltage of 20 kV and a low scan rate was found to be the optimum one. However, when using secondary electrons a lower voltage (e.g. 15 kV) can be used. Using a larger big spot size results in less noise and blurred edges of the image.

Table 8: Vickers Hardness results of CPT-B-B10 sample at three different test loads; measured using both the SEM and the optical light microscope

Load	**50 g**				**100 g**				**200 g**			
Microscope	**SEM**		**OLM**		**SEM**		**OLM**		**SEM**		**OLM**	
Test	d(µm)	H_V	d(µm)	H_V	d(µm)	H_V	d(µm)	H_V	d(µm)	H_V	d(µm)	H_V
1	5.7	2853	5.9	2663	7.2	3576	7.9	2971	10.0	3708	12.1	2533
2	5.3	3300	6.1	2491	7.2	3576	8.0	2897	10.3	3495	12.0	2575
3	5.3	3300	5.8	2756	7.4	3386	8.0	2897	10.3	3495	11.3	2904
4	5.6	2956	6.4	2263	7.4	3386	8.3	2691	10.0	3708	11.7	2709
5	5.6	2956	6.7	2065	7.3	3479	8.5	2566	10.2	3564	11.3	2904
6	5.6	2956	5.9	2663	7.2	3576	8.3	2691	10.2	3564	11.0	3064
7	5.4	3179	6.3	2336	7.6	3210	8.5	2566	10.2	3564	11.3	2904
8	5.4	3179	6.1	2491	7.4	3386	8.7	2449	10.5	3363	11.8	2663
9	5.3	3300	6.1	2491	7.5	3296	8.3	2691	10.5	3363	12.2	2487
10	5.4	3179	5.5	3064	7.4	3386	8.0	2897	10.3	3495	12.1	2533
Avg	5.5	**3116**	6.1	**2528**	7.4	**3426**	8.3	**2732**	10.3	**3532**	11.7	**2728**
StdDev	0.1	**161**	0.3	**265**	0.1	**119**	0.3	**167**	0.2	**112**	0.4	**192**

OLM = Optical light microscope and SEM = scanning electron microscope and H_V values in this table are given as kg/mm^2.

4.2 MECHANICAL PROPERTIES

4.2.1 Hot Pressed SiC

Different indentation equations yielded different results as shown in Table 9. Statistically there was a variation between the mean K_{IC} values obtained by the five different equations.

Equation AA yielded the mean K_{IC} that was similar to the values obtained using the conventional method as seen in Table 1.

Table 9: Summary of the H_V and K_{IC} values of the 5 mm HP SiC (detailed results in Appendix 1.1)

***P* (N)**	***H*V (GPa)**		***K*IC, MPa.√m**				
			Median crack			**Palmqvist crack**	
	SEM	**OLM**	**A**	**B**	**C**	**AA**	**BB**
0.98	25	27	2.5	3.2	3.0	2.9	2.9
1.96	25	25	2.5	3.1	2.9	3.2	3.0
2.94	23	24	2.2	2.8	2.5	3.1	2.9
4.91	23	22	2.3	2.8	2.4	3.4	3.0
9.81	22	23	2.4	3.0	2.6	3.6	3.4
Average	**23**	**25**	**2.4**	**3.0**	**2.7**	**3.2**	**3.0**
StdDev	1.0	1.8	0.1	0.2	0.2	0.2	0.2

4.2.2 CVD SiC shell in TRISO particles

A summary on the mechanical properties of the CVD SiC in TRISO particles are shown in Table 10, with detailed results shown in Table 22 to Table 26, appendix 7.7. The average K_{IC} values measured were comparable to the K_{IC} values in the literature shown in Table 1 although the preparation conditions of the SiC are unknown. These conditions include the microstructure (grain size), heat treatment, impurity content, texture (quality), CVD growth direction and inclusions. For instance, Kodama *et al* [9] reported that for HP SiC a maximum K_{1C} for SiC was measured at the average grain size of ~0.7 µm, and at finer or coarser grain sizes than ~0.7 µm, K_{1C} decreased. For CVD SiC, a maximum K_{1C} of ~ 4 MPa.√m was obtained at the average grain size of 1 to 3 µm. The reason for the grain size dependence of K_{1C} was reported to be residual internal stress and resultant micro-crack forming in CVD SIC.

In this investigation, it has also been found that the SiC was tougher when tested on the curved-surface as compared to the tests conducted on the cross-section. The minimum K_{IC} value was obtained by subtracting five times the standard deviation from the average K_{IC} values. This minimum K_{IC} value was used in this investigation for further studies. Sigma is a measure of how

confident researchers about their results are. Using the average (μ) K_{IC} minus five times the standard deviation (5σ) represents a conservative approach. This approach will allow 1 in 3.5 million CVD SiC in TRISO fuel particles manufactured with fracture toughness below the minimum K_{IC} value. In simple terms, 5σ indicates that 99.9999713% of the fracture toughness values should lie within five standard deviations of the mean value. This approach will assume a lower bound pressure for safe operation of the pebble bed reactor as discussed in the next section.

Table 10: K_{IC} and H_V values of the CVD SiC layer in TRISO-coated fuel particles. The last column shows the maximum pressure that a batch of particles can withstand at a LBB condition.

Batch	**Number of Cracks**	**Thickness (μm)**	**K_{IC} (MPa.m$^{1/2}$)**			**$H_{V(0.1)}$ (GPa)**		**P_{max} (MPa) @ LBB condition**
			Min (μ - 5σ)	Mean (μ)	StdDev (σ)	Mean (μ)	StdDev (σ)	
CPT-T-G165	376	28	1.43	3.13	0.34	30	3.6	21
CPT-T-G148	184	36	1.67	3.07	0.28	32	2.6	28
CPT-T-G131	244	39	1.65	3.15	0.30	32	2.7	29
CPT-B-B10 (curved-surface)	232	51	2.52	3.47	0.19	26	1.4	50
CPT-B-B10 (cross-section)	400	51	1.77	3.17	0.28	32	2.3	35

4.2.3 The Relation between Initial Crack Length and Internal Pressure

The minimum acceptable K_{IC} value for the successful operation in the Pebble bed using the LBB concept is probably the average value minus 5 times the standard deviation (μ - 5σ). The (μ - 5σ) value represent a probability of 1 in 3.5 million particles with a K_{IC} value less than the minimum [i.e. (μ - 5σ)] and represents a conservative approach.

The internal pressure that the CVD SiC layer can withstand depends on the size of the initial defect and K_{IC} of the CVD SiC layer as shown in Figure 19. A summary of the data used to plot the graph in Figure 19 are in Table 11. The graph indicates the relationship between the initial

crack length and the internal pressure. Equation 7, Equation 8, Equation 9 and Equation 10 were used to plot these graphs. These equations have been used to estimate the maximum internal pressure at the minimum K_{IC} value (i.e. $\mu - 5\sigma$) up to an estimated crack length equal to half the wall thickness as shown in Table 11.

In practice the distribution of crack lengths in a batch of particles are not known. A conservative approach would be to assume that K_{IC} values less than ($\mu - 5\sigma$) would also apply to those particles that has a crack length equal to the shell thickness i.e. the leak before break condition (LBB). Such particles would obviously leak the internal contents to the surrounding environment.

Figure 19 shows how the safe internal pressure depends on the minimum fracture toughness ($K_{IC} = \mu - 5\sigma$) and the crack length. Figure 19 shows the lower bound safe pressure for particles with the minimum fracture toughness and with through thickness cracks (LBB). Table 10 also shows the maximum pressure that a batch of particles with the minimum fracture toughness less than ($\mu - 5\sigma$) can withstand when it is assumed that those particles also contain through thickness cracks.

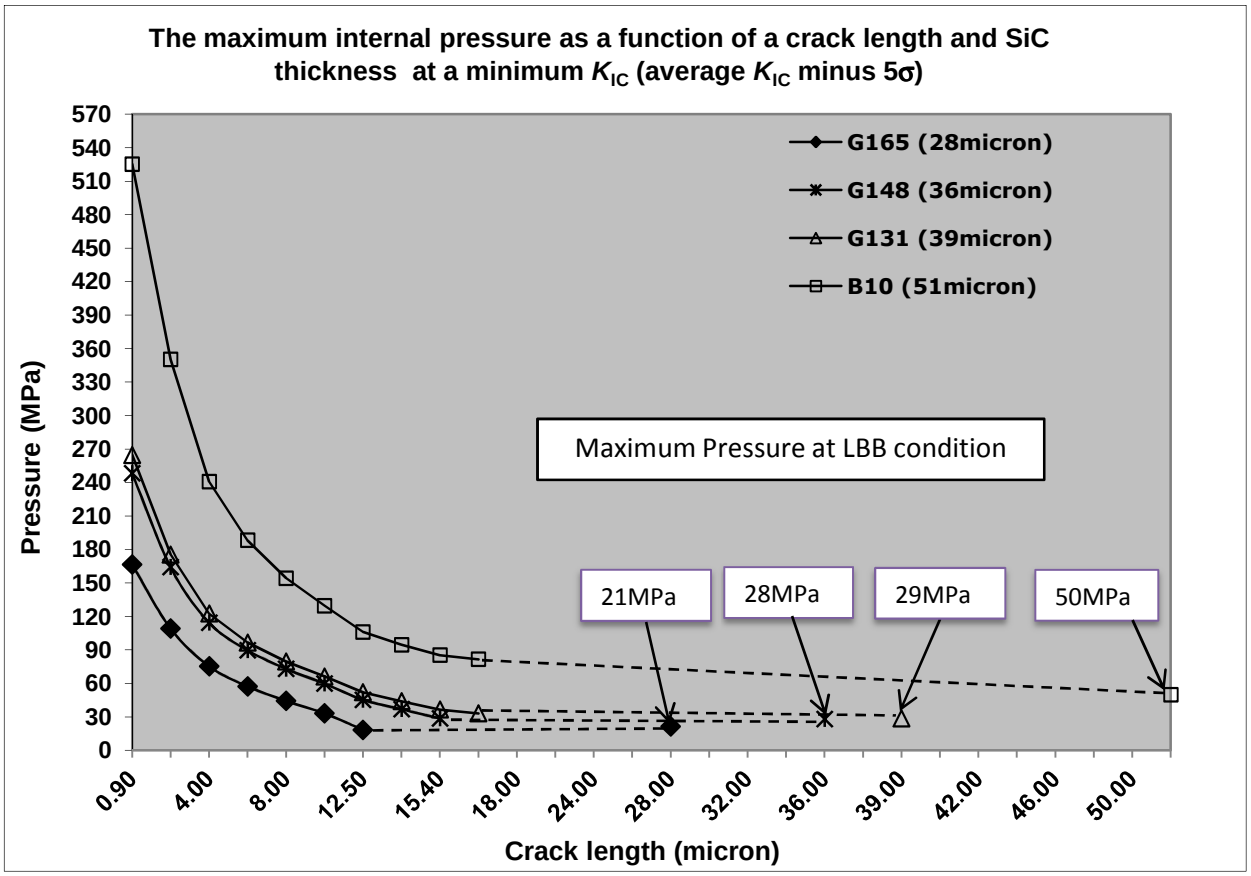

Figure 19: The maximum internal pressure that can be handled by SiC at various thicknesses of the SiC in the presence of defects at the corresponding crack length. The average curved-surface K_{IC} values minus 5σ were used to estimate the maximum internal pressure.

The following factors were taken into consideration when plotting the graphs on Figure 19:

- Only the minimum K_{IC} values as shown in Figure 20 were used (Figure 20 also shows the range of fracture toughness for the four batches tested).
- Ignoring the support that the SiC is getting from the carbon layers
- The reduction of the internal pressure applied to the SiC layer by the first two carbon layers
- Ignoring the external compression stresses from the pebble binding graphite medium and 9 MPa due to a helium gas
- Assuming that the surface crack length is twice the pressure vessel thickness (*2t*), (LBB)

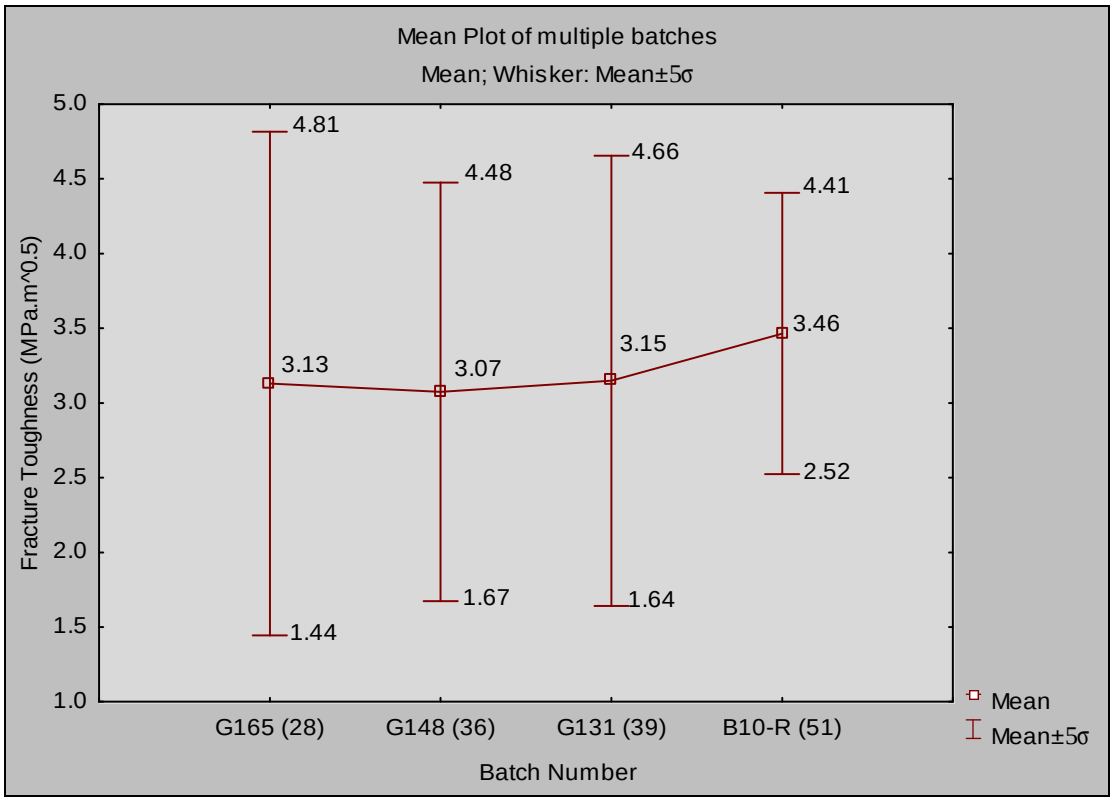

Figure 20: The minimum K_{IC} (i.e. mean K_{IC} minus 5σ) of the four batches tested.

For reference purposes the test results of sample CPT-B-10 were used as an example to give a brief description of the effect of the initial crack depth to the maximum internal pressure the SiC can handle. Assuming that the initial crack depth was less than 25 % of the material thickness (i.e. ~12.5 µm); the maximum internal pressure should be less than 106 MPa (see Table 11). This pressure is the maximum pressure beyond which a crack might propagate and lead to failure.

Table 11: The maximum internal pressure of sample G165, G148, G131 and B10 as a function of the crack depth

Sample ID (SiC thickness)	**G165 (28 µm)**	**G148 (36 µm)**	**G131 (39 µm)**	**CPT-B-10 (51 µm)**
critical crack depth, *a* (µm)	P (MPa)	P (MPa)	P (MPa)	P (MPa)
0.90	166.58	248.14	264.73	525.26
2.00	109.09	164.15	175.53	350.22
4.00	75.37	114.43	122.60	240.92
6.00	57.33	89.69	96.72	188.29
8.00	44.34	73.06	79.59	154.33
10.00	33.08	59.86	66.26	129.58
12.50	18.38	45.38	52.06	106.13
14.00		36.90	44.06	94.70
15.40		28.53	36.53	85.31
16.00			33.20	81.61
18.00				
21.90				
24.00				
25.50				
28.00	21.40			
30.00				
32.00				
34.00				
36.00		28.06		
38.00				
39.00			28.74	
40.00				
42.00				
44.00				
46.00				
48.00				
50.00				
51.00				49.83

4.3 STATISTICAL INTERPRETATION

The distribution curves shown in Figure 21 and Figure 22 are for the data taken from both the *curved surface* and *cross section* of sample CPT-B-B10 respectively. A data (i.e. mean) comparison has been done between curved surface and cross section indentation measurements. These figures show both normal and Weibull distribution curves of the K_{IC} measurements of sample CPT-B-B10, which visually fit both distributions. The results indicate that the SiC in TRISO coated fuel particles have higher K_{IC} in the curved-surface indentation with a mean K_{IC} of 3.47 MPa.m$^{1/2}$ as compared to the cross-section indentation with a mean K_{IC} of 3.17 MPa.m$^{1/2}$.

Statistically, the calculated F value (169.49) is greater than the F critical (3.86) as shown in Table 12 below and therefore, there is a significant variation between the mean K_{IC} values obtained from curved-surface indentation and that obtained from the cross-section indentation.

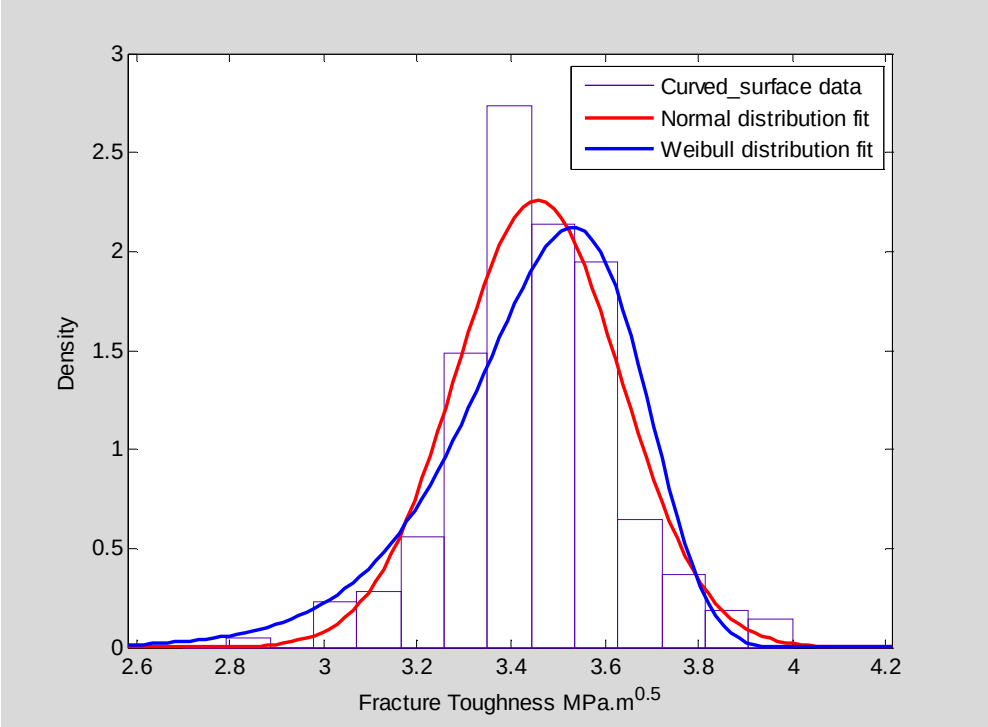

Figure 21: Distribution of K_{1C} values from batch no. CPT-B-B10, tested in the curved surface at a load of 100 g.

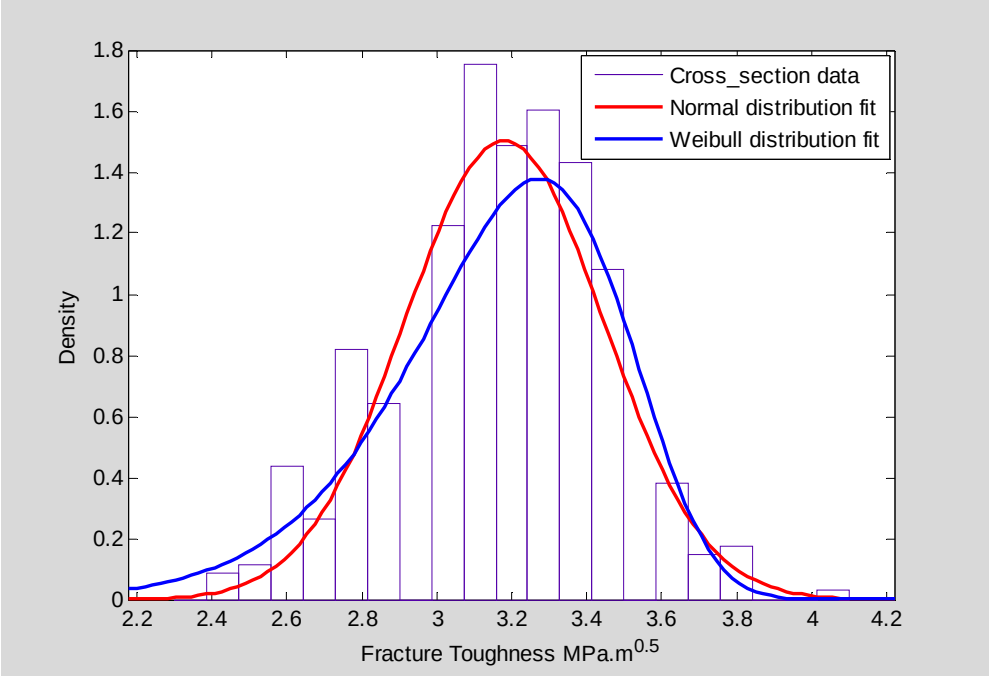

Figure 22: Distribution of K_{1C} values from batch no. CPT-B-B10, tested in the cross-section at a load of 100 g.

Table 12: Statistical variation in the mean K_{IC} results between the curved surface K_{IC} and cross-section K_{IC} of sample CPT-B-B10

Anova: Single Factor						
SUMMARY						
Groups	*Count*	*Sum*	*Average*	*Variance*		
Curved Surface indentation	232	803	3.46	0.036324		
Cross Section Indentation	232	735.7	3.17	0.078859		
ANOVA						
Source of Variation	*SS*	*df*	*MS*	***F***	*P-value*	***F crit***
Between Groups	9.761401	1	9.761401	**169.49**	3.16 E-33	**3.86**
Within Groups	26.60737	462	0.057592			
Total	36.36877	463				

The central limit theorem states that a sample size of 30 observations or more is usually large enough. More tests are necessary if the data is heavily skewed, and fewer if the data is symmetric. For all the samples tested on the curved-surface, the batch number with the least number of observations was CPT-T-G148, with 184 observations, and the batch with the highest

observation was CPT-B-10 with 232 observations. Since the number of samples used in this investigation were greater than 30 from each batch, it can be concluded that the number of samples used were enough statistically. Therefore, it can be assumed that the data is coming from a normal population.

The probability plots for the fracture toughness measurements in Appendix 7.7 were plotted in Appendix 7.8 and the statistical interpretation of these probability plots has been explained below in this section.

The standard deviation was checked (see Table 13) and showed larger variation. Since with large numbers of samples variances can often differ and equal variance is not a strict requirement, the distribution could not be plotted from the raw data. However, the central limit theorem has been applied which states that if the data set is large enough (i.e. >30) it can statistically be assumed that the distribution should be normal [58]. The Weibull and normality of the data was determined from the probability plots as shown in Appendix 7.8.

The graphical representation of fracture toughness of the six data sets is shown in Appendix 7.8, from Figure 28 to Figure 33 for the normal distribution and the Weibull distribution on the left and right of each figure respectively. The normal distribution probability plot has a logarithmic scale on the probability axis while the Weibull probability plot has a log scale on both axes.

The statistical data fit parameters and The A-D goodness of fit (GOF) test parameters for all data sets are shown in Table 13 and Table 14. The GOF test is done by comparing the alpha, α value against probability, *p* value. If the *p*-value is above the selected α-value (e.g. 0.05), the distribution pass the test and the *p*-value is below the selected α-value the test is failed.

For Data Sets CPT-T-G131 and CPT-T-G148

Visually examination of the normal probability plot and Weibull probability plot shown in Figure 28 and Figure 29 indicates that the normal distribution shows slight divergence from the fit on the lower end of the fit, while the Weibull distribution shows divergence on the lower tail end of the distribution for both data sets (i.e. CPT-T-G131 and CPT-T-G148). The parameters

obtained from the fit are shown in Table 13. The normal distribution seems to be the only appropriate fit for these two data sets. The A-D GOF test, as shown in Table 14, with the probability for both data sets being greater than 0.05, confirm that the data is from a normal distribution. However, the Weibull fit for both data sets is conservative because it predicts a higher value than actual data value.

For all curved surface data sets combined

Visually examination of the normal and Weibull probability plots shown in Figure 30 indicates that the normal distribution shows slight divergence from the fit on both tails of the distribution, while the Weibull distribution shows large divergence on the lower tail end of the distribution for all data sets. The parameters obtained from the fit are shown in Table 13. Neither normal distribution nor Weibull distribution fit the data well. However, if comparison is made, Weibull distribution is a more appropriate and conservative choice since it shows a larger divergence from the fit when compared to normal distribution.

The A-D GOF test, as shown in Table 14, also confirms that the data does not fit any distribution. However, with a probability of 0.0126, this data fit a normal distribution taking into consideration the sensitivity of the A-D GOF test, which also depends on the sample size. A-D GOF test of combined data sets involved a very large number of samples and therefore affect normal distribution. However, the Weibull fit for all combined data sets is conservative because the probability of failure for the test data is significantly below the prediction point.

For data sets CPT-T-G165, CPT-B-B10 curved surface and CPT-B-B10 cross section

Visually examination of the normal and Weibull probability plots shown from Figure 31 to Figure 33 indicates that the normal and Weibull distribution shows divergence from the fit on both tails of the distribution. However, Weibull distribution shows divergence on the lower tail end of the distribution for all three data sets. The parameters obtained from the fit are shown in Table 13.

Neither normal nor Weibull distribution fit the data. However, the Weibull fit for both data sets is conservative because the probability of failure for the test data is below predicted at the lower end of the distribution.

The Weibull plot for all data sets has been chosen because of its conservativeness not by its fit on a probability plot. The probability of failure according to the ASME code ranges between 10^{-2} and 10^{-4} [59]. For all data sets, the probability of failure, after the end of life, at the lower end of the Weibull distribution was observed and it was within the design limits of 10^{-2} and 10^{-4} as per the ASME code [59]. Therefore, the Weibull fit is conservative and we are interested only at the lower end of the distribution.

Table 13: Statistical data fit parameters

Test Location	Data Set	Normal		Weibull	
		Mean	Standard Deviation	Scale Parameter	Shape Parameter
Curved Surface	CPT-T-G165	3.1323	0.3366	3.2863	9.2739
	CPT-T-G148	3.0742	0.2799	3.2014	11.998
	CPT-T-G131	3.1474	0.2994	3.2859	10.8558
	CPT-B-B10	3.4662	0.1881	3.556	17.9665
	Combined	3.2006	0.3237	3.3468	10.6108
Cross Section	CPT-B-B10	3.1686	0.2828	3.2952	12.3849

Table 14: A-D Goodness of Fit values

Test Location	Data Set	No. of samples used	α	Normal				Weibull			
				A-D Stat	A-D adjusted	Probability	Pass	A-D Stat	A-D adjusted	Probability	Pass
Curved Surface	CPT-T-G165	372	0.05	1.8493	1.8531	0.0001	N	7.4025	7.4793	0.0000	N
	CPT-T-G148	184	0.05	0.3898	0.3914	0.2796	Y	1.4011	1.4218	0.0012	N
	CPT-T-G131	244	0.05	0.5954	0.5972	0.1188	Y	2.9312	2.9688	0.0000	N
	CPT-B-B10	232	0.05	1.0839	1.0874	0.0075	N	5.3054	5.3750	0.0000	N
	Combined	1034	0.05	0.9951	0.9958	0.0126	N	5.3309	5.3641	0.0000	N
Cross Section	CPT-B-B10	400	0.05	1.0548	1.0568	0.0089	N	0.9414	0.9509	0.0163	N

Chapter 5: Conclusions

The TRISO fuel particles will contain an internal gas pressure that is generated from fission products of the fuel kernel material. The internal pressure will cause stress that may lead to the failure of the TRISO layers and a release of the fission products to the environment. Radioactive fission products need to be retained within the fuel particle, therefore the fracture strength of the SiC layer is of concern. Thus, there is a need to determine the maximum internal pressure that the SiC layer can withstand without cracking, to ensure a safe working environment. *Therefore, the purpose of this work was to determine the integrity of the SiC shell in TRISO fuel particles. This was achieved by measuring the fracture toughness of SiC layers in order to determine the critical crack size, at pressure prevailing inside the TRISO kernel.*

The main conclusions drawn from this investigation are as follows:

- The reliability of the indentation fracture technique was tested using Chemical Vapour Deposited (CVD) SiC and Hot pressed (HP) SiC samples. However, the 0.1mm HP SiC sample was not suitable to conduct the experiments due to the surface defects (e.g. pre-existing cracks and porosities) that were causing the cracks to propagate catastrophically during the indentation test as shown in Figure 12(a). Good indentation impressions were produced on the CVD SiC sample and 0.5 mm HP SiC as shown in Figure 13 and Figure 23 to Figure 27 in Appendix 7.5.

- It has been concluded that at least four indentations instead of 100 indentations can be used to determine the K_{IC} of the CVD SiC layer, because there was no variation on the mean K_{IC} values obtained using four indentations as compared to the mean value obtained using 100 indentations. If it is not possible to make four indents on one particle because of the surface area, four particles are good enough to evaluate the fracture toughness of the SiC layer in TRISO-coated fuel particles.

- The following Evans-Davis equation gives an average K_{IC} value of the CVD SiC layer similar to the values reported in the literature. This equation has also been recommended and/or used by various authors [10, 25] such as Nogami *et al* and Pharr *et al*.

$$K_{IC} = 0.4636 \left(\frac{f}{a^{3/2}}\right)\left(\frac{E}{H_V}\right)^{2/5} 10^{F}$$

- A micro-Vickers hardness tester with a test load of 100 g was found suitable to obtain indentation impressions on the SiC samples. Compared to the light microscope the SEM was the preferred method to use for measuring both the indentation diagonal and the crack length when a 100 g test load is used.

- A very small specimen as thin as 28 µm can be used to obtain the K_{IC} of a CVD SiC layer in TRISO coated fuel particles using the indentation fracture technique. The wall thickness values of the CVD SiC layers tested were 28, 36, 39 and 51µm and their corresponding measured average K_{IC} values were 3.13, 3.07, 3.15 and 3.47 MPa.√m respectively. These values are comparable to values reported in the literature. Their corresponding minimum K_{IC} values at the *average minus 5*σ are 1.43, 1.67, 1.65 and 2.52 MPa.√m respectively.

- It was found that the K_{IC} values for the CVD SiC layer depend on the CVD growth direction. The K_{IC} values of the CVD SiC materials are not isotropic [8]. These particles (i.e. sample CPT-B-B10) have a higher K_{IC} form the test done on the curved-surface with a mean K_{IC} of 3.47 MPa.√m as compared to the cross-sectional test results with a mean K_{IC} of 3.17 MPa.√m. Since the dangerous cracks will be the ones that are propagating in the radial direction, the properties of the SiC on the curved surface are of interest.

- The internal pressure that the SiC shell can handle without failing will depend on the initial crack length and the value of K_{IC}**.** The pressure that a particle can withstand assuming the leak before break (i.e. a particle with a crack that extends right through the shell) can also be used. This represents a more conservative value for the maximum pressure allowable without fracture when the fracture toughness is known. In fact, there is a considerable wide distribution in the measured fracture toughness. Using the average fracture toughness (µ) minus five times the standard deviation (σ) represents a conservative approach. When both the LBB condition and the µ-5σ requirement are assumed, the calculated maximum allowable pressure represents an even more

conservative approach that is probably representative for the operation of the PBMR. The actual probability of particles that can be expected to fail at a particular internal pressure will depend on the actual distribution of the depth of defects as well as the distribution of the fracture toughness. Table 10 shows the maximum internal pressure allowable using the minimum K_{IC} values (*i.e. average minus 5*σ) and the LBB requirement.

- For all data sets, lower probability of failure at the lower end of the Weibull distribution on the probability plot was observed. Since we are only interested at the lower end of the distribution, the Weibull fit is conservative and therefore the choice of minimum K_{IC} would be a conservative approach.

References

1. E. Wallace, R. Matzie, R. Heiderd, J. Maddalena, *From field to factory—Taking advantage of shop manufacturing for the pebble bed modular reactor,* Nuclear Engineering and Design, **236** (2006) p 445-453
2. A.C. Kadak, *A Future For Nuclear Energy – Pebble Bed Reactors*, Massachusetts Institute of Technology, April 25, 2004
3. A.W. Mehner, W. Heit, K. Rollig, H. Ragoss and H. Muller, *Spherical fuel elements for advanced HTR manufacture and qualification by irradiation testing,* Journal of Nuclear Materials, **171** (1990) p 9-18
4. K.M. Gregory and G.B. Bennett, *Analytical solution for stresses in TRISO-coated particles*, Journal of Nuclear Materials **206** (1993) p 35-49
5. L. Wolf, G. Ballensiefen and W. Frohling, *Fuel elements of the High Temperature Pebble Bed Reactor*, Nuclear Engineering and design, **34** (1975) p 93 – 108
6. K. Niihara, *Mechanical properties of chemically vapor deposited non-oxide ceramics*, Ceramic Bulletin, **63** [9] (1984), p 1160 - 1164
7. A. Ghosh, M.G. Jenkins, K.W. White, A.S. Kobayashi and R.C. Brad, *Elevated-temperature fracture resistance of a sintered α-SiC*, Journal of the American Ceramic Society, **72** [2] (1989), p 242 – 247
8. B.V. Cockeram, *Fracture toughness and Flexural strength of chemically vapor-deposited SiC as determined using chevron-notched and surface crack in flexure specimens,* Journal of the American Ceramic Society, **87** (2004) p 1093 – 1101
9. H. Kodama and T Miyoshi, *Study of fracture behavior of very fine-grained silicon carbide ceramics*, Journal of the American Ceramic Society, **73** (1990) p 3081 – 3086
10. S. Nogami, A. Hasegawa and L. L. Snead, *Indentation fracture toughness of neutron irradiated SiC*, Journal of Nuclear Materials **307-311** (2002), p 1163-1167
11. J. Ortensi, B. Boer, A. Ougouag, THETRIS: A micro-scale temperature and gas release model for TRISO fuel, Nuclear Engineering and Design, **241** (2011) p 5018-5032
12. G.K. Miller, D.A. Petti, J.T. Maki, D.L. Knudson, An Evaluation of the effects of SiC layer thinning on failure of TRISO-coated fuel particles, Journal of Nuclear Materials **355** (2006), p 150 – 161
13. S. Williams, *CoorsTek, Inc.; P. Deny, BOOSTEC Industries (France), Overview of the production of sintered SiC optics and optical sub-assemblies [5868-04]* OPTICAL MATERIALS AND STRUCTURES TECHNOLOGIES II (OEI402), SPIE Optics and Photonics 2005, San Diego, CA

14. B. V. Cockeram, *Fracture Strength of Plate and Tubular Forms of Monolithic Silicon Carbide Produced by Chemical Vapor Deposition,* Journal of the American Ceramic. Society, **85** [3], (2002) p 603–610
15. L.L. Snead, T. Nozawa, Y. Katoh, T.S. Byun, S. Kondo and D.A. Petti, *Handbook of SiC properties for fuel performance modeling,* Journal of Nuclear Materials, **371** [1-3], (2007) p 329-377
16. R. Benz and A. Naoumidis, *Stability of un-irradiated TRISO-coated UC_2-UO_2 particles with different UC_2 contents at elevated temperatures*, Journal of Nuclear Materials, **97** [1-2], (1981) p 15-24
17. D.A. Petti, J. Buongiorno, T.J. Maki, R.R. Hobbins, G.K. Miller, *Key differences in the fabrication, irradiation and high temperature testing of U.S. and German TRISO- coated particle fuel and their implications on fuel performance*, Nuclear Engineering and Design, **222** (2003) p 281 – 297
18. C. Guéneau, S. Chatain, J.C. Dumas, J. Lechelle, C. Rado, F. Defoort, N. Dupin, B. Sundman, H, Noel, R. Konnings, Proceedings HTR 2006, *3rd International Topical Meeting on High Temperature Reactor Technology, October 1-4, 2006, Johannesburg, South Africa*
19. K.L. Choy, *Chemical vapour decomposition of coatings*, Progress in Materials Science, **48,** (2003) p 57 -170
20. J.G. Kim, E-SulKum, D.J. Choi, S.S. Kim, H.L. Lee, Y.W. Lee, and J.Y. Park, *Study of CVD SiC deposition for TRISO coated fuel material fabrication by computational simulation and actual experiment*, Journal of Ceramic Processing Research. **8** [6], (2007) p 388~392
21. K. Minato, K. Fukuda, *Chemical vapour deposition of silicon carbide for coated fuel particles,* Journal of Nuclear Materials, **149,** (1987) p 233-246
22. W.D. Callister, Jr. *Materials Science and Engineering: An Introduction*, 4th Edition, John Wiley & Sons, Inc. New.
23. W.D. Callister, *Materials Science and Engineering: An Introduction*, 3rd Edition, John Wiley & Sons, Inc. New.
24. T. Nishida, Y. Hanaki, G. Pezotti, *Effect of notch-root radius on the Fracture toughness of a fine-grained alumina,* Journal of the American Ceramic Society, **77** [6], (1994) 606
25. M. Pharr, Y. Katoh, H. Bei, *Dependence of fracture toughness on crystallographic orientation in single-crystalline cubic (β) silicon carbide*, U.S. Department of energy journal of Undergraduate research, <http://www.scied.science.doe.gov>
26. M.C. Osborne, J.C. Hay, L.L Snead and D. Steiner, *Mechanical- and Physical-property changes of neutron-irradiated chemical-vapor-deposited SiC*, Journal of the American Ceramic Society, **82,** (1999) p 2490 – 2496

27. G. Orange, H. Tanaka and G. Fantozzi, *Fracture toughness of pressureless Sintered Silicon Carbide: A comparison of K_{1C} Measurement Methods*, Ceramics International, **13,** (1987), p 159 - 165
28. R. G. Munro, *Material Properties of a Sintered alpha-SiC*, Journal of Physical and Chemical Reference Data, **26**, (1997) p 1195-1203
29. H. Zhang, E. López-Honorato, A. Javed, X. Zhao, J. Tan, P. Xiao, *A study of the microstructure and mechanical properties of SiC coatings on spherical particles*, Journal of the European Ceramic Society, **32** [8] (2012), p 1775–1786
30. D. J. Kim, D. J. Choi, *Microhardness and surface roughness of silicon carbide by chemical vapour deposition*, Journal of Materials Science Letters, **16**, (1997) p 286–289
31. S.H. Lee, Y.I. Lee, Y.W. Kim, R.J. Xie, M. Mitomo, G.D. Zhan, *Mechanical properties of hot-forged SiC ceramics*, ScriptaMaterialia, **52**, (2005) p 153–156
32. F. W. Clinard jr, G. F. Hurley, R. A. Youngman, L. W. Hobbs, *The effect of elevated-temperature neutron irradiation on fracture toughness of ceramics*, Journal of Nuclear Materials, **133 & 134**, (1985) p 701–704
33. K.H. Park, T. Hinoki and A. Kohyama, *Influence of irradiation-induced defects on fracture behaviour in highly pure SiC*, Journal of Nuclear Materials, **367–370**, Part 1, (2007) p 703–707
34. R.J. Price, *Effects of fast-neutron irradiation on pyrolytic silicon carbide*, Journal of Nuclear Materials, **33** [1], (1969) p 17-22
35. J. L. Henshall, D. J. Rowcliffe, J. W. Edington, *Fracture Toughness of Single-Crystal Silicon Carbide*, Journal of the American Ceramic Society, **60** [7-8], (1977) p 373 - 375
36. K. Minato, T. Ogawa, S. Kashimura, K. Fukuda, M. Shimizu, Y. Tayama, I. Takahashi, *Metallic impurities-silicon carbide interaction in HTGR fuel particles*, Journal of Nuclear Materials, **175** [1-2], (1990) p 14–19
37. Y.M. Lu, I.C. Leu, *Qualitative study of beta silicon carbide residual stress by Raman spectroscopy*,Thin Solid Films, **377 – 378**, (2000) p 389-393
38. C.B. Ponton and R. D. Rawlings, *Vickers indentation fracture toughness test part 1 Review of literature and formulation of standardized indentation toughness equations*, Material Science and Technology, **5**, September (1989) p 865-872
39. S.G. Hong, T.S. Byun, R.A. Lowden, L.L. Snead and Y. Katoh, *Evaluation of the Fracture Strength for Silicon Carbide Layers in the Tri-Isotropic-Coated Fuel Particle*,Journal of the American Ceramic Society, **90** [1], (2007) p 184–191
40. B.R. Lawn, A.G. Evans and D.B. Marshall, *Elastic/Plastic Indentation damage in ceramics: The median/radial crack system*, Journal of the American Ceramic Society, **63**, (1980) p 574 - 581

41. J. Gong, J Wang and Z Guan, *Indentation toughness of ceramics: A modified approach*, Journal of Material Science, **37**, (2002) p 865 - 869
42. K. Strecker, S. Ribeiro and M. Hoffmann, *Fracture toughness measurements of LPS-SiC: A comparison of the indentation technique and the SEVNB method*, Material Research, **8** [2], (2005) p 121-124
43. K.M. Liang, G. Orange and G. Fantozzi, *Evaluation by indentation of fracture toughness of ceramic materials.*, Journal of Material science, **25**, (1990) p 207-214
44. C.B. Ponton and R. D. Rawlings, *Vickers indentation fracture toughness test part 2 Applications and critical evaluation of standardized indentation toughness equations*, Material Science and Technology, **5,** October (1989) p 961-976
45. J. Qian, L.L. Diemen, Y. Zhao, *Hardness and fracture toughness of moissanite*, Diamond & Related Materials, **14**, (2005) p 1669 – 1672
46. Z. Li, A. Ghosh, A.S. Kobayashi, and R.C. Bradt, *Indentation Fracture Toughness of Sintered Silicon Carbide in the Palmqvist crack regime*, Journal of the American Ceramic Society, **72** [6], (1989) p 904 – 911
47. G.E. Dieter, *Mechanical Metallurgy*, SI metric edition, McGraw-Hill Book Company (1988) p 243-249 & 348-374
48. R.W. Hertzberg, *Deformation and fracture mechanics of engineering materials*, 4thed, 1996
49. A.K. Ntlokwana, *The efficiency of the burn-learn method in assessing the integrity of TRISO coated fuel particle layers, University of Pretoria, South Africa, July (2013)*
50. J.P.R. de Villiers, J. Göske and A. Tuling, *Disintegration in high grade titania slags: low temperature oxidation reactions and associated fracture mechanics of pseudobrookite*, Mineral Processing and Extractive Metallurgy (Trans. Inst. Min. Metall. C), **114**, June (2005)
51. D Broek, *Elementary Engineering Fracture Mechanics*, 3rd edition, Martinius Niyhoff Publishers, 1982, p 76
52. M.P. Hindley, M.N. Mitchell, D.C. Baline, A.A. Groenwold, *Observations in the statistical analysis of NBG-18 nuclear graphite strength tests*, Journal of Nuclear Materials, **420**, (2012) p 110 – 115
53. *NIST/SEMATECH e-Handbook of Statistical Methods*, http://www.itl.nist.gov/div898/handbook/eda/section3/probplot.htm, accessed on March 3, 2015
54. M.A. Stephens, *Test of fit for the logistic distribution based on the empirical distribution function*, Biometrika, **66** [3], (1979) p 591 – 595
55. M.A. Stephens, *Goodness of fit for the extreme value distribution*, Biometrika, **64** [3], (1977) p 583 – 588

56. M.A. Stephens, *EDF statistics for goodness of fit and some comparisons*, Journal of the American Statistical Association, **69** [347], September (1974) p 591 – 595
57. M.A. Stephens, *Asymptotic results for goodness-of-fit statistics with unknown parameters*, The annals of statistics, **4,** (1976) p 357 – 369
58. *NIST/SEMATECH e-Handbook of Statistical Methods*, http://www.itl.nist.gov/div898/handbook/eda/section3/eda3661.htm, accessed on April 2, 2015
59. ASME Boiler and Pressure Vessel Code, Section III Division 5 - High Temperature Reactors, rules for construction of nuclear facility components (2011) p 200 – 215

Appendices

7.1 DATA SHEET OF CVD SIC

Table 15: Physical properties of a typical CVD SiC [Source: MorganAdvancedCeramics, Physical properties of performance SiC, www.performancematerial.com, accessed on 03 September 2012]

Property	Value	Method
Density	3.21 g/cc	Sink-float and dimension
Specific Heat	0.66 J/g ° K	Pulsed laser flash
Flexural Strength	450 MPa 560 MPa	4 point bend, RT. 4 point bend, 1300°
Fracture Toughness	2.94 MPa $m^{½}$	Micro indentation
Hardness	2800	Vickers, 500 g load
Elastic Modulus (Young's Modulus)	450 GPa 430 GPa	4 point bend, RT. 4 point bend, 1300° C
Grain Size	2-10 µ m	SEM
Chemical Analysis		
Element	C	Si
Concentration ppm wt	33 wt%	67 wt%

7.2 DIFFERENT INDENTATION METHODS

Table 16: Equation for determining the fracture toughness from various authors such as Ponton and Rawlings [44]

Equation	Model	Ref. article
Radial median crack equations		
$K_{IC} = 0.043*(E*H_0)^{1/2}*(a^2/c^{3/2})$	Gong *et al*	[41]
$K_{IC} = 0.0134*(E/H_V)^{1/2}*(P/c^{3/2})$	Lawn-Evans-Marshall	[44]
$K_{IC} = 0.035*(E/H_V)^{1/4}*(P/c^{3/2})$	Tanaka	
$K_{IC} = 0.022*(E/H_V)^{2/5}*(P/c^{3/2})$	Laugier	
$K_{IC} = 0.0515*(P/c^{3/2})$	Lawn and Fuller	
$K_{IC} = 0.0363*(E/H_V)^{2/5}*(P/a^{1.5})*(a/c)^{1.56}$	JL	
$K_{IC} = 0.0824*(P/c^{3/2})$	Evans and Charles	
$K_{IC} = 0.0101*P/(ac^{1/2})$	Lawn and Swain	
$K_{IC} = 0.0160*(HP/c)^{1/2}$	Lawn and Swain#	[38]
$K_{IC} = 0.0726*(P/c^{3/2})$	Lawn and Fuller#	
$K_{IC} = 0.0752*(P/c^{3/2})$	Evans and Charles#	
$K_{IC} = 0.0950*(P/c^{3/2})$	Niihara *et al*	
Palmqvist crack equations		
$K_{IC} = 0.0143*(E/H_V)^{2/3}*(a/l)^{1/2}*(P/c^{3/2})$	Tanaka	[44]
$K_{IC} = 0.0319*P/(al^{1/2})$	Shetty-Wright-Mincerl-Clauer	
$K_{IC} = 0.0370*(HP/l)^{1/2}$	Niihara *et al*#	[38]
$K_{IC} = 0.0446*(HP/l)^{1/2}$	Shetty *et al*#	[38]

The equations are based on the materials properties of the α-SiC: E = 430 GPa, H_V = 27 GPa and v = 0.22
Where K_{1C} = fracture toughness (MPa.√m), H_V= Vickers hardness (GPa), P = load (N).a is a half diagonal length of the indent (mm), l and c are crack lengths as indicated on Figure 8, E = Young's Modulus and H is the true hardness

7.3 GENERAL FACTOR ADHERED TO WHEN CONDUCTING THE EXPERIMENTS

The following factors need to be taken into consideration when conducting the experiment using Vickers indentation fracture-toughness test to brittle materials, particularly glasses and ceramics. Although some of the following factors are explained in detail in other sections it is necessary to summarize them and should be adhered to when conducting the experiments:

- The test sample surface should be stress free before indentation; this can also be achieved by polishing the surface down to 1 µm and etching it before indentation.
- Due to the fact that the fracture toughness values which are determined using the median crack equations all decrease substantially as the test load increases, a minimum indenter load of ~50 N is recommended. Gong *et al* [41] also mentioned that the hardness value that will give reliable fracture toughness values would only be obtained at high loads (where the fracture toughness remains constant with a load increase).
- The median crack equations cannot be applied to the Palmqvist crack system. Ponton and Rawlings [44] also reported that to ensure that the crack length measurements errors are kept to a minimum, the largest indenter load that does not cause lateral crack breakthrough at the surface should be used.
- Grain size also influences the fracture toughness. Kodama [9] reported that a maximum K_{1C} for SiC appeared at the average grain sizes of ~0.7 µm, and at finer or coarser grain sizes than ~0.7 µm, K_{1C} decreased.
- The test sample should be about 2c in thickness and that adjacent indent centers should be no closer than ~4c (where c is the surface radial crack length) [44].
- If necessary, the hot-pressed SiC should be annealed prior to indentation test.
- The crack length should be measured as soon as is practicable after indentation to minimize the effect of post indentation slow cracks growth [44].
- Coating the polished specimen test surface with gold before indentation is preferable.

To avoid errors in the K_{IC} measurements, the above factors should be taken into consideration. For instance, the greatest errors that could result from the ambiguity in the actual crack-tip position can be avoided if the test surface is pre-coated with gold prior to indentation.

7.4 HARDNESS AND K_{IC} RESULTS OF 5 MM HP SIC

Table 17: Vickers hardness results of HP SiC at various test loads; measured using both the SEM and the light microscope

Load(N)	25 g				50 g				100 g				200 g				300 g				500 g				1000 g			
microscope	SEM		LM		SEM		LM		SEM		LM		SEM		LM		SEM		LM		SEM		LM		SEM		LM	
d (µm)	d	H_V	d	H_V	d	H_V	d	H_V	d	H_V	d	H_V	d	H_V	d	H_V	d	H_V	d	H_V	d	H_V	d	H_V	d	H_V	d	H_V
1	4.1	2757	4.0	2897	6.5	2194	6.0	2575	8.6	2507	8.4	2628	11.7	2709	12.8	2263	15.1	2439	15.0	2472	20.2	2272	20.0	2318	28.5	2283	27.2	2506
2	4.2	2628	4.0	2897	6.3	2336	6.0	2575	8.5	2566	8.0	2897	12.2	2491	12.2	2479	16.0	2173	15.5	2315	19.6	2413	21.0	2102	28.0	2365	28.5	2283
3	4.2	2628	4.5	2289	5.8	2756	6.2	2412	8.3	2691	8.5	2566	12.1	2533	11.8	2663	15.6	2286	15.0	2472	19.7	2389	21.0	2102	28.3	2315	29.0	2205
4	4.1	2757	3.5	3784	6.0	2575	6.0	2575	9.1	2239	8.0	2897	12.5	2373	11.8	2663	15.3	2376	15.0	2472	18.7	2651	20.5	2206	30.8	1954	29.5	2130
5	4.5	2289	4.0	2897	6.1	2491	5.7	2853	8.4	2628	8.1	2826	12.5	2373	12.3	2451	15.5	2315	15.0	2472	18.9	2595	20.0	2318	27.8	2399	27.0	2543
6	4.1	2757	4.0	2897	5.8	2756	5.5	3064	8.6	2507	8.0	2897	12.4	2412	12.5	2373	15.5	2315	15.7	2256	20.2	2272	20.4	2228	28.3	2315	27.8	2399
7	4.5	2289	4.0	2897	5.8	2756	5.5	3064	8.4	2628	8.3	2691	12.0	2575	11.7	2709	15.2	2407	14.9	2505	20.5	2206	20.9	2122	28.5	2283	27.0	2543
8	4.2	2628	3.8	3210	5.8	2756	5.4	3179	8.9	2341	8.1	2826	12.1	2533	12.1	2533	15.9	2200	15.5	2315	21.0	2102	19.5	2438	27.6	2434	27.9	2382
9	4.5	2289	4.0	2897	5.9	2663	5.5	3064	8.9	2341	8.0	2897	12.2	2491	12.5	2373	15.6	2286	15.3	2376	20.9	2122	20.5	2206	31.5	1868	27.5	2452
10	4.3	2507	3.9	3047	5.9	2663	5.6	2956	8.5	2566	8.2	2757	12.1	2533	12.1	2533	15.1	2439	14.9	2505	20.9	2122	19.6	2413	27.5	2452	28.7	2251
Ave	**4.3**	**2553**	**4.0**	**2971**	**6.0**	**2594**	**5.7**	**2832**	**8.6**	**2501**	**8.2**	**2788**	**12.2**	**2502**	**12.2**	**2504**	**15.5**	**2324**	**15.2**	**2416**	**20.1**	**2314**	**20.3**	**2245**	**28.7**	**2267**	**28.0**	**2369**
StdDev	0.2	188	0.2	350	0.2	188	0.3	259	0.2	140	0.2	116	0.2	96	0.3	138	0.3	88	0.3	87	0.8	185	0.5	116	1.3	187	0.8	139

Table 18: K_{IC} results of 5 mm HP SiC. Five different equations were used for each test load and the SEM being the analytical tool

				Assuming : Median crack (MPa.√m)			: Palmqvist crack MPa.√m)				for equation AA	
***P* (N)**	***a* (mm)**	***c* (mm)**	***H_V* (GPa)**	**A**	**B**	**C**	**AA**	**BB**	***E (GPa)*** @ RT.	**c/a**	**F**	**B**
0.25	0.00210	0.00380	25	2.2	2.6	2.4	2.3	2.2	410	1.8	-1.7112	0.2576
0.98	0.00432	0.00860	25	2.5	3.2	3.0	2.9	2.9	410	2.0	-1.7331	0.2995
1.96	0.00605	0.01380	25	2.5	3.1	2.9	3.2	3.0	410	2.3	-1.7702	0.3581
2.94	0.00775	0.01990	23	2.2	2.8	2.5	3.1	2.9	410	2.6	-1.8121	0.4096
4.91	0.00970	0.02720	23	2.3	2.8	2.4	3.4	3.0	410	2.8	-1.8507	0.4478
9.81	0.01435	0.04310	22	2.4	3.0	2.6	3.5	3.4	410	3.0	-1.8857	0.4776
Avg			24	2.4	2.9	2.6	3.0	2.9				
error			1.2	0.1	0.2	0.2	0.4	0.4				
F = (-1.59-0.34*B-2.02*B^2+11.23*B^3-24.97*B^4+16.23*B^5)											B = log (c/a)	

7.5 SEM IMAGES

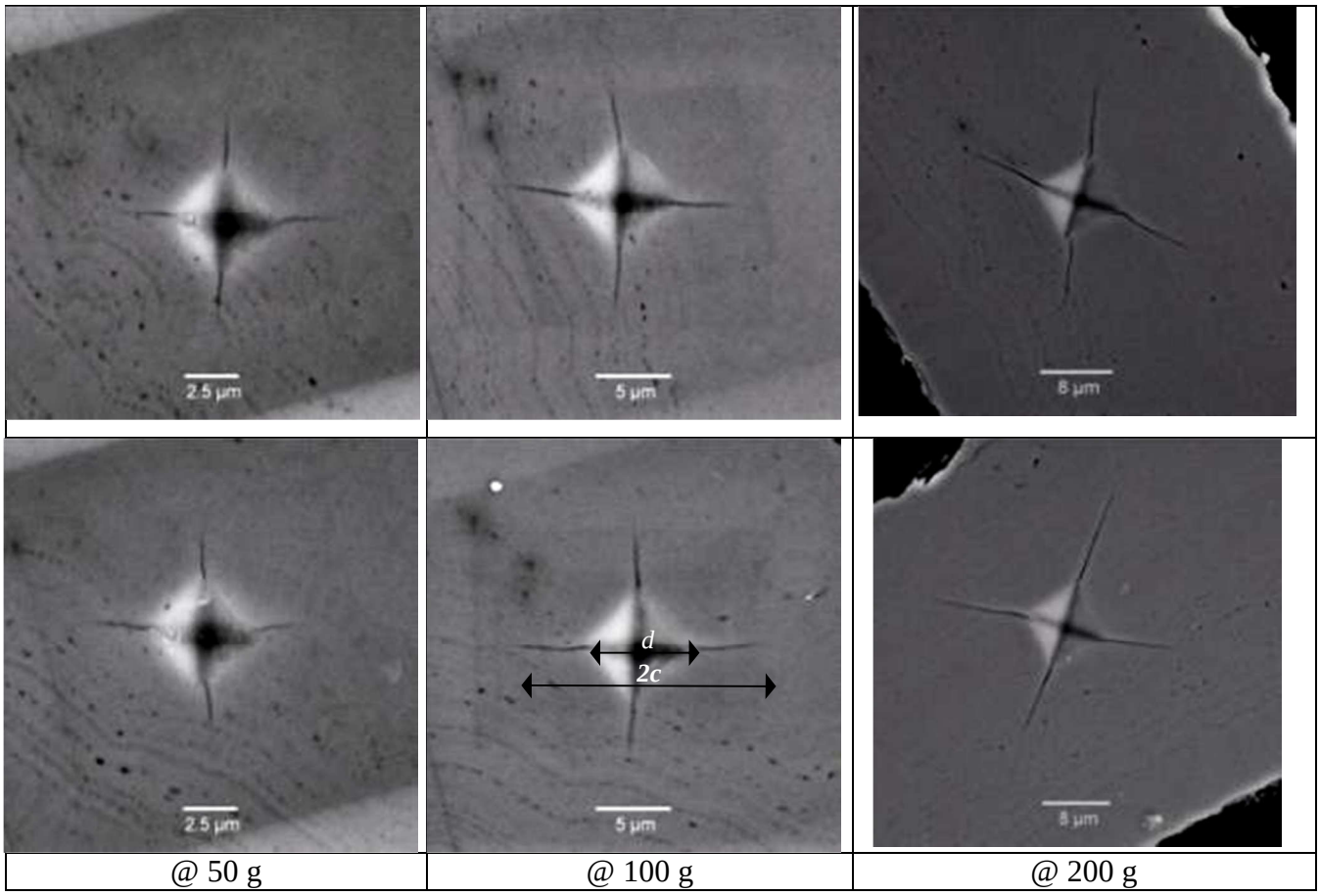

@ 50 g	@ 100 g	@ 200 g

Figure 23: SEM images of CVD SiC at three different loads showing Vickers indentations with well-defined cracks

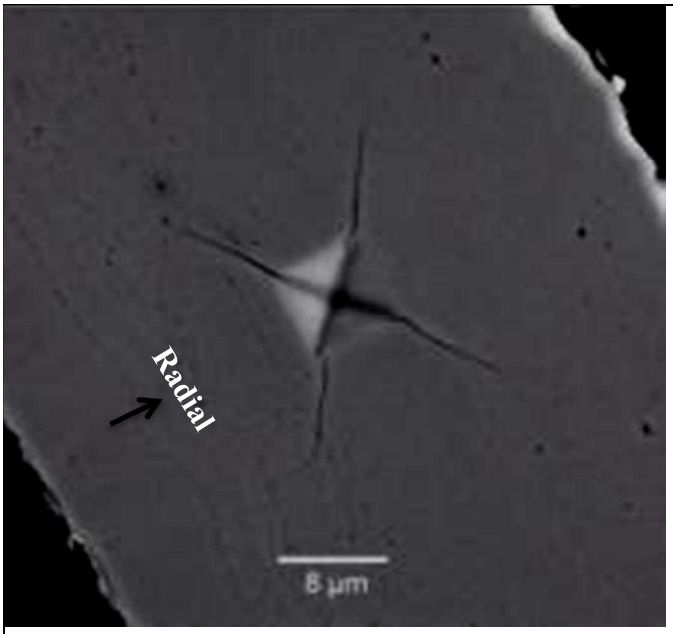

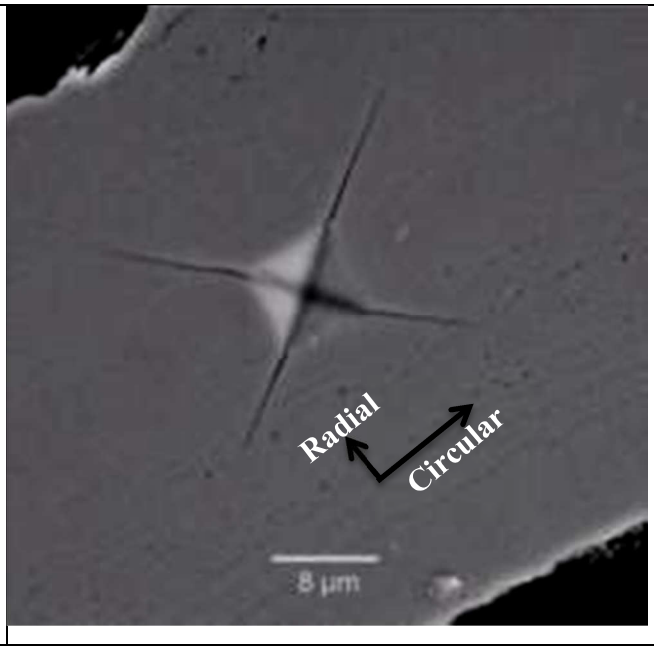

From the above SEM images, the indent corners are pointing at 45 degree in reference to the CVD growth direction (see an arrow on each image) with 200 g as a test load

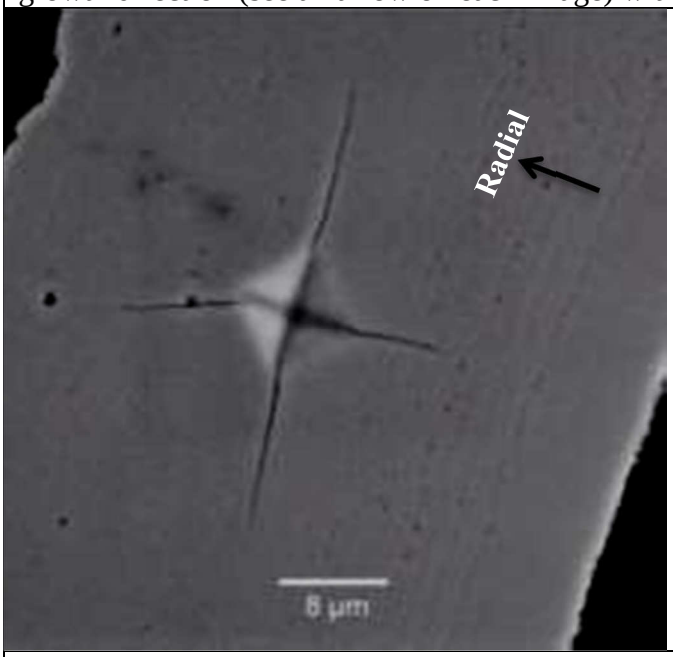

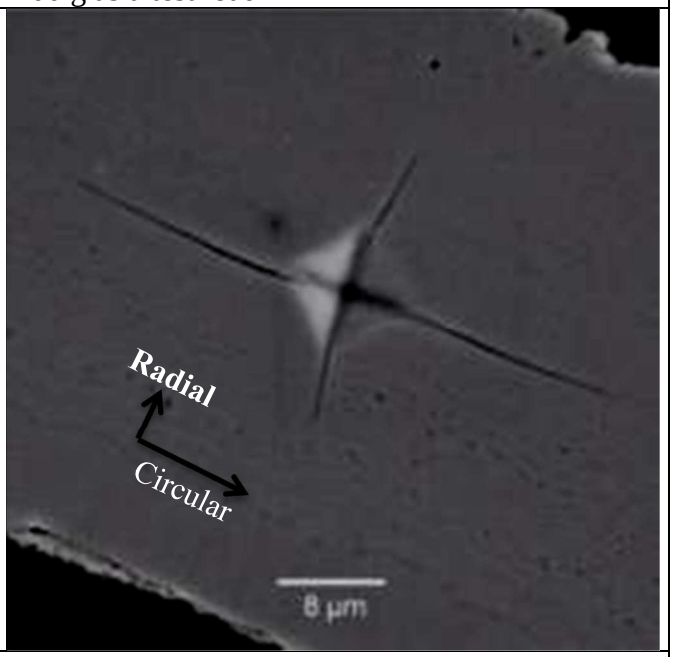

The indent corners are pointing at 90 degree in reference to the CVD growth direction (see an arrow on each image) with 200 g as a test load

Figure 24: SEM images of the CVD SiC showing how an indent orientation can influence crack propagation.

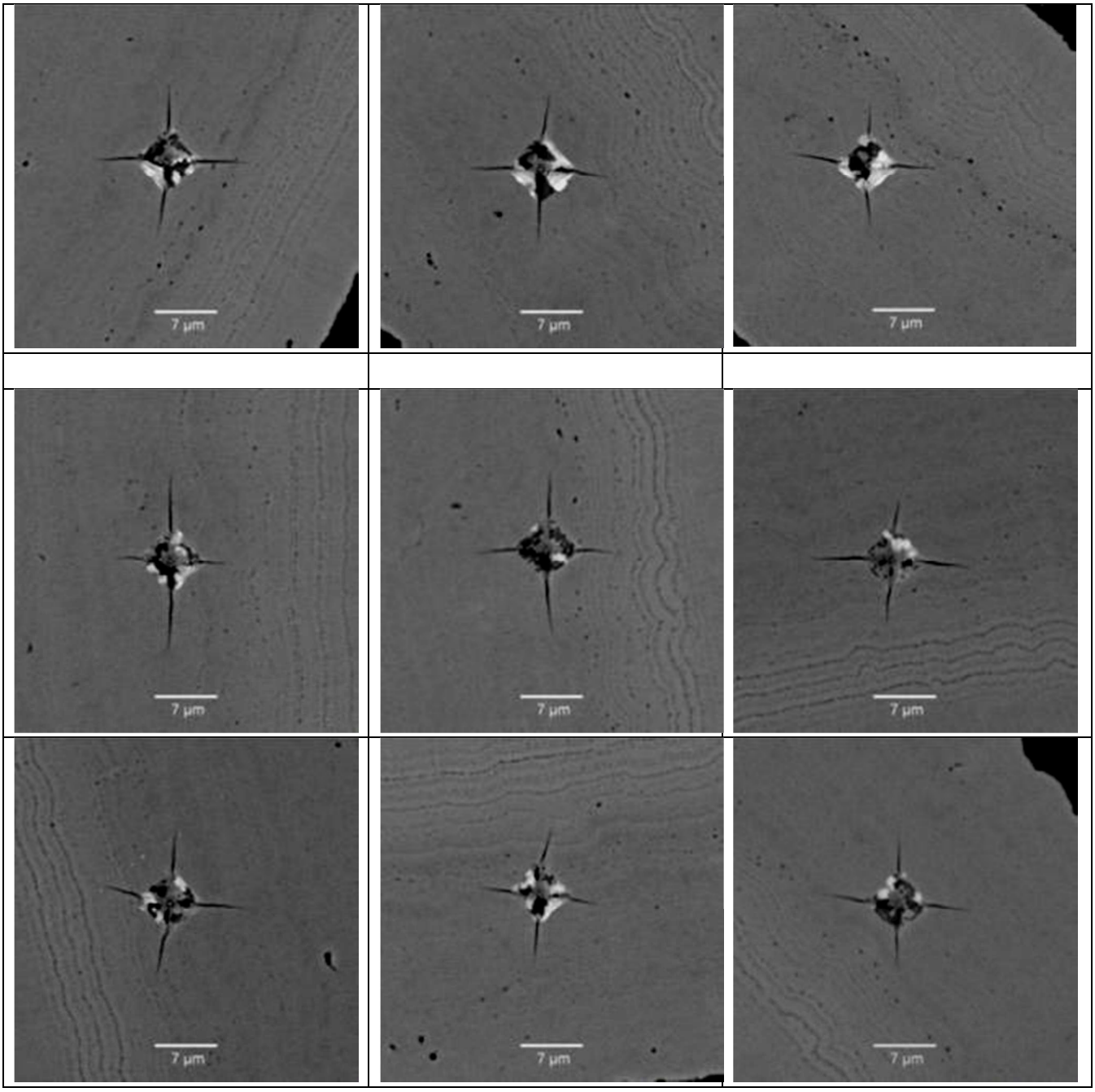

Figure 25: SEM images of the CVD SiC taken from the cross-section indentation using 100 g test load

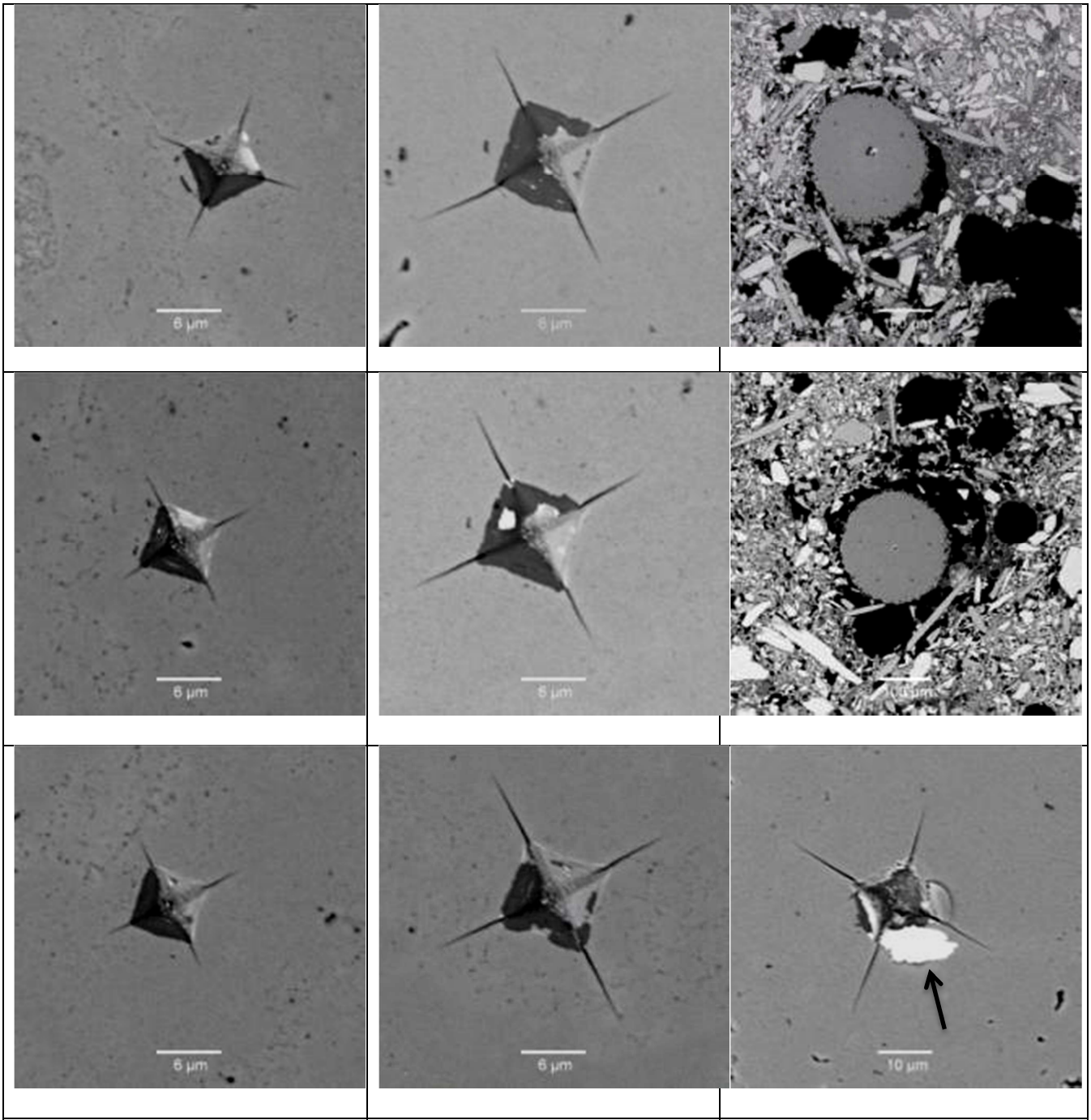

Figure 26: SEM images of the CVD SiC taken from the curved-surface indentation. The top and the middle far right images indicate how the samples were prepared for curved-surface indentation. The image on the bottom far right shows cracking due to excessive loading as indicated by the solid arrows on the image.

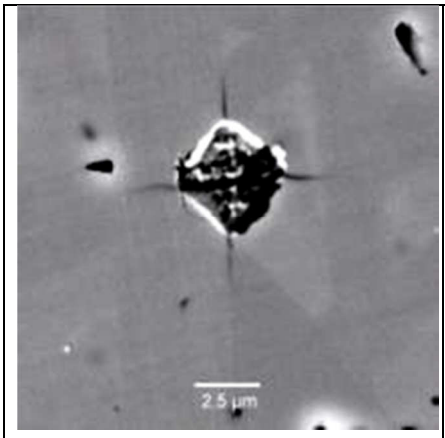	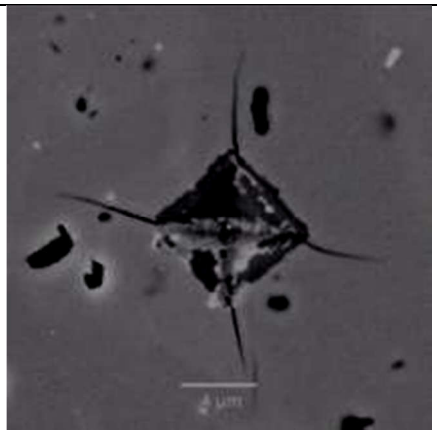	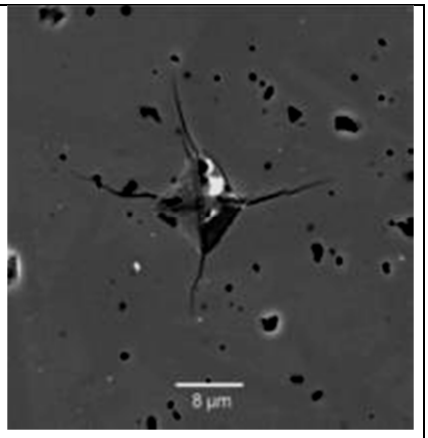
25 g	100 g	200 g
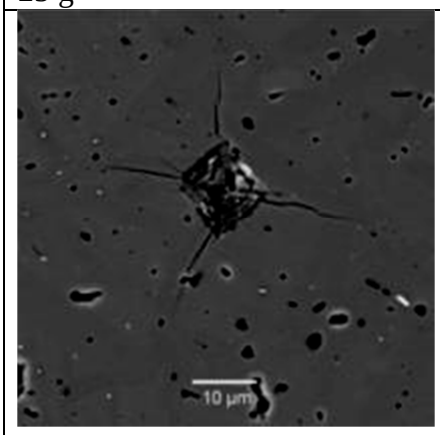	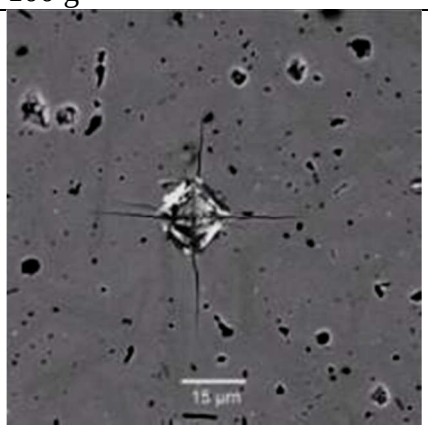	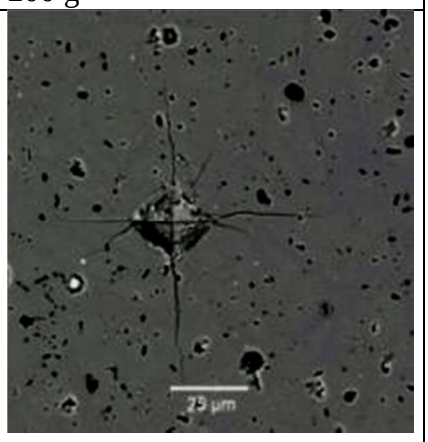
300 g	500 g	1000 g

Figure 27: SEM images of the 5mm HP SiC at various test loads, showing difficulties in making perfect crack profile as compared to the perfect crack profile obtained using the CVD SiC.

7.6 SAMPLING

Table 19: Statistical variation in the mean KIC results within 10 particles

Anova: Single Factor						
Groups	*Count*	*Sum*	*Average*	*Variance*		
CPT-B-B10 A	40	129.9	3.25	0.102045		
CPT-B-B10 B	40	124.6	3.12	0.079769		
CPT-B-B10 C	40	128.1	3.20	0.053583		
CPT-B-B10 D	40	127.2	3.18	0.046769		
CPT-B-B10 E	40	129.4	3.24	0.097205		
CPT-B-B10 F	40	122.3	3.06	0.061994		
CPT-B-B10 G	40	126.3	3.16	0.064558		
CPT-B-B10 H	40	126.5	3.16	0.067019		
CPT-B-B10 I	40	127.8	3.20	0.129718		
CPT-B-B10 J	40	125.6	3.14	0.089128		
ANOVA						
Source of Variation	*SS*	*df*	*MS*	***F***	*P-value*	***F crit***
Between Groups	1.152025	9	0.128003	**1.62**	0.108395	**1.90**
Within Groups	30.87975	390	0.079179			
Total	32.03178	399				

Table 20: Statistical variation in the mean KIC results between a group of 100 and 4 indents was done using the KIC results from sample CPT-B-B10

Anova: Single Factor						
Groups	*Count*	*Sum*	*Average*	*Variance*		
100 indents	400	1267.7	3.17	0.08028		
4 indents	16	52.9	3.31	0.08063		
ANOVA						
Source of Variation	*SS*	*df*	*MS*	***F***	*P-value*	***F crit***
Between Groups	0.288754	1	0.288754	**3.60**	0.058605	**3.86**
Within Groups	33.24115	414	0.080293			
Total	33.5299	415				

7.7 HARDNESS AND K_{IC} RESULTS OF CVD SiC

Table 21: Tabulated K_{IC} values of CVD SiC sample measured at three different test loads. Five different equations were used for each test load.

	K_{IC} (MPa.√m) @ 50 g					K_{IC} (MPa.√m) @ 100 g					K_{IC} (MPa.√m) @ 200 g					
Test 1	**A**	**B**	**C**	**AA**	**BB**	**A**	**B**	**C**	**AA**	**BB**	**A**	**B**	**C**	**AA**	**BB**	
1	1.7	2.3	3.5	2.3	2.3	2.2	2.6	2.6	3.0	2.7	1.4	1.7	1.8	2.2	2.4	
	2.2	3.0	4.1	2.6	2.7	3.5	4.2	4.2	3.7	3.6	1.8	2.1	2.2	2.7	2.6	
	2.5	3.5	4.5	2.7	3.0	3.1	3.8	3.8	3.5	3.4	2.6	3.0	3.1	3.6	3.2	
	2.5	3.4	4.5	2.7	3.0	3.3	4.0	4.0	3.6	3.5	3.0	3.6	3.7	3.9	3.5	
2	2.3	2.7	3.8	2.8	2.5	2.2	2.6	2.6	3.0	2.7	1.6	2.0	2.0	2.4	2.6	
	2.7	3.2	4.3	3.0	2.8	3.1	3.7	3.7	3.5	3.3	1.8	2.3	2.4	2.8	2.8	
	3.4	4.0	4.9	3.2	3.3	3.0	3.6	3.7	3.5	3.3	2.4	3.1	3.2	3.4	3.2	
	3.5	4.1	5.0	3.2	3.4	3.1	3.7	3.8	3.5	3.3	3.0	3.8	4.0	3.8	3.7	
3	2.2	2.6	3.7	2.7	2.4	2.2	2.8	2.9	3.0	2.8	1.5	1.9	2.0	2.3	2.5	
	2.5	3.0	4.1	2.9	2.7	3.1	3.9	4.0	3.4	3.5	2.4	3.1	3.2	3.4	3.2	
	3.0	3.6	4.6	3.1	3.1	3.1	4.0	4.1	3.4	3.5	1.8	2.2	2.3	2.7	2.7	
	2.9	3.5	4.5	3.0	3.0	2.8	3.5	3.6	3.3	3.2	2.5	3.1	3.2	3.4	3.2	
4	2.2	2.9	4.0	2.6	2.6	2.2	2.8	2.8	3.0	2.8	1.2	1.4	1.5	1.8	2.2	
	3.6	4.7	5.5	3.0	3.9	3.1	3.9	4.0	3.4	3.5	1.2	1.4	1.5	1.8	2.2	
	2.9	3.8	4.8	2.8	3.2	4.1	5.2	5.3	3.8	4.4	3.9	4.6	4.8	4.3	4.1	
	2.7	3.5	4.6	2.8	3.0	2.5	3.2	3.2	3.2	3.0	2.7	3.3	3.4	3.7	3.3	
5	2.6	3.5	4.5	2.8	3.0	2.7	3.3	3.4	3.3	3.1	1.0	1.3	1.3	1.5	2.1	
	2.9	3.9	4.9	2.9	3.3	2.5	3.1	3.1	3.2	3.0	1.2	1.5	1.5	1.8	2.2	
	3.1	4.1	5.1	2.9	3.5	3.3	4.1	4.1	3.5	3.6	2.7	3.3	3.4	3.6	3.3	
	3.0	4.0	5.0	2.9	3.4	2.5	3.1	3.1	3.2	3.0	3.3	4.1	4.2	4.0	3.8	
6	2.1	2.8	3.9	2.5	2.6	2.1	2.6	2.6	3.0	2.7	2.4	3.0	3.1	3.4	3.2	
	2.9	3.9	4.9	2.9	3.3	2.7	3.3	3.3	3.4	3.1	2.1	2.6	2.7	3.1	3.0	
	2.5	3.3	4.4	2.7	2.9	3.2	3.8	3.9	3.5	3.4	2.2	2.7	2.8	3.2	3.0	
	4.6	6.0	6.6	3.3	5.4	3.7	4.4	4.5	3.7	3.8	2.5	3.1	3.2	3.5	3.2	
7	2.4	2.9	4.0	2.8	2.6	2.4	3.3	3.3	3.0	3.1	1.5	1.8	1.9	2.2	2.5	
	3.3	4.0	4.9	3.1	3.3	2.5	3.3	3.4	3.1	3.1	2.8	3.5	3.6	3.7	3.5	
	2.9	3.6	4.6	3.0	3.0	3.2	4.3	4.4	3.4	3.8	2.1	2.6	2.7	3.1	2.9	
	2.7	3.3	4.3	2.9	2.9	2.5	3.3	3.4	3.1	3.1	3.1	3.8	4.0	3.9	3.7	
8	3.1	3.9	4.8	3.0	3.3	2.3	2.9	3.0	3.0	2.9	0.9	1.2	1.3	1.4	2.1	long crack
	2.5	3.1	4.2	2.8	2.7	2.7	3.4	3.5	3.2	3.2	3.2	4.2	4.3	3.8	3.9	short crack
	3.3	4.1	5.0	3.1	3.4	3.8	4.8	4.9	3.7	4.1	1.0	1.4	1.4	1.5	2.2	long crack
	3.3	4.1	5.0	3.1	3.4	3.3	4.2	4.3	3.5	3.7	4.6	6.0	6.2	4.3	5.1	short crack
9	3.2	3.8	4.8	3.1	3.2	2.6	3.4	3.4	3.2	3.2	1.4	1.8	1.8	2.1	2.5	
	3.5	4.1	5.0	3.2	3.4	3.0	3.9	4.0	3.4	3.5	3.1	4.1	4.2	3.8	3.8	
	3.5	4.1	5.0	3.2	3.4	2.9	3.8	3.8	3.3	3.4	1.5	1.9	2.0	2.3	2.6	
	2.9	3.4	4.4	3.0	2.9	2.9	3.7	3.8	3.3	3.4	3.0	3.9	4.1	3.7	3.7	
Average	**2.9**	**3.6**	**4.6**	**2.9**	**3.1**	**2.9**	**3.6**	**3.7**	**3.3**	**3.3**	**2.2**	**2.8**	**2.9**	**3.0**	**3.0**	
StdDev	0.5	0.7	0.6	0.2	0.5	0.5	0.6	0.6	0.2	0.4	0.9	1.1	1.1	0.8	0.7	

Table 22: The cross-section H_V and K_{IC} values of the CVD SiC samples at 100 g

Sample: CPT-B-B10		Thickness	Density	constant for H_V			**Load**	**kg**	**N**	*E (1300 °C)*	*E (Room Temp)*
		51 µm	3.16	1.854				**0.1**	**0.98**	430	450
Indent	**crack**	***a (mm)***	***a (mm)***	***l (mm)***	***c (mm)***	***Average c (mm)***	***B***	***F***	**K_{IC} (MPa.√m)**	**$H_{V\,(0.1)}$ (kg/mm2)**	**$H_{V\,(0.1)}$ (GPa)**
1	1	*0.0037*	0.0037	0.0043	0.0080	0.0078	0.34	-1.8	3.2	**3432**	**34**
	2	*0.0037*	0.0037	0.0050	0.0087		0.37	-1.8	3.0		
	3	***0.0037***	0.0037	0.0043	0.0079		0.33	-1.8	3.2		
	4		0.0037	0.0030	0.0067		0.26	-1.7	3.5		
2	5	0.0037	0.0031	0.0036	0.0067	0.0082	0.33	-1.8	4.1	**3527**	**35**
	6	0.0036	0.0031	0.0059	0.0090		0.46	-1.9	3.1		
	7	***0.0036***	0.0031	0.0059	0.0090		0.46	-1.9	3.1		
	8		0.0031	0.0050	0.0081		0.41	-1.8	3.5		
3	9	0.0035	0.0036	0.0055	0.0091	0.0077	0.40	-1.8	2.9	**3522**	**35**
	10	0.0037	0.0036	0.0045	0.0081		0.35	-1.8	3.2		
	11	***0.0036***	0.0036	0.0031	0.0067		0.27	-1.7	3.5		
	12		0.0036	0.0034	0.0070		0.28	-1.7	3.5		
4	13	0.0037	0.0037	0.0040	0.0077	0.0078	0.32	-1.7	3.3	**3479**	**34**
	14	0.0037	0.0037	0.0048	0.0085		0.36	-1.8	3.1		
	15	***0.0037***	0.0037	0.0040	0.0076		0.32	-1.7	3.3		
	16		0.0037	0.0037	0.0074		0.31	-1.7	3.4		
5	17	0.0037	0.0036	0.0058	0.0094	0.0080	0.42	-1.8	2.8	**3557**	**35**
	18	0.0035	0.0036	0.0054	0.0090		0.40	-1.8	2.9		
	19	***0.0036***	0.0036	0.0030	0.0066		0.26	-1.7	3.6		
	20		0.0036	0.0034	0.0070		0.29	-1.7	3.5		
6	21	0.0038	0.0037	0.0051	0.0088	0.0078	0.38	-1.8	3.0	**3409**	**34**
	22	0.0036	0.0037	0.0048	0.0085		0.36	-1.8	3.1		
	23	***0.0037***	0.0037	0.0030	0.0067		0.26	-1.7	3.5		
	24		0.0037	0.0037	0.0073		0.30	-1.7	3.4		
7	25	0.0034	0.0036	0.0063	0.0099	0.0082	0.44	-1.8	2.6	**3652**	**36**
	26	0.0038	0.0036	0.0063	0.0098		0.44	-1.8	2.7		
	27	***0.0036***	0.0036	0.0034	0.0069		0.29	-1.7	3.5		
	28		0.0036	0.0028	0.0063		0.25	-1.7	3.6		
8	29	0.0038	0.0036	0.0052	0.0088	0.0077	0.39	-1.8	3.0	**3493**	**34**
	30	0.0035	0.0036	0.0050	0.0086		0.37	-1.8	3.0		
	31	***0.0036***	0.0036	0.0028	0.0064		0.24	-1.7	3.6		
	32		0.0036	0.0034	0.0071		0.29	-1.7	3.4		
9	33	0.0038	0.0036	0.0059	0.0095	0.0079	0.42	-1.8	2.8	**3518**	**35**
	34	0.0035	0.0036	0.0058	0.0094		0.41	-1.8	2.8		
	35	***0.0036***	0.0036	0.0020	0.0056		0.19	-1.7	3.8		
	36		0.0036	0.0034	0.0070		0.29	-1.7	3.4		
10	37	0.0038	0.0037	0.0050	0.0087	0.0077	0.37	-1.8	3.0	**3340**	**33**
	38	0.0037	0.0037	0.0040	0.0077		0.32	-1.7	3.3		
	39	***0.0037***	0.0037	0.0040	0.0078		0.32	-1.7	3.2		
	40		0.0037	0.0030	0.0068		0.26	-1.7	3.5		

Indent	crack	*a (mm)*	*a (mm)*	*l (mm)*	*c (mm)*	*Average c (mm)*	*B*	*F*	K_{IC} (MPa.√m)	$H_{V\ (0.1)}$ (kg/mm2)	$H_{V\ (0.1)}$ (GPa)
11	41	*0.0036*	0.0034	0.0044	0.0078	0.0078	0.36	-1.8	3.4	**3527**	**35**
	42	*0.0037*	0.0034	0.0046	0.0080		0.37	-1.8	3.3		
	43	***0.0036***	0.0034	0.0041	0.0075		0.34	-1.8	3.5		
	44		0.0034	0.0046	0.0080		0.37	-1.8	3.4		
12	45	0.0039	0.0037	0.0046	0.0083	0.0084	0.35	-1.8	3.1	**3390**	**33**
	46	0.0035	0.0037	0.0049	0.0086		0.37	-1.8	3.0		
	47	***0.0037***	0.0037	0.0046	0.0083		0.35	-1.8	3.1		
	48		0.0037	0.0045	0.0082		0.34	-1.8	3.1		
13	49	0.0037	0.0039	0.0056	0.0095	0.0083	0.39	-1.8	2.8	**3127**	**31**
	50	0.0040	0.0039	0.0055	0.0093		0.38	-1.8	2.9		
	51	***0.0039***	0.0039	0.0036	0.0075		0.29	-1.7	3.3		
	52		0.0039	0.0032	0.0071		0.26	-1.7	3.4		
14	53	0.0037	0.0036	0.0059	0.0095	0.0081	0.42	-1.8	2.8	**3557**	**35**
	54	0.0036	0.0036	0.0048	0.0084		0.37	-1.8	3.1		
	55	***0.0036***	0.0036	0.0037	0.0073		0.31	-1.7	3.4		
	56		0.0036	0.0034	0.0071		0.29	-1.7	3.4		
15	57	0.0038	0.0038	0.0033	0.0071	0.0080	0.27	-1.7	3.4	**3214**	**32**
	58	0.0038	0.0038	0.0056	0.0094		0.40	-1.8	2.8		
	59	***0.0038***	0.0038	0.0031	0.0069		0.26	-1.7	3.5		
	60		0.0038	0.0050	0.0088		0.36	-1.8	3.0		
16	61	0.0033	0.0036	0.0048	0.0083	0.0075	0.37	-1.8	3.1	**3662**	**36**
	62	0.0038	0.0036	0.0038	0.0073		0.31	-1.7	3.4		
	63	***0.0036***	0.0036	0.0023	0.0059		0.22	-1.7	3.8		
	64		0.0036	0.0050	0.0085		0.38	-1.8	3.0		
17	65	0.0036	0.0036	0.0060	0.0095	0.0085	0.43	-1.8	2.8	**3647**	**36**
	66	0.0036	0.0036	0.0062	0.0097		0.44	-1.8	2.7		
	67	***0.0036***	0.0036	0.0042	0.0078		0.34	-1.8	3.3		
	68		0.0036	0.0036	0.0071		0.30	-1.7	3.4		
18	69	0.0040	0.0038	0.0059	0.0097	0.0088	0.41	-1.8	2.8	**3292**	**32**
	70	0.0036	0.0038	0.0058	0.0096		0.41	-1.8	2.8		
	71	***0.0038***	0.0038	0.0040	0.0078		0.32	-1.7	3.2		
	72		0.0038	0.0043	0.0080		0.33	-1.8	3.2		
19	73	0.0039	0.0039	0.0065	0.0104	0.0094	0.43	-1.8	2.6	**3036**	**30**
	74	0.0039	0.0039	0.0053	0.0092		0.37	-1.8	2.9		
	75	***0.0039***	0.0039	0.0044	0.0083		0.33	-1.7	3.1		
	76		0.0039	0.0059	0.0098		0.40	-1.8	2.7		
20	77	0.0037	0.0039	0.0058	0.0096	0.0086	0.40	-1.8	2.8	**3119**	**31**
	78	0.0040	0.0039	0.0058	0.0096		0.40	-1.8	2.8		
	79	***0.0039***	0.0039	0.0039	0.0078		0.30	-1.7	3.2		
	80		0.0039	0.0035	0.0073		0.28	-1.7	3.3		
21	81	*0.0038*	0.0038	0.0047	0.0085	0.0076	0.34	-1.8	3.1	**3139**	**31**
	82	*0.0039*	0.0038	0.0039	0.0078		0.31	-1.7	3.2		
	83	***0.0038***	0.0038	0.0035	0.0074		0.28	-1.7	3.3		
	84		0.0038	0.0030	0.0069		0.25	-1.7	3.4		

Indent	crack	*a (mm)*	*a (mm)*	*l (mm)*	*c (mm)*	*Average c (mm)*	*B*	*F*	K_{IC} (MPa.√m)	$H_{V\ (0.1)}$ (kg/mm2)	$H_{V\ (0.1)}$ (GPa)
22	85	0.0040	0.0040	0.0045	0.0085	0.0078	0.33	-1.8	3.1	**2922**	**29**
	86	0.0040	0.0040	0.0051	0.0091		0.36	-1.8	2.9		
	87	***0.0040***	0.0040	0.0027	0.0067		0.22	-1.7	3.5		
	88		0.0040	0.0031	0.0071		0.25	-1.7	3.4		
23	89	0.0036	0.0036	0.0055	0.0091	0.0081	0.40	-1.8	2.9	**3508**	**34**
	90	0.0037	0.0036	0.0045	0.0081		0.35	-1.8	3.2		
	91	***0.0036***	0.0036	0.0045	0.0081		0.35	-1.8	3.2		
	92		0.0036	0.0035	0.0072		0.29	-1.7	3.4		
24	93	0.0035	0.0036	0.0055	0.0091	0.0079	0.40	-1.8	2.9	**3552**	**35**
	94	0.0037	0.0036	0.0052	0.0088		0.39	-1.8	3.0		
	95	***0.0036***	0.0036	0.0033	0.0069		0.28	-1.7	3.5		
	96		0.0036	0.0030	0.0066		0.26	-1.7	3.6		
25	97	0.0039	0.0038	0.0047	0.0085	0.0082	0.35	-1.8	3.1	**3189**	**31**
	98	0.0037	0.0038	0.0049	0.0087		0.36	-1.8	3.0		
	99	***0.0038***	0.0038	0.0040	0.0078		0.31	-1.7	3.2		
	100		0.0038	0.0040	0.0078		0.31	-1.7	3.2		
26	101	0.0038	0.0038	0.0046	0.0084	0.0078	0.34	-1.8	3.1	**3240**	**32**
	102	0.0037	0.0038	0.0038	0.0076		0.30	-1.7	3.3		
	103	***0.0038***	0.0038	0.0040	0.0077		0.31	-1.7	3.2		
	104		0.0038	0.0037	0.0075		0.30	-1.7	3.3		
27	105	0.0038	0.0039	0.0046	0.0085	0.0082	0.34	-1.8	3.1	**3063**	**30**
	106	0.0040	0.0039	0.0056	0.0095		0.39	-1.8	2.8		
	107	***0.0039***	0.0039	0.0040	0.0079		0.31	-1.7	3.2		
	108		0.0039	0.0029	0.0068		0.24	-1.7	3.5		
28	109	0.0038	0.0038	0.0035	0.0073	0.0075	0.29	-1.7	3.4	**3261**	**32**
	110	0.0037	0.0038	0.0038	0.0076		0.31	-1.7	3.3		
	111	***0.0038***	0.0038	0.0034	0.0071		0.28	-1.7	3.4		
	112		0.0038	0.0040	0.0078		0.31	-1.7	3.2		
29	113	0.0039	0.0038	0.0047	0.0084	0.0080	0.35	-1.8	3.1	**3235**	**32**
	114	0.0036	0.0038	0.0059	0.0096		0.41	-1.8	2.8		
	115	***0.0038***	0.0038	0.0034	0.0072		0.28	-1.7	3.4		
	116		0.0038	0.0027	0.0065		0.24	-1.7	3.5		
30	117	0.0038	0.0038	0.0063	0.0101	0.0082	0.42	-1.8	2.6	**3197**	**31**
	118	0.0039	0.0038	0.0050	0.0088		0.36	-1.8	3.0		
	119	***0.0038***	0.0038	0.0039	0.0077		0.31	-1.7	3.2		
	120		0.0038	0.0024	0.0062		0.21	-1.7	3.6		
31	121	*0.0039*	0.0039	0.0066	0.0104	0.0089	0.43	-1.8	2.6	**3075**	**30**
	122	*0.0038*	0.0039	0.0060	0.0099		0.41	-1.8	2.7		
	123	***0.0039***	0.0039	0.0037	0.0076		0.29	-1.7	3.3		
	124		0.0039	0.0038	0.0077		0.30	-1.7	3.3		
32	125	0.0038	0.0038	0.0040	0.0078	0.0073	0.31	-1.7	3.2	**3261**	**32**
	126	0.0038	0.0038	0.0032	0.0070		0.27	-1.7	3.4		
	127	***0.0038***	0.0038	0.0033	0.0070		0.27	-1.7	3.4		
	128		0.0038	0.0038	0.0075		0.30	-1.7	3.3		

Indent	crack	*a (mm)*	*a (mm)*	*l (mm)*	*c (mm)*	*Average c (mm)*	*B*	*F*	K_{IC} (MPa.√m)	$H_{V\ (0.1)}$ (kg/mm2)	$H_{V\ (0.1)}$ (GPa)
33	129	0.0038	0.0038	0.0044	0.0082	0.0079	0.33	-1.8	3.1	**3261**	**32**
	130	0.0038	0.0038	0.0045	0.0082		0.34	-1.8	3.1		
	131	***0.0038***	0.0038	0.0045	0.0082		0.34	-1.8	3.1		
	132		0.0038	0.0034	0.0072		0.28	-1.7	3.4		
34	133	0.0036	0.0037	0.0047	0.0084	0.0081	0.36	-1.8	3.1	**3404**	**33**
	134	0.0038	0.0037	0.0048	0.0085		0.36	-1.8	3.0		
	135	***0.0037***	0.0037	0.0047	0.0084		0.35	-1.8	3.1		
	136		0.0037	0.0036	0.0073		0.30	-1.7	3.4		
35	137	0.0036	0.0035	0.0041	0.0076	0.0077	0.33	-1.8	3.3	**3720**	**37**
	138	0.0035	0.0035	0.0050	0.0085		0.38	-1.8	3.1		
	139	***0.0035***	0.0035	0.0032	0.0067		0.28	-1.7	3.5		
	140		0.0035	0.0043	0.0078		0.34	-1.8	3.3		
36	141	0.0037	0.0036	0.0049	0.0085	0.0082	0.37	-1.8	3.0	**3532**	**35**
	142	0.0036	0.0036	0.0055	0.0091		0.40	-1.8	2.9		
	143	***0.0036***	0.0036	0.0034	0.0070		0.29	-1.7	3.4		
	144		0.0036	0.0046	0.0082		0.36	-1.8	3.1		
37	145	0.0038	0.0038	0.0048	0.0087	0.0084	0.36	-1.8	3.0	**3168**	**31**
	146	0.0038	0.0038	0.0046	0.0084		0.34	-1.8	3.1		
	147	***0.0038***	0.0038	0.0040	0.0079		0.31	-1.7	3.2		
	148		0.0038	0.0047	0.0085		0.35	-1.8	3.1		
38	149	0.0040	0.0040	0.0047	0.0087	0.0079	0.34	-1.8	3.0	**2868**	**28**
	150	0.0040	0.0040	0.0047	0.0087		0.34	-1.8	3.0		
	151	***0.0040***	0.0040	0.0032	0.0072		0.25	-1.7	3.3		
	152		0.0040	0.0032	0.0072		0.25	-1.7	3.3		
39	153	0.0036	0.0037	0.0049	0.0086	0.0077	0.37	-1.8	3.0	**3390**	**33**
	154	0.0038	0.0037	0.0039	0.0076		0.31	-1.7	3.3		
	155	***0.0037***	0.0037	0.0026	0.0063		0.23	-1.7	3.6		
	156		0.0037	0.0045	0.0082		0.35	-1.8	3.1		
40	157	0.0035	0.0035	0.0055	0.0090	0.0076	0.41	-1.8	2.9	**3709**	**36**
	158	0.0036	0.0035	0.0045	0.0080		0.35	-1.8	3.2		
	159	***0.0035***	0.0035	0.0033	0.0068		0.28	-1.7	3.5		
	160		0.0035	0.0032	0.0067		0.28	-1.7	3.5		
41	161	*0.0034*	0.0034	0.0043	0.0077	0.0074	0.36	-1.8	3.3	**3974**	**39**
	162	*0.0035*	0.0034	0.0044	0.0078		0.36	-1.8	3.2		
	163	***0.0034***	0.0034	0.0035	0.0069		0.31	-1.7	3.5		
	164		0.0034	0.0035	0.0070		0.31	-1.7	3.5		
42	165	0.0039	0.0038	0.0042	0.0080	0.0078	0.32	-1.7	3.2	**3180**	**31**
	166	0.0038	0.0038	0.0033	0.0071		0.27	-1.7	3.4		
	167	***0.0038***	0.0038	0.0038	0.0076		0.30	-1.7	3.3		
	168		0.0038	0.0046	0.0084		0.34	-1.8	3.1		
43	169	0.0038	0.0037	0.0063	0.0101	0.0082	0.43	-1.8	2.6	**3323**	**33**
	170	0.0037	0.0037	0.0048	0.0085		0.36	-1.8	3.1		
	171	***0.0037***	0.0037	0.0036	0.0073		0.29	-1.7	3.4		
	172		0.0037	0.0031	0.0069		0.26	-1.7	3.5		

Indent	crack	*a (mm)*	*a (mm)*	*l (mm)*	*c (mm)*	*Average c (mm)*	*B*	*F*	K_{IC} (MPa.√m)	$H_{V\ (0.1)}$ (kg/mm2)	$H_{V\ (0.1)}$ (GPa)
44	173	0.0038	0.0037	0.0051	0.0089	0.0078	0.38	-1.8	3.0	**3318**	**33**
	174	0.0037	0.0037	0.0032	0.0069		0.27	-1.7	3.5		
	175	***0.0037***	0.0037	0.0050	0.0087		0.37	-1.8	3.0		
	176		0.0037	0.0030	0.0067		0.25	-1.7	3.5		
45	177	0.0039	0.0038	0.0050	0.0087	0.0077	0.36	-1.8	3.0	**3223**	**32**
	178	0.0037	0.0038	0.0045	0.0083		0.34	-1.8	3.1		
	179	***0.0038***	0.0038	0.0032	0.0070		0.26	-1.7	3.4		
	180		0.0038	0.0031	0.0069		0.26	-1.7	3.4		
46	181	0.0037	0.0037	0.0053	0.0090	0.0076	0.39	-1.8	2.9	**3413**	**34**
	182	0.0037	0.0037	0.0042	0.0079		0.33	-1.8	3.2		
	183	***0.0037***	0.0037	0.0032	0.0068		0.27	-1.7	3.5		
	184		0.0037	0.0030	0.0067		0.26	-1.7	3.5		
47	185	0.0035	0.0036	0.0074	0.0110	0.0083	0.48	-1.9	2.4	**3591**	**35**
	186	0.0037	0.0036	0.0072	0.0108		0.48	-1.9	2.4		
	187	***0.0036***	0.0036	0.0022	0.0058		0.21	-1.7	3.8		
	188		0.0036	0.0022	0.0058		0.21	-1.7	3.8		
48	189	0.0038	0.0037	0.0045	0.0082	0.0076	0.35	-1.8	3.1	**3451**	**34**
	190	0.0036	0.0037	0.0047	0.0084		0.36	-1.8	3.1		
	191	***0.0037***	0.0037	0.0032	0.0068		0.27	-1.7	3.5		
	192		0.0037	0.0031	0.0068		0.27	-1.7	3.5		
49	193	0.0039	0.0037	0.0041	0.0078	0.0074	0.32	-1.7	3.2	**3314**	**33**
	194	0.0036	0.0037	0.0037	0.0075		0.30	-1.7	3.3		
	195	***0.0037***	0.0037	0.0036	0.0074		0.29	-1.7	3.3		
	196		0.0037	0.0033	0.0070		0.27	-1.7	3.4		
50	197	0.0037	0.0039	0.0055	0.0094	0.0082	0.38	-1.8	2.8	**3091**	**30**
	198	0.0041	0.0039	0.0042	0.0081		0.32	-1.7	3.2		
	199	***0.0039***	0.0039	0.0039	0.0078		0.30	-1.7	3.2		
	200		0.0039	0.0036	0.0075		0.28	-1.7	3.3		
51	201	*0.0039*	0.0038	0.0037	0.0076	0.0085	0.29	-1.7	3.3	**3139**	**31**
	202	*0.0038*	0.0038	0.0035	0.0074		0.28	-1.7	3.3		
	203	***0.0038***	0.0038	0.0063	0.0102		0.42	-1.8	2.6		
	204		0.0038	0.0050	0.0089		0.36	-1.8	3.0		
52	205	0.0038	0.0039	0.0060	0.0098	0.0088	0.41	-1.8	2.7	**3127**	**31**
	206	0.0039	0.0039	0.0066	0.0104		0.43	-1.8	2.6		
	207	***0.0039***	0.0039	0.0037	0.0076		0.29	-1.7	3.3		
	208		0.0039	0.0037	0.0076		0.29	-1.7	3.3		
53	209	0.0039	0.0039	0.0050	0.0089	0.0081	0.36	-1.8	3.0	**3051**	**30**
	210	0.0039	0.0039	0.0049	0.0088		0.36	-1.8	3.0		
	211	***0.0039***	0.0039	0.0035	0.0074		0.28	-1.7	3.3		
	212		0.0039	0.0035	0.0073		0.28	-1.7	3.3		
54	213	0.0035	0.0037	0.0052	0.0089	0.0084	0.38	-1.8	2.9	**3441**	**34**
	214	0.0039	0.0037	0.0047	0.0084		0.36	-1.8	3.1		
	215	***0.0037***	0.0037	0.0034	0.0071		0.29	-1.7	3.4		
	216		0.0037	0.0056	0.0093		0.40	-1.8	2.8		

Indent	crack	*a (mm)*	*a (mm)*	*l (mm)*	*c (mm)*	*Average c (mm)*	*B*	*F*	K_{IC} (MPa.√m)	$H_{V\ (0.1)}$ (kg/mm2)	$H_{V\ (0.1)}$ (GPa)
55	217	0.0038	0.0038	0.0070	0.0108	0.0092	0.45	-1.9	2.5	**3214**	**32**
	218	0.0038	0.0038	0.0074	0.0112		0.47	-1.9	2.4		
	219	***0.0038***	0.0038	0.0037	0.0075		0.29	-1.7	3.3		
	220		0.0038	0.0037	0.0075		0.29	-1.7	3.3		
56	221	0.0039	0.0039	0.0057	0.0096	0.0087	0.39	-1.8	2.8	**3032**	**30**
	222	0.0039	0.0039	0.0047	0.0086		0.34	-1.8	3.0		
	223	***0.0039***	0.0039	0.0044	0.0083		0.33	-1.7	3.1		
	224		0.0039	0.0044	0.0083		0.33	-1.7	3.1		
57	225	0.0039	0.0040	0.0041	0.0081	0.0086	0.31	-1.7	3.1	**2933**	**29**
	226	0.0041	0.0040	0.0048	0.0088		0.34	-1.8	3.0		
	227	***0.0040***	0.0040	0.0050	0.0089		0.35	-1.8	3.0		
	228		0.0040	0.0048	0.0087		0.34	-1.8	3.0		
58	229	0.0042	0.0039	0.0046	0.0085	0.0086	0.34	-1.8	3.0	**3016**	**30**
	230	0.0036	0.0039	0.0043	0.0082		0.32	-1.7	3.1		
	231	***0.0039***	0.0039	0.0056	0.0095		0.38	-1.8	2.8		
	232		0.0039	0.0042	0.0081		0.32	-1.7	3.1		
59	233	0.0040	0.0039	0.0041	0.0079	0.0080	0.31	-1.7	3.2	**3055**	**30**
	234	0.0038	0.0039	0.0039	0.0078		0.30	-1.7	3.2		
	235	***0.0039***	0.0039	0.0042	0.0081		0.32	-1.7	3.1		
	236		0.0039	0.0042	0.0081		0.32	-1.7	3.1		
60	237	0.0040	0.0039	0.0034	0.0073	0.0075	0.27	-1.7	3.3	**3020**	**30**
	238	0.0039	0.0039	0.0036	0.0075		0.28	-1.7	3.3		
	239	***0.0039***	0.0039	0.0037	0.0076		0.29	-1.7	3.3		
	240		0.0039	0.0035	0.0075		0.28	-1.7	3.3		
61	241	*0.0038*	0.0038	0.0044	0.0082	0.0082	0.34	-1.8	3.1	**3296**	**32**
	242	*0.0037*	0.0038	0.0042	0.0079		0.33	-1.7	3.2		
	243	***0.0038***	0.0038	0.0043	0.0081		0.33	-1.8	3.2		
	244		0.0038	0.0050	0.0087		0.37	-1.8	3.0		
62	245	0.0036	0.0036	0.0052	0.0088	0.0084	0.39	-1.8	3.0	**3503**	**34**
	246	0.0037	0.0036	0.0050	0.0086		0.38	-1.8	3.0		
	247	***0.0036***	0.0036	0.0053	0.0089		0.39	-1.8	2.9		
	248		0.0036	0.0034	0.0070		0.29	-1.7	3.4		
63	249	0.0037	0.0038	0.0053	0.0091	0.0078	0.38	-1.8	2.9	**3244**	**32**
	250	0.0039	0.0038	0.0046	0.0084		0.35	-1.8	3.1		
	251	***0.0038***	0.0038	0.0029	0.0067		0.25	-1.7	3.5		
	252		0.0038	0.0033	0.0071		0.27	-1.7	3.4		
64	253	0.0038	0.0038	0.0036	0.0075	0.0073	0.29	-1.7	3.3	**3164**	**31**
	254	0.0038	0.0038	0.0037	0.0075		0.29	-1.7	3.3		
	255	***0.0038***	0.0038	0.0030	0.0068		0.25	-1.7	3.5		
	256		0.0038	0.0034	0.0072		0.28	-1.7	3.4		
65	257	0.0036	0.0036	0.0049	0.0085	0.0078	0.37	-1.8	3.1	**3547**	**35**
	258	0.0037	0.0036	0.0059	0.0095		0.42	-1.8	2.8		
	259	***0.0036***	0.0036	0.0032	0.0068		0.27	-1.7	3.5		
	260		0.0036	0.0030	0.0066		0.26	-1.7	3.6		

Indent	crack	*a (mm)*	*a (mm)*	*l (mm)*	*c (mm)*	*Average c (mm)*	*B*	*F*	K_{IC} (MPa.√m)	$H_{V\ (0.1)}$ (kg/mm^2)	$H_{V\ (0.1)}$ (GPa)
66	261	0.0038	0.0036	0.0055	0.0091	0.0081	0.40	-1.8	2.9	**3484**	**34**
	262	0.0035	0.0036	0.0050	0.0087		0.38	-1.8	3.0		
	263	***0.0036***	0.0036	0.0044	0.0080		0.34	-1.8	3.2		
	264		0.0036	0.0028	0.0065		0.25	-1.7	3.6		
67	265	0.0039	0.0039	0.0057	0.0096	0.0093	0.39	-1.8	2.8	**3047**	**30**
	266	0.0039	0.0039	0.0064	0.0103		0.42	-1.8	2.6		
	267	***0.0039***	0.0039	0.0035	0.0074		0.28	-1.7	3.3		
	268		0.0039	0.0059	0.0098		0.40	-1.8	2.7		
68	269	0.0036	0.0038	0.0044	0.0082	0.0077	0.34	-1.8	3.1	**3278**	**32**
	270	0.0039	0.0038	0.0040	0.0078		0.31	-1.7	3.2		
	271	***0.0038***	0.0038	0.0041	0.0078		0.32	-1.7	3.2		
	272		0.0038	0.0033	0.0070		0.27	-1.7	3.4		
69	273	0.0036	0.0036	0.0062	0.0098	0.0082	0.43	-1.8	2.7	**3489**	**34**
	274	0.0037	0.0036	0.0039	0.0075		0.31	-1.7	3.3		
	275	***0.0036***	0.0036	0.0036	0.0072		0.30	-1.7	3.4		
	276		0.0036	0.0046	0.0083		0.36	-1.8	3.1		
70	277	0.0037	0.0038	0.0036	0.0074	0.0081	0.29	-1.7	3.3	**3210**	**32**
	278	0.0039	0.0038	0.0043	0.0081		0.33	-1.7	3.2		
	279	***0.0038***	0.0038	0.0041	0.0079		0.32	-1.7	3.2		
	280		0.0038	0.0051	0.0089		0.37	-1.8	2.9		
71	281	*0.0038*	0.0039	0.0059	0.0098	0.0086	0.40	-1.8	2.7	**3103**	**31**
	282	*0.0040*	0.0039	0.0059	0.0098		0.40	-1.8	2.7		
	283	***0.0039***	0.0039	0.0037	0.0076		0.29	-1.7	3.3		
	284		0.0039	0.0032	0.0071		0.26	-1.7	3.4		
72	285	0.0034	0.0035	0.0057	0.0092	0.0077	0.42	-1.8	2.8	**3730**	**37**
	286	0.0037	0.0035	0.0056	0.0091		0.41	-1.8	2.9		
	287	***0.0035***	0.0035	0.0026	0.0061		0.24	-1.7	3.7		
	288		0.0035	0.0027	0.0062		0.25	-1.7	3.7		
73	289	0.0036	0.0036	0.0054	0.0090	0.0077	0.40	-1.8	2.9	**3527**	**35**
	290	0.0037	0.0036	0.0039	0.0076		0.32	-1.7	3.3		
	291	***0.0036***	0.0036	0.0036	0.0072		0.30	-1.7	3.4		
	292		0.0036	0.0033	0.0069		0.28	-1.7	3.5		
74	293	0.0039	0.0039	0.0030	0.0069	0.0084	0.25	-1.7	3.4	**3028**	**30**
	294	0.0039	0.0039	0.0040	0.0079		0.30	-1.7	3.2		
	295	***0.0039***	0.0039	0.0055	0.0094		0.38	-1.8	2.8		
	296		0.0039	0.0054	0.0093		0.38	-1.8	2.9		
75	297	0.0036	0.0036	0.0036	0.0073	0.0082	0.30	-1.7	3.4	**3498**	**34**
	298	0.0037	0.0036	0.0035	0.0071		0.29	-1.7	3.4		
	299	***0.0036***	0.0036	0.0057	0.0093		0.41	-1.8	2.8		
	300		0.0036	0.0054	0.0090		0.39	-1.8	2.9		
76	301	0.0037	0.0037	0.0044	0.0082	0.0082	0.34	-1.8	3.1	**3323**	**33**
	302	0.0038	0.0037	0.0042	0.0079		0.33	-1.7	3.2		
	303	***0.0037***	0.0037	0.0043	0.0080		0.33	-1.8	3.2		
	304		0.0037	0.0050	0.0088		0.37	-1.8	3.0		

Indent	crack	*a (mm)*	*a (mm)*	*l (mm)*	*c (mm)*	*Average c (mm)*	*B*	*F*	K_{IC} (MPa.√m)	$H_{V\ (0.1)}$ (kg/mm2)	$H_{V(0.1)}$ (GPa)
77	305	0.0038	0.0038	0.0049	0.0086	0.0081	0.36	-1.8	3.0	**3278**	**32**
	306	0.0037	0.0038	0.0043	0.0080		0.33	-1.8	3.2		
	307	***0.0038***	0.0038	0.0046	0.0084		0.35	-1.8	3.1		
	308		0.0038	0.0035	0.0072		0.28	-1.7	3.4		
78	309	0.0036	0.0038	0.0045	0.0082	0.0078	0.34	-1.8	3.1	**3265**	**32**
	310	0.0039	0.0038	0.0046	0.0084		0.35	-1.8	3.1		
	311	***0.0038***	0.0038	0.0031	0.0069		0.26	-1.7	3.5		
	312		0.0038	0.0038	0.0076		0.30	-1.7	3.3		
79	313	0.0037	0.0037	0.0041	0.0079	0.0077	0.32	-1.7	3.2	**3314**	**33**
	314	0.0037	0.0037	0.0033	0.0070		0.27	-1.7	3.4		
	315	***0.0037***	0.0037	0.0035	0.0072		0.28	-1.7	3.4		
	316		0.0037	0.0049	0.0087		0.37	-1.8	3.0		
80	317	0.0038	0.0037	0.0049	0.0086	0.0085	0.36	-1.8	3.0	**3300**	**32**
	318	0.0037	0.0037	0.0047	0.0084		0.35	-1.8	3.1		
	319	***0.0037***	0.0037	0.0040	0.0077		0.32	-1.7	3.2		
	320		0.0037	0.0054	0.0091		0.39	-1.8	2.9		
81	321	*0.0039*	0.0039	0.0039	0.0079	0.0082	0.30	-1.7	3.2	**2993**	**29**
	322	*0.0040*	0.0039	0.0039	0.0079		0.30	-1.7	3.2		
	323	***0.0039***	0.0039	0.0045	0.0084		0.33	-1.8	3.1		
	324		0.0039	0.0046	0.0086		0.34	-1.8	3.0		
82	325	0.0038	0.0039	0.0063	0.0102	0.0078	0.42	-1.8	2.6	**3127**	**31**
	326	0.0039	0.0039	0.0038	0.0077		0.30	-1.7	3.3		
	327	***0.0039***	0.0039	0.0037	0.0076		0.29	-1.7	3.3		
	328		0.0039	0.0020	0.0059		0.18	-1.7	3.7		
83	329	0.0038	0.0039	0.0042	0.0080	0.0078	0.32	-1.7	3.2	**3119**	**31**
	330	0.0039	0.0039	0.0037	0.0076		0.29	-1.7	3.3		
	331	***0.0039***	0.0039	0.0039	0.0078		0.31	-1.7	3.2		
	332		0.0039	0.0039	0.0078		0.31	-1.7	3.2		
84	333	0.0036	0.0035	0.0032	0.0067	0.0074	0.28	-1.7	3.6	**3844**	**38**
	334	0.0034	0.0035	0.0036	0.0070		0.31	-1.7	3.5		
	335	***0.0035***	0.0035	0.0041	0.0076		0.34	-1.8	3.3		
	336		0.0035	0.0047	0.0082		0.37	-1.8	3.1		
85	337	0.0039	0.0039	0.0071	0.0109	0.0086	0.45	-1.9	2.5	**3091**	**30**
	338	0.0038	0.0039	0.0069	0.0108		0.44	-1.8	2.5		
	339	***0.0039***	0.0039	0.0024	0.0063		0.21	-1.7	3.6		
	340		0.0039	0.0024	0.0063		0.21	-1.7	3.6		
86	341	0.0040	0.0039	0.0045	0.0084	0.0079	0.33	-1.8	3.1	**3001**	**29**
	342	0.0039	0.0039	0.0055	0.0094		0.38	-1.8	2.8		
	343	***0.0039***	0.0039	0.0028	0.0068		0.23	-1.7	3.5		
	344		0.0039	0.0030	0.0069		0.25	-1.7	3.4		
87	345	0.0037	0.0039	0.0050	0.0089	0.0077	0.36	-1.8	3.0	**3127**	**31**
	346	0.0040	0.0039	0.0032	0.0071		0.26	-1.7	3.4		
	347	***0.0039***	0.0039	0.0044	0.0083		0.33	-1.8	3.1		
	348		0.0039	0.0028	0.0066		0.23	-1.7	3.5		

Indent	crack	*a (mm)*	*a (mm)*	*l (mm)*	*c (mm)*	*Average c (mm)*	*B*	*F*	K_{IC} (MPa.√m)	$H_{V\ (0.1)}$ (kg/mm2)	$H_{V(0.1)}$ (GPa)
88	349	0.0039	0.0038	0.0039	0.0077	0.0077	0.30	-1.7	3.2	**3147**	**31**
	350	0.0038	0.0038	0.0038	0.0076		0.30	-1.7	3.3		
	351	***0.0038***	0.0038	0.0043	0.0082		0.33	-1.7	3.1		
	352		0.0038	0.0036	0.0075		0.29	-1.7	3.3		
89	353	0.0037	0.0038	0.0069	0.0107	0.0086	0.45	-1.8	2.5	**3147**	**31**
	354	0.0040	0.0038	0.0066	0.0104		0.43	-1.8	2.6		
	355	***0.0038***	0.0038	0.0031	0.0070		0.26	-1.7	3.4		
	356		0.0038	0.0025	0.0063		0.21	-1.7	3.6		
90	357	0.0037	0.0036	0.0058	0.0094	0.0077	0.41	-1.8	2.8	**3527**	**35**
	358	0.0035	0.0036	0.0065	0.0101		0.45	-1.8	2.6		
	359	***0.0036***	0.0036	0.0020	0.0056		0.19	-1.7	3.8		
	360		0.0036	0.0022	0.0058		0.21	-1.7	3.8		
91	361	*0.0039*	0.0039	0.0058	0.0097	0.0084	0.39	-1.8	2.8	**3005**	**30**
	362	*0.0039*	0.0039	0.0041	0.0080		0.31	-1.7	3.2		
	363	***0.0039***	0.0039	0.0049	0.0089		0.35	-1.8	3.0		
	364		0.0039	0.0030	0.0070		0.25	-1.7	3.4		
92	365	0.0039	0.0039	0.0041	0.0080	0.0081	0.31	-1.7	3.2	**2990**	**29**
	366	0.0040	0.0039	0.0036	0.0075		0.28	-1.7	3.3		
	367	***0.0039***	0.0039	0.0047	0.0086		0.34	-1.8	3.0		
	368		0.0039	0.0041	0.0080		0.31	-1.7	3.2		
93	369	0.0038	0.0038	0.0044	0.0082	0.0076	0.33	-1.8	3.1	**3139**	**31**
	370	0.0039	0.0038	0.0047	0.0086		0.35	-1.8	3.0		
	371	***0.0038***	0.0038	0.0022	0.0060		0.20	-1.7	3.7		
	372		0.0038	0.0038	0.0076		0.30	-1.7	3.3		
94	373	0.0036	0.0037	0.0055	0.0092	0.0079	0.40	-1.8	2.9	**3358**	**33**
	374	0.0038	0.0037	0.0039	0.0076		0.31	-1.7	3.3		
	375	***0.0037***	0.0037	0.0031	0.0068		0.26	-1.7	3.5		
	376		0.0037	0.0041	0.0078		0.32	-1.7	3.2		
95	377	0.0038	0.0039	0.0065	0.0103	0.0087	0.43	-1.8	2.6	**3083**	**30**
	378	0.0039	0.0039	0.0065	0.0104		0.43	-1.8	2.6		
	379	***0.0039***	0.0039	0.0034	0.0073		0.28	-1.7	3.3		
	380		0.0039	0.0028	0.0067		0.24	-1.7	3.5		
96	381	0.0043	0.0041	0.0054	0.0096	0.0089	0.36	-1.8	2.8	**2708**	**27**
	382	0.0040	0.0041	0.0051	0.0092		0.35	-1.8	2.9		
	383	***0.0041***	0.0041	0.0054	0.0095		0.36	-1.8	2.8		
	384		0.0041	0.0030	0.0071		0.24	-1.7	3.3		
97	385	0.0038	0.0038	0.0063	0.0101	0.0092	0.42	-1.8	2.6	**3189**	**31**
	386	0.0038	0.0038	0.0043	0.0081		0.33	-1.8	3.1		
	387	***0.0038***	0.0038	0.0046	0.0085		0.35	-1.8	3.1		
	388		0.0038	0.0064	0.0102		0.43	-1.8	2.6		
98	389	0.0037	0.0036	0.0031	0.0067	0.0069	0.27	-1.7	3.5	**3557**	**35**
	390	0.0036	0.0036	0.0029	0.0065		0.26	-1.7	3.6		
	391	***0.0036***	0.0036	0.0036	0.0072		0.30	-1.7	3.4		
	392		0.0036	0.0035	0.0071		0.30	-1.7	3.4		

Indent	crack	a (mm)	a (mm)	l (mm)	c (mm)	Average c (mm)	B	F	K_{IC} (MPa.√m)	$H_{V\ (0.1)}$ (kg/mm^2)	$H_{V(0.1)}$ (GPa)
99	393	0.0039	0.0038	0.0051	0.0089	0.0085	0.37	-1.8	3.0	**3227**	**32**
	394	0.0037	0.0038	0.0045	0.0083		0.34	-1.8	3.1		
	395	***0.0038***	0.0038	0.0045	0.0083		0.34	-1.8	3.1		
	396		0.0038	0.0047	0.0085		0.35	-1.8	3.1		
100	397	0.0036	0.0037	0.0024	0.0061	0.0078	0.21	-1.7	3.7	**3327**	**33**
	398	0.0039	0.0037	0.0043	0.0080		0.33	-1.8	3.2		
	399	***0.0037***	0.0037	0.0059	0.0096		0.41	-1.8	2.8		
	400		0.0037	0.0036	0.0073		0.29	-1.7	3.4		
Mean (μ)						0.0081			**3.17**		**32**
STDEVP (σ)						0.0005			**0.28**		**2.3**
99.9999713% Confidence Intervals			**μ - 5σ**						**1.75**		
			μ + 5σ						**4.58**		

Table 23: The Curved-Surface H_V and K_{IC} values of 51 µm CVD SiC sample (CPT-B-B10) at 100 g

Sample: CPT-B-B10		Thickness	Density	constant for HV			**Load**	**kg**	**N**	*E (1300oC)*	*E (Room Temp)*
		51 µm	3.16	1.854				**0.1**	**0.98**	430	450
Indent	**crack**	***2a (µm)***	***a (mm)***	***l (µm)***	***c (mm)***	***Average c (mm)***	***B***	***F***	***K_{IC} (MPa.√m)***	***$H_{V\ (0.1)}$ (kg/mm2)***	***$H_{V(0.1)}$ (GPa)***
1	1	8.1600	0.0042	2.66	0.0069	0.0067	0.21	-1.69	3.4	2640	26
	2	8.6000	0.0042	3.05	0.0072		0.24	-1.70	3.3		
	3	**8.3800**	0.0042	2.44	0.0066		0.20	-1.68	3.4		
	4		0.0042	1.92	0.0061		0.16	-1.67	3.6		
2	5	8.0100	0.0041	2.60	0.0067	0.0067	0.21	-1.69	3.5	2802	27
	6	8.2600	0.0041	2.47	0.0065		0.21	-1.69	3.6		
	7	**8.1350**	0.0041	2.40	0.0065		0.20	-1.68	3.6		
	8		0.0041	3.10	0.0072		0.25	-1.71	3.4		
3	9	7.5600	0.0038	2.76	0.0066	0.0063	0.24	-1.70	3.8	3201	31
	10	7.6600	0.0038	2.10	0.0059		0.19	-1.68	4.0		
	11	**7.6100**	0.0038	2.46	0.0063		0.22	-1.69	3.9		
	12		0.0038	2.46	0.0063		0.22	-1.69	3.9		
4	13	8.4200	0.0041	2.16	0.0063	0.0063	0.18	-1.68	3.6	2711	27
	14	8.1200	0.0041	2.16	0.0063		0.18	-1.68	3.6		
	15	**8.2700**	0.0041	2.00	0.0061		0.17	-1.67	3.6		
	16		0.0041	2.22	0.0064		0.19	-1.68	3.6		
5	17	8.6500	0.0042	2.88	0.0071	0.0065	0.23	-1.70	3.3	2643	26
	18	8.1000	0.0042	2.03	0.0062		0.17	-1.67	3.6		
	19	**8.3750**	0.0042	2.20	0.0064		0.18	-1.68	3.5		
	20		0.0042	1.95	0.0061		0.17	-1.67	3.6		
6	21	8.4000	0.0041	2.38	0.0065	0.0063	0.20	-1.68	3.6	2774	27
	22	7.9500	0.0041	2.34	0.0064		0.20	-1.68	3.6		
	23	**8.1750**	0.0041	1.93	0.0060		0.17	-1.67	3.7		
	24		0.0041	2.17	0.0063		0.18	-1.68	3.6		
7	25	8.2100	0.0042	2.37	0.0066	0.0066	0.19	-1.68	3.4	2615	26
	26	8.6300	0.0042	2.99	0.0072		0.23	-1.70	3.3		
	27	**8.4200**	0.0042	2.57	0.0068		0.21	-1.69	3.4		
	28		0.0042	1.61	0.0058		0.14	-1.66	3.6		
8	29	8.4300	0.0041	2.79	0.0069	0.0064	0.22	-1.69	3.4	2701	26
	30	8.1400	0.0041	2.23	0.0064		0.19	-1.68	3.5		
	31	**8.2850**	0.0041	2.00	0.0061		0.17	-1.67	3.6		
	32		0.0041	2.09	0.0062		0.18	-1.67	3.6		
9	33	8.4700	0.0043	2.44	0.0067	0.0063	0.20	-1.68	3.4	2545	25
	34	8.6000	0.0043	1.52	0.0058		0.13	-1.65	3.6		
	35	**8.5350**	0.0043	1.59	0.0059		0.14	-1.65	3.6		
	36		0.0043	2.58	0.0068		0.21	-1.69	3.3		
10	37	8.9600	0.0043	2.01	0.0063	0.0066	0.17	-1.67	3.5	2536	25
	38	8.1400	0.0043	2.29	0.0066		0.19	-1.68	3.4		
	39	**8.5500**	0.0043	2.03	0.0063		0.17	-1.67	3.5		
	40		0.0043	2.91	0.0072		0.23	-1.70	3.2		

Indent	crack	2a (μm)	a (mm)	l (μm)	c (mm)	Average c (mm)	B	F	K_{IC} (MPa.√m)	$H_{V\ (0.1)}$ (kg/mm2)	$H_{V(0.1)}$ (GPa)
11	41	8.3900	0.0043	2.44	0.0067	0.0061	0.20	-1.68	3.3	2504	25
	42	8.8200	0.0043	1.44	0.0057		0.13	-1.65	3.6		
	43	**8.6050**	0.0043	1.95	0.0063		0.16	-1.67	3.4		
	44		0.0043	1.51	0.0058		0.13	-1.65	3.6		
12	45	8.8000	0.0042	2.59	0.0068	0.0066	0.21	-1.69	3.4	2628	26
	46	8.0000	0.0042	2.60	0.0068		0.21	-1.69	3.4		
	47	**8.4000**	0.0042	2.10	0.0063		0.18	-1.67	3.5		
	48		0.0042	2.22	0.0064		0.18	-1.68	3.5		
13	49	8.0900	0.0041	2.40	0.0065	0.0061	0.20	-1.68	3.6	2802	27
	50	8.1800	0.0041	1.78	0.0058		0.16	-1.66	3.8		
	51	**8.1350**	0.0041	2.08	0.0061		0.18	-1.67	3.7		
	52		0.0041	1.80	0.0059		0.16	-1.66	3.8		
14	53	8.8700	0.0044	2.22	0.0066	0.0076	0.18	-1.67	3.3	2408	24
	54	8.6800	0.0044	2.67	0.0071		0.21	-1.69	3.2		
	55	**8.7750**	0.0044	3.36	0.0077		0.25	-1.71	3.1		
	56		0.0044	4.75	0.0091		0.32	-1.74	2.8		
15	57	8.1000	0.0041	2.70	0.0068	0.0064	0.22	-1.69	3.5	2812	28
	58	8.1400	0.0041	3.37	0.0074		0.26	-1.71	3.4		
	59	**8.1200**	0.0041	2.05	0.0061		0.18	-1.67	3.7		
	60		0.0041	1.10	0.0052		0.10	-1.64	4.0		
16	61	8.1400	0.0040	1.66	0.0057	0.0060	0.15	-1.66	3.8	2847	28
	62	8.0000	0.0040	1.10	0.0051		0.10	-1.64	4.0		
	63	**8.0700**	0.0040	2.15	0.0062		0.19	-1.68	3.7		
	64		0.0040	2.91	0.0069		0.24	-1.70	3.5		
17	65	8.1000	0.0042	2.03	0.0062	0.0060	0.17	-1.67	3.6	2669	26
	66	8.5700	0.0042	2.32	0.0065		0.19	-1.68	3.5		
	67	**8.3350**	0.0042	1.50	0.0057		0.13	-1.65	3.7		
	68		0.0042	1.50	0.0057		0.13	-1.65	3.7		
18	69	8.5800	0.0043	2.36	0.0066	0.0065	0.19	-1.68	3.4	2566	25
	70	8.4200	0.0043	1.81	0.0061		0.15	-1.66	3.5		
	71	**8.5000**	0.0043	2.16	0.0064		0.18	-1.67	3.4		
	72		0.0043	2.74	0.0070		0.22	-1.69	3.3		
19	73	8.1700	0.0042	1.50	0.0057	0.0065	0.13	-1.65	3.7	2656	26
	74	8.5400	0.0042	2.45	0.0066		0.20	-1.68	3.5		
	75	**8.3550**	0.0042	2.61	0.0068		0.21	-1.69	3.4		
	76		0.0042	2.92	0.0071		0.23	-1.70	3.3		
20	77	8.5600	0.0042	2.12	0.0063	0.0063	0.18	-1.67	3.5	2643	26
	78	8.1900	0.0042	2.51	0.0067		0.20	-1.69	3.4		
	79	**8.3750**	0.0042	2.27	0.0065		0.19	-1.68	3.5		
	80		0.0042	1.60	0.0058		0.14	-1.66	3.7		
21	81	8.0000	0.0040	2.51	0.0065	0.0064	0.21	-1.69	3.6	2857	28
	82	8.1100	0.0040	2.51	0.0065		0.21	-1.69	3.6		
	83	**8.0550**	0.0040	2.62	0.0066		0.22	-1.69	3.6		
	84		0.0040	1.92	0.0059		0.17	-1.7	3.8		

Indent	crack	2a (μm)	a (mm)	l (μm)	c (mm)	Average c (mm)	B	F	K_{IC} (MPa.√m)	$H_{V\ (0.1)}$ (kg/mm2)	$H_{V(0.1)}$ (GPa)
22	85	8.1400	0.0041	1.90	0.0060	0.0067	0.16	-1.67	3.7	2737	27
	86	8.3200	0.0041	2.43	0.0065		0.20	-1.68	3.5		
	87	**8.2300**	0.0041	2.63	0.0067		0.21	-1.69	3.5		
	88		0.0041	3.41	0.0075		0.26	-1.71	3.3		
23	89	8.0000	0.0041	1.44	0.0056	0.0064	0.13	-1.65	3.8	2698	26
	90	8.5800	0.0041	3.67	0.0078		0.28	-1.72	3.2		
	91	**8.2900**	0.0041	2.37	0.0065		0.20	-1.68	3.5		
	92		0.0041	1.70	0.0058		0.15	-1.66	3.7		
24	93	8.5800	0.0042	2.63	0.0068	0.0068	0.21	-1.69	3.4	2631	26
	94	8.2100	0.0042	2.58	0.0068		0.21	-1.69	3.4		
	95	**8.3950**	0.0042	2.56	0.0068		0.21	-1.69	3.4		
	96		0.0042	2.70	0.0069		0.22	-1.69	3.4		
25	97	8.4200	0.0043	1.70	0.0060	0.0064	0.14	-1.66	3.5	2507	25
	98	8.7800	0.0043	2.31	0.0066		0.19	-1.68	3.4		
	99	**8.6000**	0.0043	2.31	0.0066		0.19	-1.68	3.4		
	100		0.0043	2.24	0.0065		0.18	-1.68	3.4		
26	101	8.2100	0.0042	2.26	0.0064	0.0062	0.19	-1.68	3.5	2650	26
	102	8.5200	0.0042	1.80	0.0060		0.16	-1.66	3.6		
	103	**8.3650**	0.0042	1.47	0.0057		0.13	-1.65	3.7		
	104		0.0042	2.48	0.0067		0.20	-1.68	3.4		
27	105	8.5700	0.0043	1.62	0.0059	0.0066	0.14	-1.66	3.6	2554	25
	106	8.4700	0.0043	2.48	0.0067		0.20	-1.68	3.4		
	107	**8.5200**	0.0043	2.60	0.0069		0.21	-1.69	3.3		
	108		0.0043	2.74	0.0070		0.22	-1.69	3.3		
28	109	8.1700	0.0041	2.08	0.0062	0.0061	0.18	-1.67	3.6	2711	27
	110	8.3700	0.0041	1.11	0.0052		0.10	-1.64	3.9		
	111	**8.2700**	0.0041	2.04	0.0062		0.17	-1.67	3.6		
	112		0.0041	2.63	0.0068		0.21	-1.69	3.5		
29	113	8.3500	0.0042	2.53	0.0067	0.0065	0.20	-1.69	3.4	2618	26
	114	8.4800	0.0042	2.29	0.0065		0.19	-1.68	3.5		
	115	**8.4150**	0.0042	2.05	0.0063		0.17	-1.67	3.5		
	116		0.0042	2.40	0.0066		0.20	-1.68	3.4		
30	117	8.6000	0.0043	2.16	0.0064	0.0065	0.18	-1.67	3.4	2545	25
	118	8.4700	0.0043	1.88	0.0061		0.16	-1.66	3.5		
	119	**8.5350**	0.0043	3.52	0.0078		0.26	-1.71	3.1		
	120		0.0043	1.48	0.0057		0.13	-1.65	3.6		
31	121	8.3500	0.0042	2.42	0.0067	0.0068	0.20	-1.68	3.4	2584	25
	122	8.5900	0.0042	2.62	0.0069		0.21	-1.69	3.4		
	123	**8.4700**	0.0042	2.75	0.0070		0.22	-1.69	3.3		
	124		0.0042	2.29	0.0065		0.19	-1.68	3.4		
32	125	8.6000	0.0043	1.86	0.0061	0.0063	0.16	-1.66	3.5	2536	25
	126	8.5000	0.0043	1.82	0.0061		0.15	-1.66	3.5		
	127	**8.5500**	0.0043	2.08	0.0064		0.17	-1.67	3.4		
	128		0.0043	2.27	0.0065		0.18	-1.68	3.4		

Indent	crack	2a (μm)	a (mm)	l (μm)	c (mm)	Average c (mm)	B	F	K_{IC} (MPa.√m)	$H_{V\ (0.1)}$ (kg/mm2)	$H_{V(0.1)}$ (GPa)
33	129	8.5000	0.0043	2.62	0.0069	0.0068	0.21	-1.69	3.3	2530	25
	130	8.6200	0.0043	2.62	0.0069		0.21	-1.69	3.3		
	131	**8.5600**	0.0043	2.65	0.0069		0.21	-1.69	3.3		
	132		0.0043	2.20	0.0065		0.18	-1.67	3.4		
34	133	8.2500	0.0041	2.51	0.0066	0.0067	0.21	-1.69	3.5	2708	27
	134	8.3000	0.0041	2.27	0.0064		0.19	-1.68	3.5		
	135	**8.2750**	0.0041	2.77	0.0069		0.22	-1.69	3.4		
	136		0.0041	2.73	0.0069		0.22	-1.69	3.4		
35	137	8.4400	0.0042	3.19	0.0074	0.0067	0.25	-1.71	3.3	2646	26
	138	8.3000	0.0042	2.59	0.0068		0.21	-1.69	3.4		
	139	**8.3700**	0.0042	2.17	0.0064		0.18	-1.67	3.5		
	140		0.0042	2.05	0.0062		0.17	-1.67	3.5		
36	141	8.2700	0.0042	2.50	0.0067	0.0066	0.20	-1.69	3.4	2637	26
	142	8.5000	0.0042	2.50	0.0067		0.20	-1.69	3.4		
	143	**8.3850**	0.0042	1.85	0.0060		0.16	-1.66	3.6		
	144		0.0042	2.89	0.0071		0.23	-1.70	3.3		
37	145	8.3300	0.0042	3.24	0.0074	0.0067	0.25	-1.71	3.3	2685	26
	146	8.2900	0.0042	1.75	0.0059		0.15	-1.66	3.7		
	147	**8.3100**	0.0042	2.71	0.0069		0.22	-1.69	3.4		
	148		0.0042	2.59	0.0067		0.21	-1.69	3.4		
38	149	8.3000	0.0041	2.07	0.0062	0.0070	0.18	-1.67	3.6	2761	27
	150	8.0900	0.0041	3.26	0.0074		0.25	-1.71	3.4		
	151	**8.1950**	0.0041	3.42	0.0075		0.26	-1.71	3.3		
	152		0.0041	2.99	0.0071		0.24	-1.70	3.4		
39	153	8.3200	0.0042	1.24	0.0054	0.0068	0.11	-1.64	3.8	2656	26
	154	8.3900	0.0042	2.87	0.0070		0.23	-1.70	3.4		
	155	**8.3550**	0.0042	3.52	0.0077		0.27	-1.72	3.2		
	156		0.0042	2.99	0.0072		0.23	-1.70	3.3		
40	157	8.1800	0.0041	2.46	0.0066	0.0068	0.20	-1.69	3.5	2747	27
	158	8.2500	0.0041	2.91	0.0070		0.23	-1.70	3.4		
	159	**8.2150**	0.0041	2.61	0.0067		0.21	-1.69	3.5		
	160		0.0041	2.70	0.0068		0.22	-1.69	3.5		
41	161	8.6300	0.0043	3.10	0.0074	0.0068	0.23	-1.70	3.2	2481	24
	162	8.6600	0.0043	2.50	0.0068		0.20	-1.68	3.3		
	163	**8.6450**	0.0043	2.23	0.0066		0.18	-1.67	3.4		
	164		0.0043	2.15	0.0065		0.18	-1.67	3.4		
42	165	8.6600	0.0043	2.17	0.0065	0.0068	0.18	-1.67	3.4	2518	25
	166	8.5000	0.0043	2.39	0.0067		0.19	-1.68	3.3		
	167	**8.5800**	0.0043	2.59	0.0069		0.21	-1.69	3.3		
	168		0.0043	2.83	0.0071		0.22	-1.69	3.2		
43	169	8.6800	0.0043	3.73	0.0080	0.0069	0.27	-1.72	3.1	2498	25
	170	8.5500	0.0043	2.70	0.0070		0.21	-1.69	3.3		
	171	**8.6150**	0.0043	2.26	0.0066		0.18	-1.68	3.4		
	172		0.0043	1.51	0.0058		0.13	-1.65	3.6		

Indent	crack	2a (μm)	a (mm)	l (μm)	c (mm)	Average c (mm)	B	F	K_{IC} (MPa.√m)	$H_{V\ (0.1)}$ (kg/mm2)	$H_{V(0.1)}$ (GPa)
44	173	8.7800	0.0043	3.91	0.0083	0.0075	0.28	-1.72	3.0	2461	24
	174	8.5800	0.0043	2.17	0.0065		0.18	-1.67	3.3		
	175	**8.6800**	0.0043	2.90	0.0072		0.22	-1.69	3.2		
	176		0.0043	3.70	0.0080		0.27	-1.72	3.0		
45	177	8.4800	0.0042	2.38	0.0066	0.0069	0.19	-1.68	3.4	2578	25
	178	8.4800	0.0042	2.05	0.0063		0.17	-1.67	3.5		
	179	**8.4800**	0.0042	2.46	0.0067		0.20	-1.68	3.4		
	180		0.0042	3.79	0.0080		0.28	-1.72	3.1		
46	181	8.5800	0.0043	1.59	0.0058	0.0067	0.14	-1.65	3.6	2560	25
	182	8.4400	0.0043	2.46	0.0067		0.20	-1.68	3.4		
	183	**8.5100**	0.0043	3.63	0.0079		0.27	-1.72	3.1		
	184		0.0043	2.26	0.0065		0.19	-1.68	3.4		
47	185	7.7000	0.0039	3.42	0.0073	0.0066	0.27	-1.72	3.5	3071	30
	186	7.8400	0.0039	3.12	0.0070		0.26	-1.71	3.6		
	187	**7.7700**	0.0039	1.96	0.0058		0.18	-1.67	3.9		
	188		0.0039	2.29	0.0062		0.20	-1.68	3.8		
48	189	8.8600	0.0043	1.68	0.0060	0.0064	0.14	-1.66	3.5	2484	24
	190	8.4200	0.0043	2.09	0.0064		0.17	-1.67	3.4		
	191	**8.6400**	0.0043	1.80	0.0061		0.15	-1.66	3.5		
	192		0.0043	2.72	0.0070		0.21	-1.69	3.2		
49	193	8.4200	0.0042	2.36	0.0066	0.0066	0.19	-1.68	3.4	2606	26
	194	8.4500	0.0042	2.20	0.0064		0.18	-1.68	3.5		
	195	**8.4350**	0.0042	1.84	0.0061		0.16	-1.66	3.6		
	196		0.0042	3.10	0.0073		0.24	-1.70	3.3		
50	197	8.4500	0.0042	2.42	0.0066	0.0066	0.20	-1.68	3.5	2678	26
	198	8.1900	0.0042	2.50	0.0067		0.20	-1.69	3.5		
	199	**8.3200**	0.0042	2.31	0.0065		0.19	-1.68	3.5		
	200		0.0042	2.33	0.0065		0.19	-1.68	3.5		
51	201	8.2700	0.0041	2.61	0.0068	0.0063	0.21	-1.69	3.5	2698	26
	202	8.3100	0.0041	2.42	0.0066		0.20	-1.68	3.5		
	203	**8.2900**	0.0041	1.95	0.0061		0.17	-1.67	3.6		
	204		0.0041	1.67	0.0058		0.15	-1.66	3.7		
52	205	8.3500	0.0042	1.82	0.0061	0.0067	0.16	-1.66	3.6	2590	25
	206	8.5700	0.0042	2.71	0.0069		0.22	-1.69	3.3		
	207	**8.4600**	0.0042	2.70	0.0069		0.21	-1.69	3.3		
	208		0.0042	2.55	0.0068		0.20	-1.69	3.4		
53	209	8.3700	0.0042	3.42	0.0076	0.0065	0.26	-1.71	3.2	2615	26
	210	8.4700	0.0042	1.87	0.0061		0.16	-1.66	3.6		
	211	**8.4200**	0.0042	1.88	0.0061		0.16	-1.66	3.6		
	212		0.0042	1.92	0.0061		0.16	-1.67	3.6		
54	213	8.9800	0.0043	1.36	0.0057	0.0066	0.12	-1.64	3.6	2501	25
	214	8.2400	0.0043	2.02	0.0063		0.17	-1.67	3.4		
	215	**8.6100**	0.0043	3.41	0.0077		0.25	-1.71	3.1		
	216		0.0043	2.25	0.0066		0.18	-1.68	3.4		

Indent	crack	2a (µm)	a (mm)	l (µm)	c (mm)	Average c (mm)	B	F	K_{IC} (MPa.√m)	$H_{V\ (0.1)}$ (kg/mm2)	$H_{V(0.1)}$ (GPa)
55	217	8.5200	0.0043	2.75	0.0070	0.0066	0.22	-1.69	3.3	2521	25
	218	8.6300	0.0043	2.85	0.0071		0.22	-1.69	3.2		
	219	**8.5750**	0.0043	1.66	0.0059		0.14	-1.66	3.5		
	220		0.0043	2.00	0.0063		0.17	-1.67	3.4		
56	221	8.8700	0.0043	1.41	0.0057	0.0068	0.12	-1.65	3.6	2464	24
	222	8.4800	0.0043	1.52	0.0059		0.13	-1.65	3.5		
	223	**8.6750**	0.0043	3.67	0.0080		0.27	-1.72	3.0		
	224		0.0043	3.27	0.0076		0.24	-1.70	3.1		
57	225	8.2700	0.0043	3.08	0.0074	0.0064	0.23	-1.70	3.2	2507	25
	226	8.9300	0.0043	1.94	0.0062		0.16	-1.67	3.5		
	227	**8.6000**	0.0043	1.03	0.0053		0.09	-1.63	3.7		
	228		0.0043	2.50	0.0068		0.20	-1.68	3.3		
58	229	8.8800	0.0044	1.17	0.0055	0.0065	0.10	-1.64	3.6	2424	24
	230	8.6100	0.0044	1.53	0.0059		0.13	-1.65	3.5		
	231	**8.7450**	0.0044	2.61	0.0070		0.20	-1.69	3.2		
	232		0.0044	3.01	0.0074		0.23	-1.70	3.1		
Mean (µ)						0.0066			**3.47**		**26**
STDEVP (σ)						0.0001			**0.19**		**1.4**
99.9999713% Confidence Intervals			**µ - 5σ**						**2.53**		**23**
			µ + 5σ						**4.40**		**29**

Table 24: The Curved-Surface H_V and K_{IC} values of 39 µm CVD SiC sample (CPT-T-G131) at 100 g

Sample: CPT-T-G131		Thickness	Density	constant for HV			Load	kg	N	*E (1300oC)*	*E (Room Temp)*
		39 □m	3.19	1.854				0.1	0.98	430	450
Indent	**crack**	***2a (µm)***	***a (mm)***	***l (µm)***	***c (mm)***	***Average c (mm)***	***B***	***F***	K_{IC} (MPa.√m)	$H_{V\ (0.1)}$ (kg/mm2)	$H_{V(0.1)}$ (GPa)
1	1	7.96	0.0040	4.11	0.0081	0.0083	0.31	-1.74	3.0	**2952**	**29**
	2	7.89	0.0040	3.68	0.0076		0.29	-1.73	3.1		
	3	**7.93**	0.0040	3.77	0.0077		0.29	-1.73	3.1		
	4		0.0040	5.68	0.0096		0.39	-1.79	2.6		
2	5	7.62	0.0038	5.40	0.0092	0.0084	0.38	-1.79	2.8	**3193**	**31**
	6	7.62	0.0038	3.68	0.0075		0.29	-1.73	3.2		
	7	**7.62**	0.0038	5.03	0.0088		0.37	-1.78	2.9		
	8		0.0038	4.16	0.0080		0.32	-1.75	3.1		
3	9	7.05	0.0036	5.88	0.0095	0.0086	0.42	-1.82	2.8	**3493**	**34**
	10	7.52	0.0036	3.87	0.0075		0.31	-1.74	3.4		
	11	**7.29**	0.0036	5.14	0.0088		0.38	-1.79	3.0		
	12		0.0036	4.96	0.0086		0.37	-1.78	3.1		
4	13	7.00	0.0034	3.48	0.0069	0.0071	0.31	-1.74	3.8	**4027**	**40**
	14	6.57	0.0034	3.71	0.0071		0.32	-1.75	3.7		
	15	**6.79**	0.0034	3.97	0.0074		0.34	-1.76	3.6		
	16		0.0034	3.58	0.0070		0.31	-1.74	3.8		
5	17	7.02	0.0036	4.47	0.0081	0.0081	0.35	-1.76	3.2	**3503**	**34**
	18	7.53	0.0036	4.86	0.0085		0.37	-1.78	3.1		
	19	**7.28**	0.0036	5.26	0.0089		0.39	-1.79	3.0		
	20		0.0036	3.09	0.0067		0.27	-1.72	3.6		
6	21	7.10	0.0035	3.95	0.0075	0.0075	0.33	-1.75	3.5	**3730**	**37**
	22	7.00	0.0035	2.95	0.0065		0.26	-1.71	3.8		
	23	**7.05**	0.0035	4.10	0.0076		0.34	-1.75	3.4		
	24		0.0035	4.74	0.0083		0.37	-1.78	3.2		
7	25	7.06	0.0036	4.09	0.0077	0.0079	0.33	-1.75	3.4	**3606**	**35**
	26	7.28	0.0036	5.15	0.0087		0.39	-1.79	3.1		
	27	**7.17**	0.0036	3.99	0.0076		0.32	-1.75	3.4		
	28		0.0036	3.96	0.0075		0.32	-1.75	3.4		
8	29	6.54	0.0035	3.89	0.0074	0.0076	0.33	-1.75	3.6	**3844**	**38**
	30	7.35	0.0035	3.22	0.0067		0.28	-1.73	3.8		
	31	**6.95**	0.0035	5.65	0.0091		0.42	-1.82	3.0		
	32		0.0035	3.62	0.0071		0.31	-1.74	3.6		
9	33	7.53	0.0037	4.48	0.0082	0.0075	0.34	-1.76	3.1	**3367**	**33**
	34	7.31	0.0037	3.24	0.0070		0.27	-1.72	3.5		
	35	**7.42**	0.0037	3.52	0.0072		0.29	-1.73	3.4		
	36		0.0037	3.77	0.0075		0.30	-1.74	3.3		
10	37	7.76	0.0039	3.67	0.0076	0.0077	0.29	-1.73	3.1	**3020**	**30**
	38	7.91	0.0039	4.17	0.0081		0.31	-1.74	3.0		
	39	**7.84**	0.0039	3.06	0.0070		0.25	-1.71	3.3		
	40		0.0039	4.18	0.0081		0.32	-1.74	3.0		

Indent	crack	2a (μm)	a (mm)	l (μm)	c (mm)	Average c (mm)	B	F	K_{IC} (MPa.√m)	$H_{V\ (0.1)}$ (kg/mm2)	$H_{V(0.1)}$ (GPa)
11	41	7.49	0.0038	5.89	0.0097	0.0084	0.41	-1.81	2.7	3252	32
	42	7.61	0.0038	4.43	0.0082		0.34	-1.76	3.1		
	43	**7.55**	0.0038	3.36	0.0071		0.28	-1.72	3.4		
	44		0.0038	4.74	0.0085		0.35	-1.77	3.0		
12	45	7.52	0.0039	4.49	0.0084	0.0079	0.33	-1.75	3.0	3032	30
	46	8.12	0.0039	4.37	0.0083		0.33	-1.75	3.0		
	47	**7.82**	0.0039	3.73	0.0076		0.29	-1.73	3.1		
	48		0.0039	3.19	0.0071		0.26	-1.71	3.2		
13	49	7.62	0.0039	4.98	0.0089	0.0087	0.36	-1.77	2.9	3087	30
	50	7.88	0.0039	3.80	0.0077		0.30	-1.73	3.1		
	51	**7.75**	0.0039	6.25	0.0101		0.42	-1.82	2.6		
	52		0.0039	4.26	0.0081		0.32	-1.75	3.0		
14	53	7.61	0.0038	2.98	0.0068	0.0081	0.25	-1.71	3.4	3189	31
	54	7.64	0.0038	5.73	0.0095		0.40	-1.80	2.7		
	55	**7.63**	0.0038	5.64	0.0095		0.39	-1.80	2.8		
	56		0.0038	2.70	0.0065		0.23	-1.70	3.5		
15	57	7.67	0.0037	5.39	0.0091	0.0081	0.39	-1.79	2.9	3318	33
	58	7.28	0.0037	4.16	0.0079		0.32	-1.75	3.2		
	59	**7.48**	0.0037	3.68	0.0074		0.30	-1.73	3.3		
	60		0.0037	4.15	0.0079		0.32	-1.75	3.2		
16	61	7.50	0.0038	5.14	0.0089	0.0081	0.37	-1.78	2.9	3235	32
	62	7.64	0.0038	4.19	0.0080		0.32	-1.75	3.1		
	63	**7.57**	0.0038	4.37	0.0082		0.33	-1.75	3.1		
	64		0.0038	3.64	0.0074		0.29	-1.73	3.3		
17	65	7.85	0.0040	3.87	0.0078	0.0087	0.30	-1.73	3.1	2971	29
	66	7.95	0.0040	5.30	0.0093		0.37	-1.78	2.7		
	67	**7.90**	0.0040	4.83	0.0088		0.35	-1.76	2.8		
	68		0.0040	5.00	0.0090		0.36	-1.77	2.8		
18	69	6.81	0.0035	4.95	0.0085	0.0075	0.38	-1.79	3.2	3768	37
	70	7.22	0.0035	4.47	0.0080		0.36	-1.77	3.3		
	71	**7.02**	0.0035	3.60	0.0071		0.31	-1.74	3.6		
	72		0.0035	2.91	0.0064		0.26	-1.71	3.8		
19	73	7.47	0.0037	3.37	0.0070	0.0075	0.28	-1.72	3.5	3474	34
	74	7.14	0.0037	4.38	0.0080		0.34	-1.76	3.2		
	75	**7.31**	0.0037	3.94	0.0076		0.32	-1.74	3.3		
	76		0.0037	3.81	0.0075		0.31	-1.74	3.4		
20	77	7.44	0.0037	4.58	0.0083	0.0081	0.35	-1.76	3.1	3309	32
	78	7.53	0.0037	5.55	0.0093		0.39	-1.80	2.8		
	79	**7.49**	0.0037	3.00	0.0067		0.26	-1.71	3.5		
	80		0.0037	4.11	0.0079		0.32	-1.75	3.2		
21	81	6.54	0.0035	4.08	0.0075	0.0080	0.34	-1.76	3.5	3872	38
	82	7.30	0.0035	4.05	0.0075		0.34	-1.76	3.5		
	83	**6.92**	0.0035	4.89	0.0084		0.38	-1.79	3.3		
	84		0.0035	5.08	0.0085		0.39	-1.80	3.2		

Indent	crack	2a (μm)	a (mm)	l (μm)	c (mm)	Average c (mm)	B	F	K_{IC} (MPa.√m)	$H_{V\ (0.1)}$ (kg/mm2)	$H_{V(0.1)}$ (GPa)
22	85	7.69	0.0038	5.17	0.0090	0.0086	0.37	-1.78	2.9	3180	31
	86	7.58	0.0038	4.87	0.0087		0.36	-1.77	3.0		
	87	**7.64**	0.0038	4.49	0.0083		0.34	-1.76	3.1		
	88		0.0038	4.68	0.0085		0.35	-1.76	3.0		
23	89	7.91	0.0039	4.32	0.0082	0.0086	0.32	-1.75	3.0	3071	30
	90	7.63	0.0039	5.50	0.0094		0.38	-1.79	2.8		
	91	**7.77**	0.0039	4.24	0.0081		0.32	-1.75	3.1		
	92		0.0039	4.77	0.0087		0.35	-1.76	2.9		
24	93	7.25	0.0037	5.52	0.0092	0.0084	0.40	-1.80	2.9	3358	33
	94	7.61	0.0037	4.04	0.0078		0.32	-1.74	3.3		
	95	**7.43**	0.0037	4.38	0.0081		0.34	-1.76	3.2		
	96		0.0037	4.69	0.0084		0.35	-1.77	3.1		
25	97	7.88	0.0039	5.97	0.0098	0.0086	0.40	-1.81	2.7	3087	30
	98	7.62	0.0039	3.80	0.0077		0.30	-1.73	3.2		
	99	**7.75**	0.0039	5.24	0.0091		0.37	-1.78	2.8		
	100		0.0039	3.71	0.0076		0.29	-1.73	3.2		
26	101	7.50	0.0038	4.92	0.0088	0.0087	0.36	-1.77	2.9	3135	31
	102	7.88	0.0038	5.16	0.0090		0.37	-1.78	2.9		
	103	**7.69**	0.0038	4.98	0.0088		0.36	-1.77	2.9		
	104		0.0038	4.16	0.0080		0.32	-1.74	3.1		
27	105	7.10	0.0036	2.77	0.0064	0.0078	0.25	-1.71	3.7	3503	34
	106	7.45	0.0036	4.87	0.0085		0.37	-1.78	3.1		
	107	**7.28**	0.0036	4.60	0.0082		0.35	-1.77	3.2		
	108		0.0036	4.39	0.0080		0.34	-1.76	3.3		
28	109	7.28	0.0037	6.04	0.0097	0.0084	0.42	-1.82	2.8	3390	33
	110	7.51	0.0037	4.11	0.0078		0.32	-1.75	3.3		
	111	**7.40**	0.0037	3.47	0.0072		0.29	-1.73	3.4		
	112		0.0037	5.30	0.0090		0.39	-1.79	3.0		
29	113	7.62	0.0037	4.53	0.0082	0.0073	0.35	-1.76	3.2	3358	33
	114	7.24	0.0037	4.19	0.0079		0.33	-1.75	3.2		
	115	**7.43**	0.0037	3.40	0.0071		0.28	-1.72	3.4		
	116		0.0037	2.02	0.0057		0.19	-1.68	3.8		
30	117	7.95	0.0038	5.16	0.0089	0.0081	0.38	-1.78	3.0	3283	32
	118	7.08	0.0038	4.69	0.0084		0.35	-1.77	3.1		
	119	**7.52**	0.0038	2.71	0.0065		0.24	-1.70	3.6		
	120		0.0038	4.65	0.0084		0.35	-1.76	3.1		
31	121	7.13	0.0036	3.84	0.0074	0.0078	0.32	-1.74	3.5	3571	35
	122	7.28	0.0036	5.5	0.0091		0.40	-1.81	3.0		
	123	**7.21**	0.0036	3.46	0.0071		0.29	-1.73	3.6		
	124		0.0036	4.01	0.0076		0.32	-1.75	3.4		
32	125	6.95	0.0035	4.61	0.0082	0.0075	0.36	-1.77	3.3	3693	36
	126	7.22	0.0035	3.83	0.0074		0.32	-1.74	3.5		
	127	**7.09**	0.0035	3.53	0.0071		0.30	-1.73	3.6		
	128		0.0035	3.98	0.0075		0.33	-1.75	3.5		

Indent	crack	2a (μm)	a (mm)	l (μm)	c (mm)	Average c (mm)	B	F	K_{IC} (MPa.√m)	$H_{V\ (0.1)}$ (kg/mm2)	$H_{V(0.1)}$ (GPa)
33	129	7.22	0.0037	4.37	0.0081	0.0075	0.34	-1.76	3.2	**3409**	**33**
	130	7.53	0.0037	3.97	0.0077		0.32	-1.74	3.3		
	131	**7.38**	0.0037	3.84	0.0075		0.31	-1.74	3.4		
	132		0.0037	3.19	0.0069		0.27	-1.72	3.5		
34	133	7.30	0.0036	3.96	0.0076	0.0079	0.32	-1.74	3.4	**3503**	**34**
	134	7.25	0.0036	4.08	0.0077		0.33	-1.75	3.4		
	135	**7.28**	0.0036	4.26	0.0079		0.34	-1.76	3.3		
	136		0.0036	4.94	0.0086		0.37	-1.78	3.1		
35	137	7.91	0.0039	5.79	0.0097	0.0091	0.40	-1.80	2.7	**3091**	**30**
	138	7.58	0.0039	4.77	0.0086		0.35	-1.76	3.0		
	139	**7.75**	0.0039	5.5	0.0094		0.38	-1.79	2.8		
	140		0.0039	5.03	0.0089		0.36	-1.77	2.9		
36	141	8.14	0.0040	4.04	0.0080	0.0082	0.30	-1.74	3.0	**2933**	**29**
	142	7.76	0.0040	4.28	0.0083		0.32	-1.74	3.0		
	143	**7.95**	0.0040	4.42	0.0084		0.32	-1.75	2.9		
	144		0.0040	4.14	0.0081		0.31	-1.74	3.0		
37	145	8.06	0.0039	5.13	0.0091	0.0086	0.36	-1.77	2.8	**2990**	**29**
	146	7.69	0.0039	3.27	0.0072		0.26	-1.71	3.2		
	147	**7.88**	0.0039	5.18	0.0091		0.36	-1.77	2.8		
	148		0.0039	5.15	0.0091		0.36	-1.77	2.8		
38	149	7.62	0.0039	5.61	0.0095	0.0091	0.39	-1.79	2.7	**3087**	**30**
	150	7.88	0.0039	3.88	0.0078		0.30	-1.73	3.2		
	151	**7.75**	0.0039	5.43	0.0093		0.38	-1.79	2.8		
	152		0.0039	5.97	0.0098		0.40	-1.81	2.7		
39	153	7.95	0.0039	4.17	0.0081	0.0087	0.31	-1.74	3.1	**3024**	**30**
	154	7.71	0.0039	5.12	0.0090		0.36	-1.77	2.8		
	155	**7.83**	0.0039	4.93	0.0088		0.35	-1.77	2.9		
	156		0.0039	4.9	0.0088		0.35	-1.77	2.9		
40	157	7.25	0.0036	5.38	0.0090	0.0077	0.40	-1.80	3.0	**3581**	**35**
	158	7.14	0.0036	4.37	0.0080		0.35	-1.76	3.3		
	159	**7.20**	0.0036	2.20	0.0058		0.21	-1.69	3.9		
	160		0.0036	4.37	0.0080		0.35	-1.76	3.3		
41	161	7.55	0.0038	3.97	0.0077	0.0077	0.31	-1.74	3.3	**3278**	**32**
	162	7.49	0.0038	4.06	0.0078		0.32	-1.74	3.2		
	163	**7.52**	0.0038	3.68	0.0074		0.30	-1.73	3.3		
	164		0.0038	3.85	0.0076		0.31	-1.74	3.3		
42	165	7.74	0.0036	2.51	0.0061	0.0073	0.23	-1.70	3.8	**3513**	**34**
	166	6.79	0.0036	4.99	0.0086		0.38	-1.78	3.1		
	167	**7.27**	0.0036	2.05	0.0057		0.19	-1.68	3.9		
	168		0.0036	5.07	0.0087		0.38	-1.79	3.1		
43	169	7.48	0.0037	4.78	0.0085	0.0072	0.36	-1.77	3.1	**3300**	**32**
	170	7.51	0.0037	2.50	0.0062		0.22	-1.69	3.6		
	171	**7.50**	0.0037	2.44	0.0062		0.22	-1.69	3.7		
	172		0.0037	3.94	0.0077		0.31	-1.74	3.3		

Indent	crack	2a (μm)	a (mm)	l (μm)	c (mm)	Average c (mm)	B	F	K_{IC} (MPa.√m)	$H_{V\ (0.1)}$ (kg/mm2)	$H_{V(0.1)}$ (GPa)
44	173	7.68	0.0038	3.74	0.0075	0.0072	0.30	-1.73	3.3	3292	32
	174	7.33	0.0038	3.41	0.0072		0.28	-1.72	3.4		
	175	**7.51**	0.0038	3.32	0.0071		0.28	-1.72	3.4		
	176		0.0038	3.27	0.0070		0.27	-1.72	3.4		
45	177	7.28	0.0036	3.99	0.0075	0.0078	0.33	-1.75	3.5	3662	36
	178	6.95	0.0036	3.67	0.0072		0.31	-1.74	3.6		
	179	**7.12**	0.0036	3.96	0.0075		0.32	-1.75	3.5		
	180		0.0036	5.49	0.0090		0.41	-1.81	3.0		
46	181	7.35	0.0037	3.55	0.0072	0.0074	0.29	-1.73	3.4	3432	34
	182	7.35	0.0037	3.96	0.0076		0.32	-1.74	3.3		
	183	**7.35**	0.0037	3.19	0.0069		0.27	-1.72	3.5		
	184		0.0037	4.18	0.0079		0.33	-1.75	3.3		
47	185	7.31	0.0036	3.48	0.0071	0.0076	0.29	-1.73	3.5	3498	34
	186	7.25	0.0036	4.94	0.0086		0.37	-1.78	3.1		
	187	**7.28**	0.0036	3.99	0.0076		0.32	-1.75	3.4		
	188		0.0036	3.56	0.0072		0.30	-1.73	3.5		
48	189	7.91	0.0039	5.01	0.0089	0.0087	0.36	-1.77	2.9	3091	30
	190	7.58	0.0039	4.79	0.0087		0.35	-1.76	2.9		
	191	**7.75**	0.0039	4.77	0.0086		0.35	-1.76	3.0		
	192		0.0039	4.78	0.0087		0.35	-1.76	2.9		
49	193	8.43	0.0042	5.51	0.0097	0.0091	0.36	-1.77	2.5	2600	26
	194	8.46	0.0042	4.17	0.0084		0.30	-1.73	2.8		
	195	**8.45**	0.0042	4.74	0.0090		0.33	-1.75	2.7		
	196		0.0042	5.06	0.0093		0.34	-1.76	2.6		
50	197	8.23	0.0040	5.32	0.0093	0.0085	0.37	-1.78	2.7	2926	29
	198	7.69	0.0040	3.74	0.0077		0.29	-1.73	3.1		
	199	**7.96**	0.0040	5.83	0.0098		0.39	-1.80	2.6		
	200		0.0040	3.19	0.0072		0.26	-1.71	3.2		
51	201	7.88	0.0039	4.44	0.0083	0.0084	0.33	-1.75	3.0	3087	30
	202	7.62	0.0039	3.80	0.0077		0.30	-1.73	3.2		
	203	**7.75**	0.0039	5.14	0.0090		0.37	-1.78	2.9		
	204		0.0039	4.64	0.0085		0.34	-1.76	3.0		
52	205	7.71	0.0039	4.11	0.0080	0.0086	0.31	-1.74	3.1	3024	30
	206	7.95	0.0039	4.96	0.0089		0.36	-1.77	2.9		
	207	**7.83**	0.0039	5.09	0.0090		0.36	-1.77	2.8		
	208		0.0039	4.46	0.0084		0.33	-1.75	3.0		
53	209	7.95	0.0039	5.14	0.0091	0.0088	0.36	-1.77	2.8	3024	30
	210	7.71	0.0039	6.34	0.0103		0.42	-1.82	2.5		
	211	**7.83**	0.0039	5.09	0.0090		0.36	-1.77	2.8		
	212		0.0039	2.82	0.0067		0.24	-1.70	3.4		
54	213	6.92	0.0037	4.77	0.0085	0.0086	0.36	-1.77	3.1	3377	33
	214	7.90	0.0037	5.13	0.0088		0.38	-1.78	3.0		
	215	**7.41**	0.0037	4.99	0.0087		0.37	-1.78	3.0		
	216		0.0037	4.75	0.0085		0.36	-1.77	3.1		

Indent	crack	2a (μm)	a (mm)	l (μm)	c (mm)	Average c (mm)	B	F	K_{IC} (MPa.√m)	$H_{V\ (0.1)}$ (kg/mm2)	$H_{V(0.1)}$ (GPa)
55	217	8.02	0.0039	4.38	0.0083	0.0089	0.33	-1.75	3.0	3009	30
	218	7.68	0.0039	6.13	0.0101		0.41	-1.81	2.6		
	219	**7.85**	0.0039	5.59	0.0095		0.38	-1.79	2.7		
	220		0.0039	3.99	0.0079		0.30	-1.74	3.1		
56	221	7.71	0.0040	5.37	0.0093	0.0090	0.37	-1.78	2.7	2937	29
	222	8.18	0.0040	3.42	0.0074		0.27	-1.72	3.1		
	223	**7.95**	0.0040	6.41	0.0104		0.42	-1.82	2.5		
	224		0.0040	4.89	0.0089		0.35	-1.76	2.8		
57	225	7.28	0.0037	6.07	0.0098	0.0089	0.42	-1.82	2.7	3418	34
	226	7.45	0.0037	5.24	0.0089		0.38	-1.79	3.0		
	227	**7.37**	0.0037	5.63	0.0093		0.40	-1.81	2.9		
	228		0.0037	3.76	0.0074		0.31	-1.74	3.4		
58	229	7.71	0.0038	4.49	0.0083	0.0085	0.34	-1.76	3.0	3160	31
	230	7.61	0.0038	4.66	0.0085		0.35	-1.76	3.0		
	231	**7.66**	0.0038	4.33	0.0082		0.33	-1.75	3.1		
	232		0.0038	5.25	0.0091		0.37	-1.78	2.8		
59	233	7.68	0.0038	4.36	0.0082	0.0083	0.33	-1.75	3.1	3147	31
	234	7.67	0.0038	3.39	0.0072		0.27	-1.72	3.3		
	235	**7.68**	0.0038	4.35	0.0082		0.33	-1.75	3.1		
	236		0.0038	5.80	0.0096		0.40	-1.80	2.7		
60	237	7.71	0.0039	5.09	0.0090	0.0087	0.36	-1.77	2.8	3079	30
	238	7.81	0.0039	5.17	0.0091		0.37	-1.78	2.8		
	239	**7.76**	0.0039	3.77	0.0077		0.29	-1.73	3.1		
	240		0.0039	5.25	0.0091		0.37	-1.78	2.8		
61	241	7.68	0.0039	3.99	0.0079	0.0087	0.30	-1.74	3.1	3009	30
	242	8.02	0.0039	6.95	0.0109		0.44	-1.85	2.4		
	243	**7.85**	0.0039	5.15	0.0091		0.36	-1.77	2.8		
	244		0.0039	3.14	0.0071		0.26	-1.71	3.2		
Mean (μ)						0.0079			**3.15**		**32**
STDEVP (σ)						0.0021			**0.30**		**2.7**
99.9999713% Confidence Intervals			**μ - 5σ**						**1.66**		
			μ + 5σ						**4.64**		

Table 25: The Curved-Surface H_V and K_{IC} values of 36 µm CVD SiC sample (CPT-T-G148) at 100 g

Sample: G148		Thickness	Density	constant for HV			Load	kg	N	*E (1300oC)*	*E (Room Temp)*
		36 mm	3.18	1.854				0.1	0.98	430	450
Indent	**crack**	***2a (µm)***	***a (mm)***	***l (µm)***	***c (mm)***	***Average c (mm)***	***B***	***F***	**K_{IC} (MPa.√m)**	**$H_{V\ (0.1)}$ (kg/mm2)**	**$H_{V(0.1)}$ (GPa)**
1	1	7.3200	0.0037	3.48	0.0072	0.0082	0.29	-1.73	3.5	3423	34
	2	7.4000	0.0037	4.76	0.0084		0.36	-1.77	3.1		
	3	**7.3600**	0.0037	5.06	0.0087		0.38	-1.78	3.0		
	4		0.0037	4.75	0.0084		0.36	-1.77	3.1		
2	5	7.4500	0.0038	5.41	0.0092	0.0084	0.38	-1.79	2.8	3160	31
	6	7.8700	0.0038	3.13	0.0070		0.26	-1.71	3.4		
	7	**7.6600**	0.0038	3.84	0.0077		0.30	-1.73	3.2		
	8		0.0038	6.06	0.0099		0.41	-1.81	2.7		
3	9	7.8700	0.0039	4.23	0.0081	0.0090	0.32	-1.74	3.0	3024	30
	10	7.7900	0.0039	5.30	0.0092		0.37	-1.78	2.8		
	11	**7.8300**	0.0039	5.55	0.0095		0.38	-1.79	2.7		
	12		0.0039	5.43	0.0093		0.38	-1.79	2.8		
4	13	7.8700	0.0039	6.45	0.0104	0.0088	0.42	-1.82	2.5	2993	29
	14	7.8700	0.0039	5.05	0.0090		0.36	-1.77	2.8		
	15	**7.8700**	0.0039	4.99	0.0089		0.36	-1.77	2.8		
	16		0.0039	2.80	0.0067		0.23	-1.70	3.3		
5	17	8.1900	0.0039	4.24	0.0082	0.0083	0.32	-1.74	3.0	3005	29
	18	7.5200	0.0039	4.11	0.0080		0.31	-1.74	3.1		
	19	**7.8550**	0.0039	5.53	0.0095		0.38	-1.79	2.7		
	20		0.0039	3.41	0.0073		0.27	-1.72	3.2		
6	21	7.3500	0.0038	6.88	0.0107	0.0096	0.45	-1.85	2.5	3214	32
	22	7.8400	0.0038	5.87	0.0097		0.41	-1.81	2.7		
	23	**7.5950**	0.0038	4.91	0.0087		0.36	-1.77	3.0		
	24		0.0038	5.60	0.0094		0.39	-1.80	2.8		
7	25	7.3900	0.0037	2.91	0.0066	0.0080	0.25	-1.71	3.6	3423	34
	26	7.3300	0.0037	4.11	0.0078		0.33	-1.75	3.3		
	27	**7.3600**	0.0037	4.56	0.0082		0.35	-1.76	3.2		
	28		0.0037	5.74	0.0094		0.41	-1.81	2.9		
8	29	7.5000	0.0038	4.69	0.0084	0.0076	0.35	-1.77	3.1	3296	32
	30	7.5000	0.0038	3.50	0.0073		0.29	-1.73	3.4		
	31	**7.5000**	0.0038	3.83	0.0076		0.31	-1.74	3.3		
	32		0.0038	3.20	0.0070		0.27	-1.72	3.5		
9	33	7.9000	0.0039	4.79	0.0087	0.0087	0.35	-1.76	2.9	3059	30
	34	7.6700	0.0039	4.69	0.0086		0.34	-1.76	3.0		
	35	**7.7850**	0.0039	5.32	0.0092		0.37	-1.78	2.8		
	36		0.0039	4.50	0.0084		0.33	-1.75	3.0		
10	37	7.1200	0.0036	3.23	0.0069	0.0081	0.28	-1.72	3.6	3513	34
	38	7.4100	0.0036	5.66	0.0093		0.41	-1.81	2.9		
	39	**7.2650**	0.0036	5.31	0.0089		0.39	-1.80	3.0		
	40		0.0036	3.86	0.0075		0.31	-1.74	3.4		

Indent	crack	2a (μm)	a (mm)	l (μm)	c (mm)	Average c (mm)	B	F	K_{IC} (MPa.√m)	$H_{V\ (0.1)}$ (kg/mm2)	$H_{V(0.1)}$ (GPa)
11	41	7.2500	0.0036	4.64	0.0083	0.0082	0.36	-1.77	3.2	3498	34
	42	7.3100	0.0036	4.92	0.0086		0.37	-1.78	3.1		
	43	**7.2800**	0.0036	3.40	0.0070		0.29	-1.73	3.5		
	44		0.0036	5.10	0.0087		0.38	-1.79	3.1		
12	45	8.2600	0.0041	7.02	0.0111	0.0093	0.43	-1.83	2.3	2721	27
	46	8.2500	0.0041	6.30	0.0104		0.40	-1.81	2.4		
	47	**8.2550**	0.0041	4.61	0.0087		0.33	-1.75	2.8		
	48		0.0041	2.70	0.0068		0.22	-1.69	3.2		
13	49	7.2500	0.0036	5.02	0.0086	0.0079	0.38	-1.79	3.1	3576	35
	50	7.1500	0.0036	4.66	0.0083		0.36	-1.77	3.2		
	51	**7.2000**	0.0036	3.79	0.0074		0.31	-1.74	3.5		
	52		0.0036	3.63	0.0072		0.30	-1.74	3.5		
14	53	7.8100	0.0040	3.66	0.0076	0.0085	0.28	-1.72	3.1	2959	29
	54	8.0200	0.0040	4.88	0.0088		0.35	-1.76	2.9		
	55	**7.9150**	0.0040	4.43	0.0084		0.33	-1.75	3.0		
	56		0.0040	5.02	0.0090		0.36	-1.77	2.8		
15	57	7.4900	0.0038	4.17	0.0080	0.0081	0.32	-1.75	3.1	3168	31
	58	7.8100	0.0038	4.84	0.0087		0.36	-1.77	3.0		
	59	**7.6500**	0.0038	4.23	0.0081		0.32	-1.75	3.1		
	60		0.0038	3.87	0.0077		0.30	-1.74	3.2		
16	61	7.8300	0.0039	5.02	0.0089	0.0087	0.36	-1.77	2.9	3047	30
	62	7.7700	0.0039	3.97	0.0079		0.30	-1.74	3.1		
	63	**7.8000**	0.0039	4.82	0.0087		0.35	-1.76	2.9		
	64		0.0039	5.51	0.0094		0.38	-1.79	2.8		
17	65	7.8900	0.0039	3.20	0.0071	0.0074	0.26	-1.71	3.3	3075	30
	66	7.6400	0.0039	3.83	0.0077		0.30	-1.73	3.2		
	67	**7.7650**	0.0039	2.74	0.0066		0.23	-1.70	3.4		
	68		0.0039	4.14	0.0080		0.32	-1.74	3.1		
18	69	7.8900	0.0039	6.09	0.0100	0.0086	0.41	-1.81	2.6	3075	30
	70	7.6400	0.0039	3.86	0.0077		0.30	-1.73	3.2		
	71	**7.7650**	0.0039	4.79	0.0087		0.35	-1.76	2.9		
	72		0.0039	4.09	0.0080		0.31	-1.74	3.1		
19	73	7.8300	0.0040	4.02	0.0080	0.0086	0.30	-1.73	3.0	2875	28
	74	8.2300	0.0040	4.59	0.0086		0.33	-1.75	2.9		
	75	**8.0300**	0.0040	4.71	0.0087		0.34	-1.76	2.8		
	76		0.0040	4.86	0.0089		0.34	-1.76	2.8		
20	77	7.4900	0.0039	5.27	0.0091	0.0083	0.37	-1.78	2.8	3127	31
	78	7.9100	0.0039	4.32	0.0082		0.33	-1.75	3.1		
	79	**7.7000**	0.0039	2.90	0.0068		0.24	-1.70	3.4		
	80		0.0039	5.38	0.0092		0.38	-1.79	2.8		
21	81	7.8400	0.0038	4.85	0.0086	0.0084	0.36	-1.77	3.0	3235	32
	82	7.3000	0.0038	5.39	0.0092		0.38	-1.79	2.9		
	83	**7.5700**	0.0038	3.60	0.0074		0.29	-1.73	3.3		
	84		0.0038	4.60	0.0084		0.35	-1.76	3.1		

Indent	crack	2a (μm)	a (mm)	l (μm)	c (mm)	Average c (mm)	B	F	K_{IC} (MPa.√m)	$H_{V\ (0.1)}$ (kg/mm^2)	$H_{V(0.1)}$ (GPa)
22	85	7.4600	0.0037	4.77	0.0085	0.0079	0.36	-1.77	3.1	3404	33
	86	7.3000	0.0037	4.73	0.0084		0.36	-1.77	3.1		
	87	**7.3800**	0.0037	3.18	0.0069		0.27	-1.72	3.5		
	88		0.0037	4.09	0.0078		0.32	-1.75	3.3		
23	89	7.8400	0.0038	6.75	0.0105	0.0092	0.44	-1.85	2.5	3235	32
	90	7.3000	0.0038	5.22	0.0090		0.38	-1.78	2.9		
	91	**7.5700**	0.0038	4.14	0.0079		0.32	-1.75	3.2		
	92		0.0038	5.37	0.0092		0.38	-1.79	2.9		
24	93	7.8000	0.0039	4.32	0.0082	0.0087	0.33	-1.75	3.1	3083	30
	94	7.7100	0.0039	4.84	0.0087		0.35	-1.77	2.9		
	95	**7.7550**	0.0039	4.08	0.0080		0.31	-1.74	3.1		
	96		0.0039	6.11	0.0100		0.41	-1.81	2.6		
25	97	7.2700	0.0037	3.26	0.0070	0.0085	0.27	-1.72	3.5	3349	33
	98	7.6100	0.0037	5.14	0.0089		0.38	-1.78	3.0		
	99	**7.4400**	0.0037	6.31	0.0100		0.43	-1.83	2.7		
	100		0.0037	4.49	0.0082		0.34	-1.76	3.2		
26	101	7.6800	0.0038	5.03	0.0089	0.0085	0.36	-1.77	2.9	3135	31
	102	7.7000	0.0038	4.25	0.0081		0.32	-1.75	3.1		
	103	**7.6900**	0.0038	4.64	0.0085		0.34	-1.76	3.0		
	104		0.0038	4.64	0.0085		0.34	-1.76	3.0		
27	105	7.8700	0.0039	3.88	0.0078	0.0083	0.30	-1.73	3.1	2978	29
	106	7.9100	0.0039	4.19	0.0081		0.31	-1.74	3.0		
	107	**7.8900**	0.0039	4.30	0.0082		0.32	-1.75	3.0		
	108		0.0039	5.10	0.0090		0.36	-1.77	2.8		
28	109	7.3300	0.0037	4.31	0.0080	0.0088	0.34	-1.75	3.2	3377	33
	110	7.4900	0.0037	5.70	0.0094		0.40	-1.81	2.8		
	111	**7.4100**	0.0037	6.62	0.0103		0.45	-1.85	2.6		
	112		0.0037	3.72	0.0074		0.30	-1.73	3.4		
29	113	7.3300	0.0037	5.56	0.0092	0.0081	0.40	-1.80	2.9	3432	34
	114	7.3700	0.0037	4.09	0.0078		0.32	-1.75	3.3		
	115	**7.3500**	0.0037	3.77	0.0074		0.31	-1.74	3.4		
	116		0.0037	4.23	0.0079		0.33	-1.75	3.3		
30	117	7.3700	0.0038	3.48	0.0072	0.0084	0.28	-1.72	3.4	3278	32
	118	7.6700	0.0038	4.36	0.0081		0.33	-1.75	3.2		
	119	**7.5200**	0.0038	5.00	0.0088		0.37	-1.78	3.0		
	120		0.0038	5.55	0.0093		0.39	-1.80	2.8		
31	121	7.6400	0.0038	5.49	0.0093	0.0085	0.39	-1.79	2.8	3164	31
	122	7.6700	0.0038	5.01	0.0088		0.36	-1.77	2.9		
	123	**7.6550**	0.0038	4.94	0.0088		0.36	-1.77	2.9		
	124		0.0038	3.41	0.0072		0.28	-1.72	3.3		
32	125	7.5100	0.0038	4.86	0.0086	0.0088	0.36	-1.77	3.0	3296	32
	126	7.4900	0.0038	5.00	0.0088		0.37	-1.78	3.0		
	127	**7.5000**	0.0038	4.59	0.0083		0.35	-1.76	3.1		
	128		0.0038	5.70	0.0095		0.40	-1.80	2.8		

Indent	crack	2a (μm)	a (mm)	l (μm)	c (mm)	Average c (mm)	B	F	K_{IC} (MPa.√m)	$H_{V\ (0.1)}$ (kg/mm2)	$H_{V(0.1)}$ (GPa)
33	129	7.6400	0.0035	5.40	0.0089	0.0076	0.40	-1.81	3.1	3688	36
	130	6.5400	0.0035	3.46	0.0070		0.30	-1.73	3.6		
	131	**7.0900**	0.0035	3.95	0.0075		0.33	-1.75	3.5		
	132		0.0035	3.57	0.0071		0.30	-1.73	3.6		
34	133	7.3600	0.0038	5.24	0.0090	0.0080	0.38	-1.78	2.9	3201	31
	134	7.8600	0.0038	4.85	0.0087		0.36	-1.77	3.0		
	135	**7.6100**	0.0038	4.15	0.0080		0.32	-1.75	3.2		
	136		0.0038	2.56	0.0064		0.22	-1.69	3.5		
35	137	6.8500	0.0034	4.80	0.0082	0.0078	0.38	-1.79	3.4	4087	40
	138	6.6200	0.0034	4.76	0.0081		0.38	-1.79	3.4		
	139	**6.7350**	0.0034	4.53	0.0079		0.37	-1.78	3.5		
	140		0.0034	3.58	0.0069		0.31	-1.74	3.8		
36	141	7.5700	0.0038	7.34	0.0111	0.0090	0.47	-1.87	2.4	3223	32
	142	7.6000	0.0038	6.58	0.0104		0.44	-1.84	2.6		
	143	**7.5850**	0.0038	3.90	0.0077		0.31	-1.74	3.2		
	144		0.0038	3.16	0.0070		0.26	-1.71	3.4		
37	145	7.0500	0.0036	5.72	0.0094	0.0085	0.41	-1.81	2.9	3513	34
	146	7.4800	0.0036	5.49	0.0091		0.40	-1.80	3.0		
	147	**7.2650**	0.0036	4.37	0.0080		0.34	-1.76	3.3		
	148		0.0036	4.02	0.0077		0.32	-1.75	3.4		
38	149	7.4800	0.0039	5.38	0.0093	0.0089	0.38	-1.79	2.8	3091	30
	150	8.0100	0.0039	4.54	0.0084		0.34	-1.76	3.0		
	151	**7.7450**	0.0039	3.91	0.0078		0.30	-1.74	3.1		
	152		0.0039	6.34	0.0102		0.42	-1.82	2.6		
39	153	7.7900	0.0038	5.48	0.0092	0.0091	0.39	-1.79	2.9	3265	32
	154	7.2800	0.0038	5.96	0.0097		0.41	-1.81	2.7		
	155	**7.5350**	0.0038	6.02	0.0098		0.41	-1.82	2.7		
	156		0.0038	3.71	0.0075		0.30	-1.73	3.3		
40	157	7.4300	0.0037	5.90	0.0096	0.0091	0.41	-1.82	2.8	3386	33
	158	7.3700	0.0037	3.83	0.0075		0.31	-1.74	3.3		
	159	**7.4000**	0.0037	6.27	0.0100		0.43	-1.83	2.7		
	160		0.0037	5.54	0.0092		0.40	-1.80	2.9		
41	161	7.0000	0.0036	4.81	0.0084	0.0082	0.37	-1.78	3.2	3616	35
	162	7.3200	0.0036	4.10	0.0077		0.33	-1.75	3.4		
	163	**7.1600**	0.0036	5.16	0.0087		0.39	-1.79	3.1		
	164		0.0036	4.40	0.0080		0.35	-1.76	3.3		
42	165	7.4300	0.0037	3.60	0.0073	0.0074	0.29	-1.73	3.4	3358	33
	166	7.4300	0.0037	3.88	0.0076		0.31	-1.74	3.3		
	167	**7.4300**	0.0037	3.19	0.0069		0.27	-1.72	3.5		
	168		0.0037	4.04	0.0078		0.32	-1.74	3.3		
43	169	7.3000	0.0037	6.48	0.0101	0.0082	0.44	-1.84	2.7	3446	34
	170	7.3700	0.0037	4.58	0.0082		0.35	-1.77	3.2		
	171	**7.3350**	0.0037	3.85	0.0075		0.31	-1.74	3.4		
	172		0.0037	3.29	0.0070		0.28	-1.72	3.5		

Indent	crack	2a (μm)	a (mm)	l (μm)	c (mm)	Average c (mm)	B	F	K_{IC} (MPa.√m)	$H_{V\ (0.1)}$ (kg/mm2)	$H_{V(0.1)}$ (GPa)
44	173	7.3100	0.0036	5.19	0.0088	0.0091	0.39	-1.79	3.1	3571	35
	174	7.1000	0.0036	5.59	0.0092		0.41	-1.81	3.0		
	175	**7.2050**	0.0036	5.63	0.0092		0.41	-1.81	2.9		
	176		0.0036	5.57	0.0092		0.41	-1.81	3.0		
45	177	7.1100	0.0036	4.04	0.0076	0.0082	0.33	-1.75	3.5	3673	36
	178	7.1000	0.0036	3.73	0.0073		0.31	-1.74	3.5		
	179	**7.1050**	0.0036	4.96	0.0085		0.38	-1.79	3.2		
	180		0.0036	5.96	0.0095		0.43	-1.83	2.9		
46	181	6.7800	0.0035	4.73	0.0082	0.0083	0.37	-1.78	3.3	3849	38
	182	7.1000	0.0035	4.28	0.0078		0.35	-1.76	3.5		
	183	**6.9400**	0.0035	5.00	0.0085		0.39	-1.79	3.3		
	184		0.0035	5.37	0.0088		0.41	-1.81	3.1		
Mean (μ)						0.0084			**3.07**		**32**
STDEVP (σ)						0.0005			**0.28**		**2.6**
99.9999713% Confidence Intervals			**μ - 5σ**						**1.68**		
			μ + 5σ						**4.47**		

Table 26: The Curved-Surface H_V and K_{IC} values of 28 µm CVD SiC sample (CPT-T-G165) at 100 g

Sample: G165		Thickness	Density	constant for HV			Test Load	kg	N	*E (1300oC)*	*E (RT)*
		28 □m	3.180	1.854				0.1	0.98	430	450
Indent	**crack**	***2a (µm)***	***a (mm)***	***l (µm)***	***c (mm)***	***Average c (mm)***	***B***	***F***	***K_{IC} (MPa.√m)***	***$H_{V\ (0.1)}$ (kg/mm2)***	***$H_{V(0.1)}$ (GPa)***
1	1	9.30	0.0046	4.73	0.0093	0.0092	0.307	-1.74	2.5	2190	21
	2	9.10	0.0046	4.46	0.0091		0.294	-1.73	2.6		
	3	**9.20**	0.0046	3.54	0.0081		0.248	-1.71	2.7		
	4		0.0046	5.56	0.0102		0.344	-1.76	2.4		
2	5	6.96	0.0035	5.25	0.0088	0.0079	0.397	-1.80	3.3	3746	37
	6	7.11	0.0035	4.13	0.0076		0.337	-1.76	3.6		
	7	**7.04**	0.0035	3.65	0.0072		0.309	-1.74	3.7		
	8		0.0035	4.69	0.0082		0.368	-1.78	3.4		
3	9	8.49	0.0043	3.14	0.0074	0.0092	0.238	-1.70	3.0	2498	25
	10	8.74	0.0043	4.60	0.0089		0.316	-1.74	2.7		
	11	**8.62**	0.0043	5.32	0.0096		0.349	-1.76	2.6		
	12		0.0043	6.54	0.0108		0.401	-1.80	2.4		
4	13	7.96	0.0039	2.93	0.0068	0.0072	0.245	-1.71	3.5	3107	30
	14	7.49	0.0039	2.48	0.0063		0.215	-1.69	3.6		
	15	**7.73**	0.0039	3.37	0.0072		0.272	-1.72	3.4		
	16		0.0039	4.61	0.0085		0.341	-1.76	3.1		
5	17	7.92	0.0040	4.72	0.0087	0.0083	0.338	-1.76	3.0	2890	28
	18	8.10	0.0040	4.05	0.0081		0.303	-1.74	3.1		
	19	**8.01**	0.0040	3.33	0.0073		0.263	-1.71	3.3		
	20		0.0040	4.88	0.0089		0.346	-1.76	2.9		
6	21	8.12	0.0041	3.83	0.0080	0.0081	0.284	-1.72	3.0	2701	26
	22	8.45	0.0041	3.71	0.0079		0.278	-1.72	3.1		
	23	**8.29**	0.0041	4.77	0.0089		0.333	-1.75	2.8		
	24		0.0041	3.39	0.0075		0.260	-1.71	3.1		
7	25	7.93	0.0040	3.55	0.0076	0.0075	0.274	-1.72	3.2	2854	28
	26	8.19	0.0040	4.56	0.0086		0.329	-1.75	3.0		
	27	**8.06**	0.0040	2.85	0.0069		0.232	-1.70	3.3		
	28		0.0040	2.84	0.0069		0.232	-1.70	3.4		
8	29	8.14	0.0042	4.46	0.0086	0.0088	0.317	-1.74	2.9	2682	26
	30	8.49	0.0042	4.13	0.0083		0.300	-1.73	3.0		
	31	**8.32**	0.0042	5.76	0.0099		0.378	-1.78	2.6		
	32		0.0042	4.08	0.0082		0.297	-1.73	3.0		
9	33	8.29	0.0041	4.85	0.0089	0.0086	0.339	-1.76	2.9	2761	27
	34	8.10	0.0041	3.09	0.0072		0.244	-1.70	3.2		
	35	**8.20**	0.0041	4.95	0.0090		0.344	-1.76	2.8		
	36		0.0041	5.21	0.0093		0.356	-1.77	2.8		
10	37	7.81	0.0039	4.93	0.0088	0.0083	0.356	-1.77	3.0	3079	30
	38	7.71	0.0039	5.07	0.0090		0.363	-1.77	3.0		
	39	**7.76**	0.0039	3.48	0.0074		0.278	-1.72	3.4		
	40		0.0039	4.20	0.0081		0.319	-1.74	3.2		

Indent	crack	2a (μm)	a (mm)	l (μm)	c (mm)	Average c (mm)	B	F	K_{IC} (MPa.√m)	$H_{V\ (0.1)}$ (kg/mm2)	$H_{V(0.1)}$ (GPa)
11	41	8.67	0.0043	4.37	0.0087	0.0083	0.305	-1.74	2.8	2507	25
	42	8.53	0.0043	3.26	0.0076		0.245	-1.71	3.0		
	43	**8.60**	0.0043	3.45	0.0078		0.256	-1.71	3.0		
	44		0.0043	5.03	0.0093		0.336	-1.76	2.7		
12	45	7.53	0.0039	3.99	0.0079	0.0087	0.307	-1.74	3.2	3075	30
	46	8.00	0.0039	4.05	0.0079		0.310	-1.74	3.2		
	47	**7.77**	0.0039	5.58	0.0095		0.387	-1.79	2.9		
	48		0.0039	5.58	0.0095		0.387	-1.79	2.9		
13	49	7.51	0.0037	3.30	0.0070	0.0079	0.275	-1.72	3.6	3309	32
	50	7.46	0.0037	4.80	0.0085		0.358	-1.77	3.2		
	51	**7.49**	0.0037	5.46	0.0092		0.391	-1.80	3.0		
	52		0.0037	3.12	0.0069		0.263	-1.71	3.6		
14	53	8.33	0.0042	7.44	0.0116	0.0098	0.443	-1.85	2.3	2637	26
	54	8.44	0.0042	6.35	0.0105		0.400	-1.80	2.5		
	55	**8.39**	0.0042	4.13	0.0083		0.298	-1.73	2.9		
	56		0.0042	4.48	0.0087		0.316	-1.74	2.9		
15	57	7.89	0.0039	4.56	0.0085	0.0084	0.333	-1.75	3.0	2974	29
	58	7.90	0.0039	4.46	0.0084		0.328	-1.75	3.1		
	59	**7.90**	0.0039	5.10	0.0090		0.360	-1.77	2.9		
	60		0.0039	3.65	0.0076		0.284	-1.72	3.3		
16	61	8.29	0.0041	4.98	0.0091	0.0081	0.346	-1.76	2.8	2764	27
	62	8.09	0.0041	4.69	0.0088		0.331	-1.75	2.9		
	63	**8.19**	0.0041	3.49	0.0076		0.268	-1.72	3.1		
	64		0.0041	2.88	0.0070		0.231	-1.70	3.3		
17	65	7.96	0.0039	5.79	0.0097	0.0079	0.397	-1.80	2.8	3083	30
	66	7.55	0.0039	4.34	0.0082		0.326	-1.75	3.2		
	67	**7.76**	0.0039	4.14	0.0080		0.315	-1.74	3.2		
	68		0.0039	1.71	0.0056		0.159	-1.66	3.8		
18	69	7.95	0.0040	4.05	0.0080	0.0076	0.306	-1.74	3.2	2963	29
	70	7.87	0.0040	3.76	0.0077		0.290	-1.73	3.2		
	71	**7.91**	0.0040	2.88	0.0068		0.238	-1.70	3.4		
	72		0.0040	3.69	0.0076		0.286	-1.73	3.2		
19	73	8.01	0.0040	5.05	0.0090	0.0085	0.355	-1.77	2.9	2919	29
	74	7.93	0.0040	3.29	0.0073		0.261	-1.71	3.3		
	75	**7.97**	0.0040	3.46	0.0074		0.271	-1.72	3.3		
	76		0.0040	6.29	0.0103		0.411	-1.81	2.6		
20	77	7.90	0.0039	3.34	0.0073	0.0084	0.267	-1.72	3.3	3005	29
	78	7.81	0.0039	5.18	0.0091		0.365	-1.78	2.9		
	79	**7.86**	0.0039	4.21	0.0081		0.316	-1.74	3.1		
	80		0.0039	5.16	0.0091		0.364	-1.77	2.9		
21	81	8.04	0.0041	4.52	0.0086	0.0084	0.325	-1.75	3.0	2815	28
	82	8.19	0.0041	3.99	0.0080		0.297	-1.73	3.1		
	83	**8.12**	0.0041	3.09	0.0071		0.246	-1.71	3.3		
	84		0.0041	5.77	0.0098		0.384	-1.79	2.7		

Indent	crack	2a (μm)	a (mm)	l (μm)	c (mm)	Average c (mm)	B	F	K_{IC} (MPa.√m)	$H_{V\ (0.1)}$ (kg/mm2)	$H_{V(0.1)}$ (GPa)
22	85	7.55	0.0037	4.38	0.0080	0.0080	0.342	-1.76	3.4	3455	34
	86	7.10	0.0037	4.40	0.0081		0.343	-1.76	3.4		
	87	**7.33**	0.0037	3.52	0.0072		0.292	-1.73	3.6		
	88		0.0037	4.97	0.0086		0.372	-1.78	3.2		
23	89	7.37	0.0037	3.16	0.0068	0.0077	0.269	-1.72	3.7	3432	34
	90	7.33	0.0037	4.27	0.0079		0.335	-1.75	3.4		
	91	**7.35**	0.0037	4.45	0.0081		0.345	-1.76	3.3		
	92		0.0037	4.03	0.0077		0.322	-1.75	3.5		
24	93	8.37	0.0041	4.55	0.0086	0.0078	0.326	-1.75	2.9	2802	27
	94	7.90	0.0041	2.14	0.0062		0.184	-1.68	3.5		
	95	**8.14**	0.0041	4.16	0.0082		0.306	-1.74	3.0		
	96		0.0041	3.90	0.0080		0.292	-1.73	3.1		
25	97	7.11	0.0036	4.15	0.0077	0.0075	0.335	-1.75	3.5	3642	36
	98	7.16	0.0036	4.15	0.0077		0.335	-1.75	3.5		
	99	**7.14**	0.0036	3.73	0.0073		0.311	-1.74	3.7		
	100		0.0036	3.77	0.0073		0.313	-1.74	3.7		
26	101	7.03	0.0036	3.78	0.0073	0.0075	0.314	-1.74	3.7	3647	36
	102	7.23	0.0036	3.72	0.0073		0.310	-1.74	3.7		
	103	**7.13**	0.0036	3.79	0.0074		0.315	-1.74	3.6		
	104		0.0036	4.51	0.0081		0.355	-1.77	3.4		
27	105	7.17	0.0036	4.95	0.0086	0.0084	0.375	-1.78	3.3	3552	35
	106	7.28	0.0036	5.13	0.0087		0.384	-1.79	3.2		
	107	**7.23**	0.0036	3.53	0.0071		0.296	-1.73	3.7		
	108		0.0036	5.58	0.0092		0.406	-1.81	3.1		
28	109	6.99	0.0035	5.32	0.0088	0.0078	0.401	-1.80	3.2	3778	37
	110	7.02	0.0035	4.83	0.0083		0.376	-1.78	3.4		
	111	**7.01**	0.0035	3.23	0.0067		0.284	-1.72	3.9		
	112		0.0035	3.94	0.0074		0.327	-1.75	3.7		
29	113	7.41	0.0037	3.03	0.0067	0.0070	0.262	-1.71	3.7	3470	34
	114	7.21	0.0037	3.27	0.0069		0.278	-1.72	3.7		
	115	**7.31**	0.0037	3.47	0.0071		0.290	-1.73	3.6		
	116		0.0037	3.47	0.0071		0.290	-1.73	3.6		
30	117	7.59	0.0038	5.63	0.0094	0.0087	0.398	-1.80	2.9	3292	32
	118	7.42	0.0038	3.79	0.0075		0.303	-1.74	3.4		
	119	**7.51**	0.0038	5.34	0.0091		0.384	-1.79	3.0		
	120		0.0038	4.90	0.0087		0.363	-1.77	3.1		
31	121	7.37	0.0036	2.53	0.0061	0.0075	0.232	-1.70	4.0	3611	35
	122	6.96	0.0036	5.22	0.0088		0.390	-1.80	3.2		
	123	**7.17**	0.0036	3.26	0.0068		0.281	-1.72	3.8		
	124		0.0036	4.83	0.0084		0.371	-1.78	3.3		
32	125	7.03	0.0035	3.71	0.0072	0.0070	0.314	-1.74	3.8	3800	37
	126	6.94	0.0035	3.71	0.0072		0.314	-1.74	3.8		
	127	**6.99**	0.0035	3.08	0.0066		0.275	-1.72	4.0		
	128		0.0035	3.34	0.0068		0.291	-1.73	3.9		

Indent	crack	2a (μm)	a (mm)	l (μm)	c (mm)	Average c (mm)	B	F	K_{IC} (MPa.√m)	$H_{V\ (0.1)}$ (kg/mm2)	$H_{V(0.1)}$ (GPa)
33	129	6.77	0.0035	4.12	0.0076	0.0073	0.340	-1.76	3.7	3838	38
	130	7.13	0.0035	5.20	0.0087		0.397	-1.80	3.3		
	131	**6.95**	0.0035	3.25	0.0067		0.287	-1.73	3.9		
	132		0.0035	2.68	0.0062		0.248	-1.71	4.1		
34	133	7.84	0.0040	4.00	0.0080	0.0083	0.302	-1.73	3.1	2926	29
	134	8.08	0.0040	3.83	0.0078		0.293	-1.73	3.2		
	135	**7.96**	0.0040	4.81	0.0088		0.344	-1.76	3.0		
	136		0.0040	4.74	0.0087		0.341	-1.76	3.0		
35	137	7.31	0.0036	4.26	0.0079	0.0075	0.338	-1.76	3.5	3547	35
	138	7.15	0.0036	4.00	0.0076		0.324	-1.75	3.5		
	139	**7.23**	0.0036	4.46	0.0081		0.349	-1.76	3.4		
	140		0.0036	2.87	0.0065		0.254	-1.71	3.8		
36	141	6.58	0.0034	2.87	0.0063	0.0071	0.267	-1.72	4.2	4045	40
	142	6.96	0.0034	3.66	0.0070		0.318	-1.74	3.9		
	143	**6.77**	0.0034	3.53	0.0069		0.310	-1.74	4.0		
	144		0.0034	4.62	0.0080		0.374	-1.78	3.6		
37	145	7.12	0.0036	3.65	0.0072	0.0068	0.306	-1.74	3.7	3657	36
	146	7.12	0.0036	2.20	0.0058		0.209	-1.69	4.1		
	147	**7.12**	0.0036	3.72	0.0073		0.311	-1.74	3.7		
	148		0.0036	3.38	0.0069		0.290	-1.73	3.8		
38	149	7.80	0.0037	3.75	0.0075	0.0078	0.302	-1.73	3.5	3340	33
	150	7.10	0.0037	2.96	0.0067		0.254	-1.71	3.7		
	151	**7.45**	0.0037	4.87	0.0086		0.363	-1.77	3.2		
	152		0.0037	4.52	0.0082		0.345	-1.76	3.3		
39	153	7.69	0.0039	5.86	0.0097	0.0080	0.401	-1.80	2.8	3115	31
	154	7.74	0.0039	2.97	0.0068		0.248	-1.71	3.5		
	155	**7.72**	0.0039	3.25	0.0071		0.265	-1.72	3.4		
	156		0.0039	4.31	0.0082		0.326	-1.75	3.2		
40	157	7.66	0.0038	5.48	0.0093	0.0080	0.390	-1.79	3.0	3261	32
	158	7.42	0.0038	5.61	0.0094		0.396	-1.80	2.9		
	159	**7.54**	0.0038	3.23	0.0070		0.269	-1.72	3.6		
	160		0.0038	2.57	0.0063		0.226	-1.70	3.7		
41	161	8.15	0.0040	3.00	0.0070	0.0078	0.244	-1.70	3.4	2919	29
	162	7.79	0.0040	3.35	0.0073		0.265	-1.71	3.3		
	163	**7.97**	0.0040	4.46	0.0084		0.326	-1.75	3.0		
	164		0.0040	4.32	0.0083		0.319	-1.74	3.1		
42	165	7.89	0.0039	3.55	0.0075	0.0074	0.281	-1.72	3.3	3032	30
	166	7.75	0.0039	3.47	0.0074		0.276	-1.72	3.3		
	167	**7.82**	0.0039	3.71	0.0076		0.290	-1.73	3.3		
	168		0.0039	3.41	0.0073		0.272	-1.72	3.3		
43	169	8.27	0.0040	5.04	0.0091	0.0083	0.353	-1.77	2.9	2875	28
	170	7.79	0.0040	4.85	0.0089		0.344	-1.76	2.9		
	171	**8.03**	0.0040	3.70	0.0077		0.284	-1.72	3.2		
	172		0.0040	3.63	0.0076		0.280	-1.72	3.2		

Indent	crack	2a (μm)	a (mm)	l (μm)	c (mm)	Average c (mm)	B	F	K_{IC} (MPa.√m)	$H_{V\ (0.1)}$ (kg/mm2)	$H_{V(0.1)}$ (GPa)
44	173	8.78	0.0042	5.39	0.0096	0.0088	0.360	-1.77	2.7	2656	26
	174	7.93	0.0042	4.49	0.0087		0.317	-1.74	2.9		
	175	**8.36**	0.0042	4.69	0.0089		0.327	-1.75	2.8		
	176		0.0042	3.79	0.0080		0.280	-1.72	3.0		
45	177	8.21	0.0039	6.12	0.0100	0.0088	0.409	-1.81	2.7	3028	30
	178	7.44	0.0039	6.16	0.0101		0.411	-1.81	2.7		
	179	**7.83**	0.0039	3.14	0.0071		0.256	-1.71	3.4		
	180		0.0039	3.96	0.0079		0.304	-1.74	3.2		
46	181	8.35	0.0041	3.73	0.0078	0.0083	0.283	-1.72	3.1	2808	28
	182	7.90	0.0041	5.36	0.0094		0.365	-1.78	2.8		
	183	**8.13**	0.0041	3.88	0.0079		0.291	-1.73	3.1		
	184		0.0041	4.15	0.0082		0.306	-1.74	3.0		
47	185	7.94	0.0039	5.99	0.0098	0.0085	0.408	-1.81	2.8	3127	31
	186	7.46	0.0039	5.31	0.0092		0.376	-1.78	2.9		
	187	**7.70**	0.0039	4.41	0.0083		0.332	-1.75	3.2		
	188		0.0039	2.73	0.0066		0.233	-1.70	3.6		
48	189	8.11	0.0040	4.51	0.0085	0.0078	0.330	-1.75	3.0	2945	29
	190	7.76	0.0040	3.70	0.0077		0.286	-1.73	3.2		
	191	**7.94**	0.0040	3.73	0.0077		0.288	-1.73	3.2		
	192		0.0040	3.31	0.0073		0.263	-1.71	3.3		
49	193	7.55	0.0038	3.50	0.0073	0.0084	0.282	-1.72	3.4	3152	31
	194	7.79	0.0038	5.21	0.0090		0.373	-1.78	3.0		
	195	**7.67**	0.0038	5.19	0.0090		0.372	-1.78	3.0		
	196		0.0038	4.27	0.0081		0.325	-1.75	3.2		
50	197	8.09	0.0039	4.15	0.0081	0.0081	0.314	-1.74	3.2	3020	30
	198	7.58	0.0039	4.18	0.0081		0.315	-1.74	3.2		
	199	**7.84**	0.0039	4.20	0.0081		0.316	-1.74	3.2		
	200		0.0039	4.09	0.0080		0.310	-1.74	3.2		
51	201	8.03	0.0040	3.65	0.0076	0.0078	0.284	-1.72	3.2	2963	29
	202	7.79	0.0040	2.88	0.0068		0.238	-1.70	3.4		
	203	**7.91**	0.0040	4.55	0.0085		0.333	-1.75	3.0		
	204		0.0040	4.11	0.0081		0.309	-1.74	3.1		
52	205	7.93	0.0039	3.62	0.0076	0.0085	0.283	-1.72	3.3	2990	29
	206	7.82	0.0039	4.76	0.0087		0.344	-1.76	3.0		
	207	**7.88**	0.0039	5.39	0.0093		0.375	-1.78	2.9		
	208		0.0039	4.59	0.0085		0.336	-1.75	3.0		
53	209	8.51	0.0042	3.65	0.0079	0.0089	0.269	-1.72	3.0	2572	25
	210	8.47	0.0042	4.87	0.0091		0.332	-1.75	2.7		
	211	**8.49**	0.0042	4.32	0.0086		0.305	-1.74	2.8		
	212		0.0042	5.80	0.0100		0.374	-1.78	2.6		
54	213	8.19	0.0041	5.03	0.0091	0.0087	0.350	-1.76	2.8	2812	28
	214	8.05	0.0041	6.33	0.0104		0.408	-1.81	2.6		
	215	**8.12**	0.0041	3.61	0.0077		0.276	-1.72	3.2		
	216		0.0041	3.56	0.0076		0.273	-1.72	3.2		

Indent	crack	2a (μm)	a (mm)	l (μm)	c (mm)	Average c (mm)	B	F	K_{IC} (MPa.√m)	$H_{V\ (0.1)}$ (kg/mm2)	$H_{V(0.1)}$ (GPa)
55	217	7.82	0.0039	5.43	0.0093	0.0089	0.381	-1.79	2.9	3111	31
	218	7.62	0.0039	5.78	0.0096		0.397	-1.80	2.8		
	219	**7.72**	0.0039	4.52	0.0084		0.337	-1.76	3.1		
	220		0.0039	4.52	0.0084		0.337	-1.76	3.1		
56	221	8.00	0.0040	5.48	0.0095	0.0088	0.375	-1.78	2.8	2893	28
	222	8.01	0.0040	5.62	0.0096		0.381	-1.79	2.8		
	223	**8.01**	0.0040	3.58	0.0076		0.277	-1.72	3.2		
	224		0.0040	4.42	0.0084		0.323	-1.75	3.0		
57	225	7.88	0.0040	4.11	0.0081	0.0082	0.309	-1.74	3.1	2941	29
	226	8.00	0.0040	5.31	0.0093		0.369	-1.78	2.9		
	227	**7.94**	0.0040	4.18	0.0082		0.312	-1.74	3.1		
	228		0.0040	3.31	0.0073		0.263	-1.71	3.3		
58	229	8.06	0.0040	3.77	0.0078	0.0079	0.288	-1.73	3.2	2879	28
	230	7.99	0.0040	3.77	0.0078		0.288	-1.73	3.2		
	231	**8.03**	0.0040	3.96	0.0080		0.298	-1.73	3.1		
	232		0.0040	3.92	0.0079		0.296	-1.73	3.1		
59	233	8.06	0.0040	4.89	0.0089	0.0080	0.348	-1.76	2.9	2922	29
	234	7.87	0.0040	3.98	0.0080		0.301	-1.73	3.1		
	235	**7.97**	0.0040	3.46	0.0074		0.272	-1.72	3.3		
	236		0.0040	3.57	0.0076		0.278	-1.72	3.2		
60	237	8.41	0.0041	3.46	0.0075	0.0088	0.268	-1.72	3.2	2826	28
	238	7.79	0.0041	5.52	0.0096		0.373	-1.78	2.7		
	239	**8.10**	0.0041	5.42	0.0095		0.369	-1.78	2.8		
	240		0.0041	4.63	0.0087		0.331	-1.75	2.9		
61	241	8.71	0.0041	5.68	0.0098	0.0089	0.375	-1.78	2.7	2708	27
	242	7.84	0.0041	4.63	0.0088		0.326	-1.75	2.9		
	243	**8.28**	0.0041	4.12	0.0083		0.300	-1.73	3.0		
	244		0.0041	4.69	0.0088		0.329	-1.75	2.9		
62	245	7.97	0.0039	5.43	0.0093	0.0082	0.378	-1.78	2.9	3020	30
	246	7.70	0.0039	4.95	0.0089		0.355	-1.77	3.0		
	247	**7.84**	0.0039	2.20	0.0061		0.194	-1.68	3.6		
	248		0.0039	4.37	0.0083		0.325	-1.75	3.1		
63	249	7.78	0.0039	5.06	0.0089	0.0089	0.363	-1.77	3.0	3099	30
	250	7.69	0.0039	5.60	0.0095		0.389	-1.79	2.9		
	251	**7.74**	0.0039	4.36	0.0082		0.328	-1.75	3.2		
	252		0.0039	5.01	0.0089		0.361	-1.77	3.0		
64	253	7.45	0.0038	4.41	0.0082	0.0086	0.333	-1.75	3.2	3168	31
	254	7.85	0.0038	5.14	0.0090		0.370	-1.78	3.0		
	255	**7.65**	0.0038	4.09	0.0079		0.316	-1.74	3.3		
	256		0.0038	5.64	0.0095		0.393	-1.80	2.9		
65	257	8.06	0.0040	4.20	0.0082	0.0087	0.311	-1.74	3.1	2865	28
	258	8.03	0.0040	5.08	0.0091		0.355	-1.77	2.9		
	259	**8.05**	0.0040	4.47	0.0085		0.325	-1.75	3.0		
	260		0.0040	4.88	0.0089		0.345	-1.76	2.9		

Indent	crack	2a (μm)	a (mm)	l (μm)	c (mm)	Average c (mm)	B	F	K_{IC} (MPa.√m)	$H_{V\ (0.1)}$ (kg/mm2)	$H_{V(0.1)}$ (GPa)
66	261	8.21	0.0042	4.86	0.0090	0.0078	0.336	-1.75	2.8	2669	26
	262	8.46	0.0042	3.12	0.0073		0.243	-1.70	3.1		
	263	**8.34**	0.0042	4.11	0.0083		0.298	-1.73	2.9		
	264		0.0042	2.30	0.0065		0.191	-1.68	3.3		
67	265	7.68	0.0040	4.57	0.0085	0.0085	0.334	-1.75	3.0	2967	29
	266	8.13	0.0040	5.63	0.0096		0.385	-1.79	2.8		
	267	**7.91**	0.0040	3.21	0.0072		0.258	-1.71	3.3		
	268		0.0040	4.62	0.0086		0.336	-1.76	3.0		
68	269	8.07	0.0040	5.02	0.0090	0.0087	0.355	-1.77	2.9	2933	29
	270	7.83	0.0040	3.65	0.0076		0.283	-1.72	3.2		
	271	**7.95**	0.0040	4.79	0.0088		0.343	-1.76	3.0		
	272		0.0040	5.26	0.0092		0.366	-1.78	2.9		
69	273	7.04	0.0035	2.69	0.0062	0.0070	0.248	-1.71	4.1	3795	37
	274	6.94	0.0035	4.12	0.0076		0.338	-1.76	3.6		
	275	**6.99**	0.0035	4.40	0.0079		0.354	-1.77	3.5		
	276		0.0035	2.74	0.0062		0.251	-1.71	4.1		
70	277	8.18	0.0040	4.49	0.0085	0.0088	0.327	-1.75	3.0	2890	28
	278	7.84	0.0040	5.64	0.0096		0.382	-1.79	2.8		
	279	**8.01**	0.0040	5.64	0.0096		0.382	-1.79	2.8		
	280		0.0040	3.42	0.0074		0.268	-1.72	3.2		
71	281	7.40	0.0037	3.88	0.0076	0.0080	0.310	-1.74	3.4	3340	33
	282	7.50	0.0037	4.90	0.0086		0.365	-1.77	3.2		
	283	**7.45**	0.0037	4.28	0.0080		0.332	-1.75	3.3		
	284		0.0037	3.98	0.0077		0.316	-1.74	3.4		
72	285	7.93	0.0039	6.61	0.0106	0.0092	0.427	-1.83	2.6	2978	29
	286	7.85	0.0039	5.30	0.0092		0.370	-1.78	2.9		
	287	**7.89**	0.0039	6.07	0.0100		0.405	-1.81	2.7		
	288		0.0039	3.13	0.0071		0.254	-1.71	3.4		
73	289	8.43	0.0042	4.45	0.0087	0.0085	0.312	-1.74	2.8	2597	25
	290	8.47	0.0042	4.59	0.0088		0.319	-1.74	2.8		
	291	**8.45**	0.0042	3.43	0.0077		0.258	-1.71	3.0		
	292		0.0042	4.51	0.0087		0.316	-1.74	2.8		
74	293	8.11	0.0038	4.52	0.0083	0.0080	0.340	-1.76	3.2	3193	31
	294	7.13	0.0038	4.34	0.0082		0.330	-1.75	3.2		
	295	**7.62**	0.0038	3.80	0.0076		0.300	-1.73	3.4		
	296		0.0038	4.02	0.0078		0.313	-1.74	3.3		
75	297	7.89	0.0039	4.07	0.0080	0.0084	0.311	-1.74	3.2	3059	30
	298	7.68	0.0039	5.28	0.0092		0.372	-1.78	2.9		
	299	**7.79**	0.0039	4.39	0.0083		0.328	-1.75	3.1		
	300		0.0039	4.13	0.0080		0.314	-1.74	3.2		
76	301	9.53	0.0048	6.29	0.0111	0.0097	0.364	-1.77	2.2	2022	20
	302	9.62	0.0048	6.28	0.0111		0.364	-1.77	2.2		
	303	**9.58**	0.0048	3.10	0.0079		0.217	-1.69	2.6		
	304		0.0048	3.81	0.0086		0.254	-1.71	2.5		

Indent	crack	2a (μm)	a (mm)	l (μm)	c (mm)	Average c (mm)	B	F	K_{IC} (MPa.√m)	$H_{V\ (0.1)}$ (kg/mm2)	$H_{V(0.1)}$ (GPa)
77	305	7.94	0.0040	5.81	0.0098	0.0086	0.392	-1.80	2.7	2956	29
	306	7.90	0.0040	3.93	0.0079		0.299	-1.73	3.2		
	307	**7.92**	0.0040	4.48	0.0084		0.329	-1.75	3.1		
	308		0.0040	4.38	0.0083		0.323	-1.75	3.1		
78	309	7.95	0.0040	5.14	0.0091	0.0083	0.361	-1.77	2.9	2945	29
	310	7.92	0.0040	4.52	0.0085		0.330	-1.75	3.0		
	311	**7.94**	0.0040	4.01	0.0080		0.303	-1.74	3.2		
	312		0.0040	3.69	0.0077		0.286	-1.73	3.2		
79	313	8.16	0.0039	2.94	0.0069	0.0077	0.242	-1.70	3.4	2990	29
	314	7.59	0.0039	3.25	0.0072		0.261	-1.71	3.4		
	315	**7.88**	0.0039	4.17	0.0081		0.314	-1.74	3.1		
	316		0.0039	4.51	0.0084		0.332	-1.75	3.1		
80	317	8.15	0.0041	4.76	0.0088	0.0083	0.338	-1.76	2.9	2826	28
	318	8.05	0.0041	4.21	0.0083		0.310	-1.74	3.0		
	319	**8.10**	0.0041	4.71	0.0088		0.335	-1.75	2.9		
	320		0.0041	3.18	0.0072		0.252	-1.71	3.3		
81	321	7.92	0.0039	4.53	0.0084	0.0082	0.335	-1.75	3.1	3051	30
	322	7.67	0.0039	4.96	0.0089		0.357	-1.77	3.0		
	323	**7.80**	0.0039	3.71	0.0076		0.290	-1.73	3.3		
	324		0.0039	4.07	0.0080		0.311	-1.74	3.2		
82	325	7.95	0.0040	4.20	0.0082	0.0081	0.314	-1.74	3.1	2956	29
	326	7.89	0.0040	5.44	0.0094		0.375	-1.78	2.8		
	327	**7.92**	0.0040	3.77	0.0077		0.290	-1.73	3.2		
	328		0.0040	3.16	0.0071		0.255	-1.71	3.4		
83	329	7.77	0.0040	4.61	0.0086	0.0081	0.336	-1.75	3.0	2967	29
	330	8.04	0.0040	4.45	0.0084		0.328	-1.75	3.1		
	331	**7.91**	0.0040	4.65	0.0086		0.338	-1.76	3.0		
	332		0.0040	2.80	0.0068		0.233	-1.70	3.4		
84	333	8.67	0.0042	5.97	0.0102	0.0087	0.383	-1.79	2.5	2612	26
	334	8.18	0.0042	4.59	0.0088		0.320	-1.75	2.8		
	335	**8.43**	0.0042	3.30	0.0075		0.251	-1.71	3.1		
	336		0.0042	4.06	0.0083		0.293	-1.73	2.9		
85	337	7.70	0.0038	5.57	0.0094	0.0078	0.389	-1.79	2.9	3131	31
	338	7.69	0.0038	5.97	0.0098		0.407	-1.81	2.8		
	339	**7.70**	0.0038	2.83	0.0067		0.239	-1.70	3.6		
	340		0.0038	1.60	0.0054		0.151	-1.66	3.9		
86	341	8.10	0.0041	2.89	0.0069	0.0085	0.234	-1.70	3.3	2819	28
	342	8.12	0.0041	4.69	0.0087		0.334	-1.75	2.9		
	343	**8.11**	0.0041	4.94	0.0090		0.346	-1.76	2.9		
	344		0.0041	5.39	0.0094		0.367	-1.78	2.8		
87	345	7.63	0.0039	4.64	0.0085	0.0083	0.341	-1.76	3.1	3075	30
	346	7.90	0.0039	4.94	0.0088		0.356	-1.77	3.0		
	347	**7.77**	0.0039	4.15	0.0080		0.316	-1.74	3.2		
	348		0.0039	3.74	0.0076		0.293	-1.73	3.3		

Indent	crack	2a (μm)	a (mm)	l (μm)	c (mm)	Average c (mm)	B	F	K_{IC} (MPa.√m)	$H_{V\ (0.1)}$ (kg/mm2)	$H_{V(0.1)}$ (GPa)
88	349	8.38	0.0041	5.39	0.0095	0.0085	0.365	-1.78	2.7	2771	27
	350	7.98	0.0041	5.13	0.0092		0.353	-1.77	2.8		
	351	**8.18**	0.0041	3.70	0.0078		0.280	-1.72	3.1		
	352		0.0041	3.44	0.0075		0.265	-1.71	3.2		
89	353	8.13	0.0040	3.27	0.0073	0.0080	0.258	-1.71	3.2	2847	28
	354	8.01	0.0040	2.89	0.0069		0.235	-1.70	3.3		
	355	**8.07**	0.0040	4.65	0.0087		0.333	-1.75	3.0		
	356		0.0040	5.00	0.0090		0.350	-1.76	2.9		
90	357	7.75	0.0039	3.16	0.0071	0.0072	0.257	-1.71	3.4	3009	30
	358	7.95	0.0039	3.20	0.0071		0.259	-1.71	3.4		
	359	**7.85**	0.0039	3.20	0.0071		0.259	-1.71	3.4		
	360		0.0039	3.39	0.0073		0.270	-1.72	3.3		
91	361	7.63	0.0039	3.60	0.0075	0.0076	0.283	-1.72	3.3	3020	30
	362	8.04	0.0039	3.67	0.0076		0.287	-1.73	3.3		
	363	**7.84**	0.0039	3.82	0.0077		0.296	-1.73	3.2		
	364		0.0039	3.66	0.0076		0.287	-1.73	3.3		
92	365	9.03	0.0045	3.37	0.0079	0.0087	0.242	-1.70	2.8	2269	22
	366	9.05	0.0045	3.51	0.0080		0.250	-1.71	2.8		
	367	**9.04**	0.0045	4.68	0.0092		0.309	-1.74	2.6		
	368		0.0045	4.98	0.0095		0.323	-1.75	2.5		
93	373	8.37	0.0042	3.56	0.0077	0.0080	0.267	-1.72	3.0	2643	26
	374	8.38	0.0042	4.33	0.0085		0.308	-1.74	2.9		
	375	**8.38**	0.0042	3.53	0.0077		0.266	-1.72	3.0		
	376		0.0042	3.91	0.0081		0.286	-1.73	3.0		
Mean (μ)						0.0082			**3.13**		**30**
STDEVP (σ)						0.0004			**0.34**		**3.6**
99.9999713% Confidence Intervals			**μ - 5σ**						**1.45**		
			μ + 5σ						**4.81**		

7.8 FRACTURE TOUGHNESS PROBABILITY PLOTS OF THE CVD SiC SAMPLES

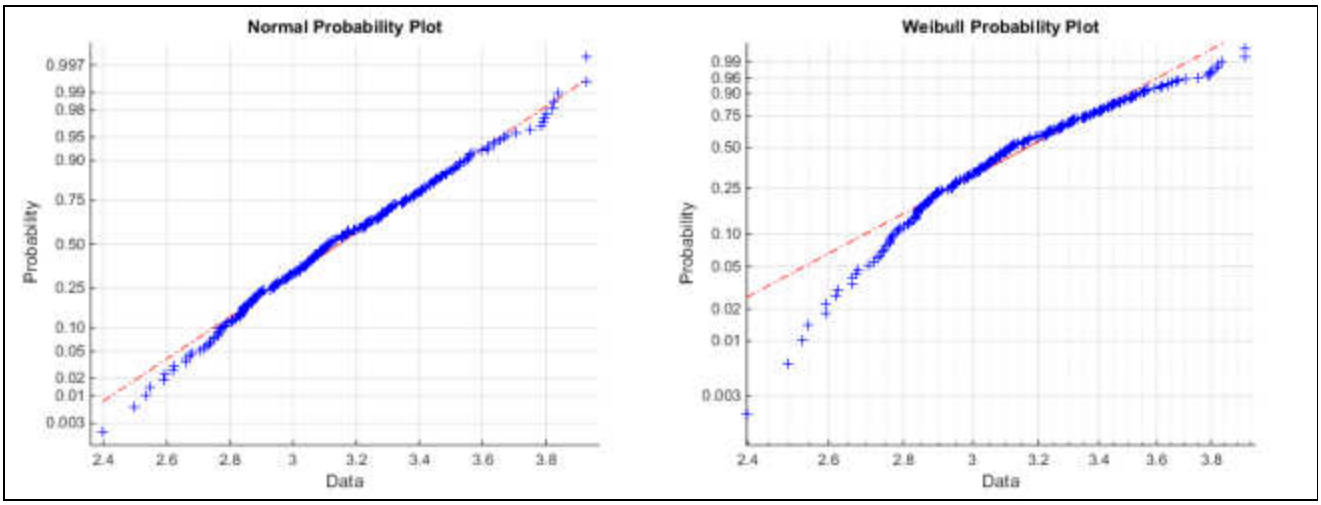

Figure 28: **Curved surface** K_{IC} normal and Weibull probability plots for data set CPT-T-G131

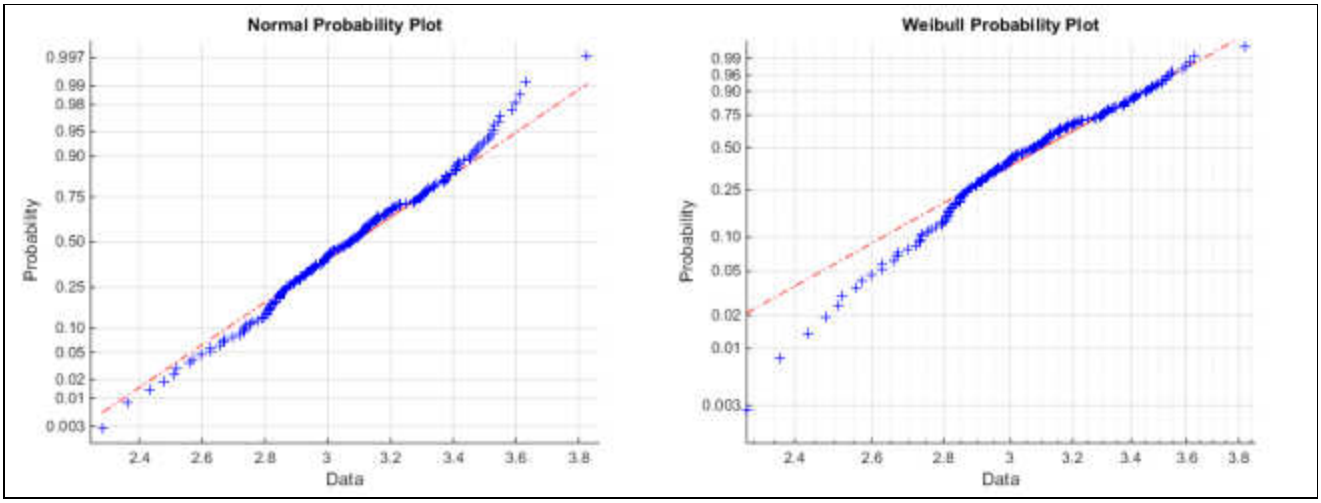

Figure 29: **Curved surface** K_{IC} normal and Weibull probability plots for data CPT-T-G148

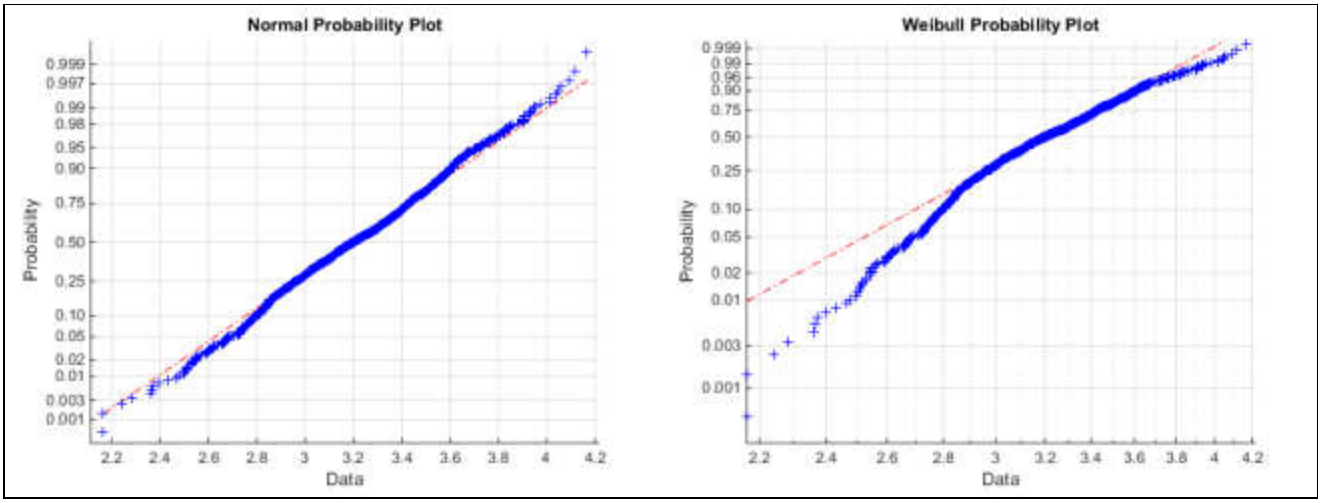

Figure 30: **Curved surface** K_{IC} normal and Weibull probability plots for all combined data sets

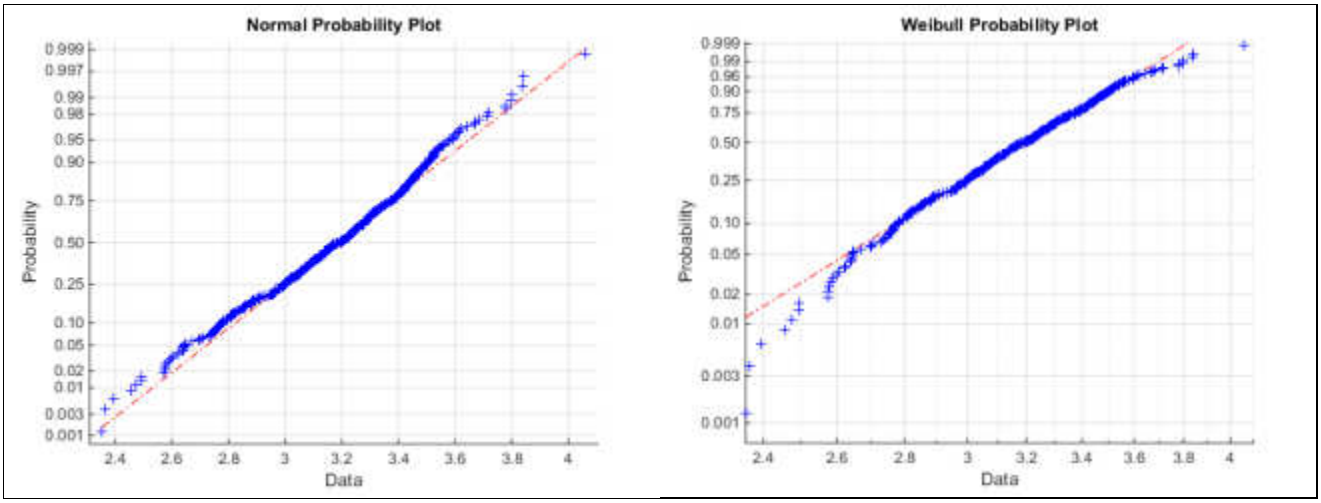

Figure 31: **Cross Sectional** K_{IC} normal and Weibull probability plots for data set CPT-B-B10

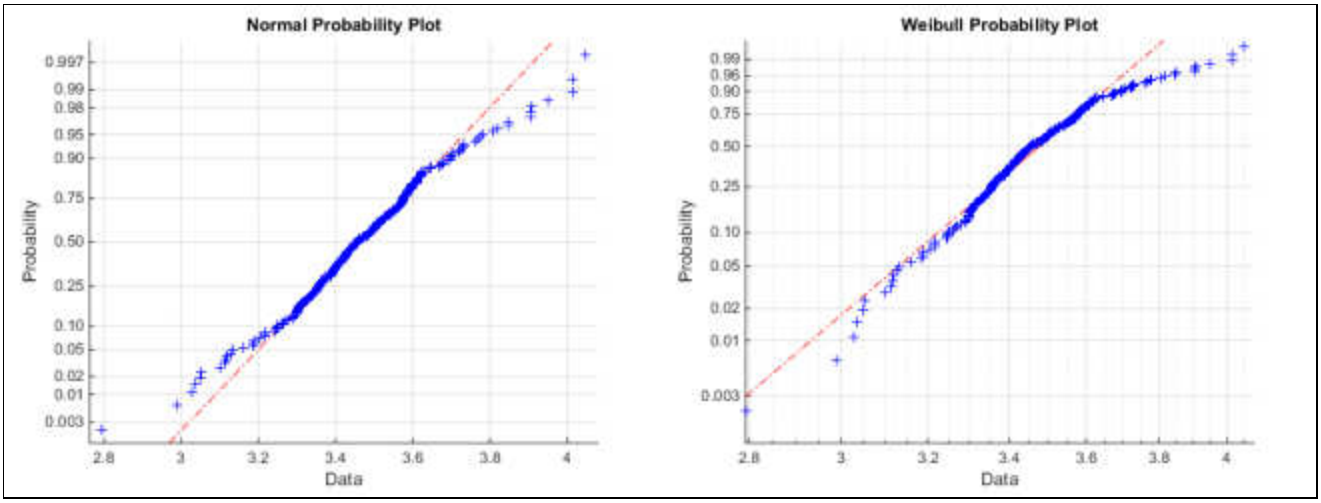

Figure 32: **Curved surface** K_{IC} normal and Weibull probability plots for data set CPT-B-B10

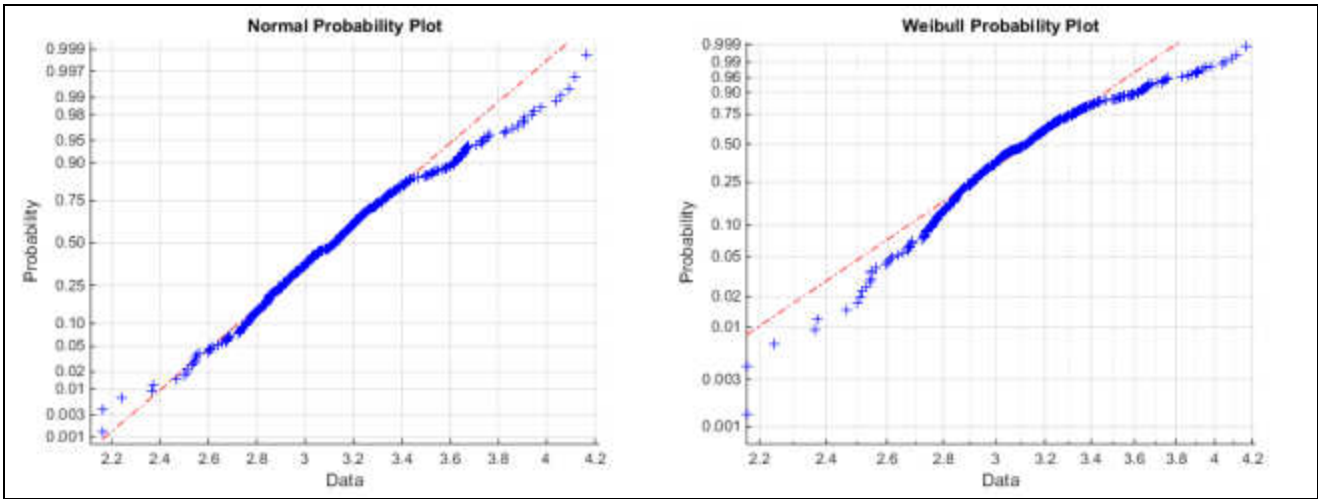

Figure 33: **Curved surface** K_{IC} normal and Weibull probability plots for data set CPT-T-G165